January 2013

# An Investigation Of Climate Patterns On Earth-Like Planets Using The NASA GISS Global Climate Model II

Robert Mark Elowitz

# AN INVESTIGATION OF CLIMATE PATTERNS ON EARTH-LIKE PLANETS USING THE NASA GISS GLOBAL CLIMATE MODEL II

by

Robert Mark Elowitz
Bachelor of Science, University of Arizona, 1985

A Thesis

Submitted to the Graduate Faculty

of the

University of North Dakota

In partial fulfillment of the requirements

for the degree of

Master of Science

Grand Forks, North Dakota
May
2013

This thesis, submitted by R. Mark Elowitz in partial fulfillment of the requirements for the Degree of Master of Science from the University of North Dakota, has been read by the Faculty Advisor under whom the work has been done and is hereby approved.

_____
Dr. Paul S. Hardersen

_____
Dr. Xiquan Dong

_____
Dr. Ronald Fevig

This thesis is being submitted by the appointed advisory committee as having met all of the requirements of the Graduate School at the University of North Dakota and is hereby approved.

_____
Dean of the Graduate School

_____
Date

# PERMISSION

Title: An Investigation of Climate Patterns on Earth-like Planets Using the NASA GISS Global Climate Model II

Department: Space Studies

Degree: Master of Science

In presenting this thesis in partial fulfillment of the requirements for a graduate degree from the University of North Dakota, I agree that the library of this University shall make it freely available for inspection. I further agree that permission for extensive copying for scholarly purposes may be granted by the professor who supervised my thesis work or, in her absence, by the chairperson of the department or the dean of the Graduate School. It is understood that any copying or publication or other use of this thesis or part thereof for financial gain shall not be allowed without my written permission. It is also understood that due recognition shall be given to me and to the University of North Dakota in any scholarly use which may be made of any material in my thesis.

Robert Mark Elowitz
March 19, 2013

TABLE OF CONTENTS

LIST OF FIGURES

LIST OF TABLES

Table Page

ACKNOWLEDGMENTS

I wish to express my sincere appreciation to the members of my advisory committee for their guidance and support during my time in the master's program at the University of North Dakota.

To Kathy and Bill

ABSTRACT

To determine the capability of NASA's GISS GCM-II global climate model, the user-friendly EdGCM interface to the 3-D climate model code was evaluated by simulating global climate patterns that Earth-like planets may experience. The simulation scenarios involved different greenhouse gas emissions trends, planetary orbital parameters, and solar irradiance variations. It is found that the EdGCM interface to the GCM-II 3-D climate model is capable of studying climate patterns on hypothetical Earth-like planets, with some limitations involved. Studying extreme climate patterns on Earth-like planets as a function of planetary obliquity, orbital eccentricity, atmospheric composition, solar irradiance variations, and location with the host star's habitable zone is needed to determine whether such planets are habitable for life as we know it. Studying the behavior of climate on hypothetical Earth-like planet also provides insight into the future climate of our own planet. A database of climate models based on hypothetical Earth-like worlds will provide a valuable resource to the astrobiology community in support of future detections of exoplanets with masses, sizes, and composition similar to Earth. At present, most studies involved the use of 1-D, or 2-D climate models to explore planetary climate on Earth-like planets. This is due to the difficulty of using very complex 3-D climate model codes that typically have poor user interfaces or interfaces that are very difficult to use. EdGCM provides scientists with a user-friendly interface to a full 3-D climate model capable of simulating the climate on Earth-like planets.

However, EdGCM  is extremely limited in studying global climate on exo-Earth planets outside our solar system. The user is able to change the simulation initial conditions, including different greenhouse gas concentrations and their associated trends, solar irradiance and its trend over time,  planetary obliquity and orbit eccentricity, and heliocentric distance by specifying the appropriate solar irradiance. The results of simulations carried out in this research indicate positive results, with the exception of some of the more extreme cases. The EdGCM interface to GCM-II would be a valuable addition to universities with astrobiology programs involved in studying climate on Earth-like planets with one major modification. The ability to change the land mass configuration that is currently based on Earth's continents to any arbitrary land mass configuration would allow the creation of a database of climate model simulations of an array of hypothetical Earth-like worlds that will soon be discovered by current and future space-based planet-finding missions.

# CHAPTER I

## INTRODUCTION

This thesis will investigate the effects of climate forcing, including variations in solar irradiance over time, and variation in Earth's orbital parameters on the climate of Earth as well as earthlike planets that may be discovered by current or future space-based planet finding missions. This work investigates both linear and non-linear trends in greenhouse gas emissions over several hundred years. The effects on climate from a variation in solar irradiance will be explored. It is known that earth's climate has been significantly affected by changes in solar irradiance over short periods of time as demonstrated by the Maunder Minimum, a period of low solar activity that occurred between 1645 and 1715. During this period of low sunspot number, the Earth experienced colder climate conditions over many regions (Shindell, 2009). The change in solar irradiance during the Maunder Minimum is correlated with the number of measured sunspots, and the resulting change in solar luminosity appears to be correlated with the so-called "Little Ice Age" during the $17^{th}$ century. The Little Ice Age marked a period of colder temperatures, especially in the northern hemisphere. This work will investigate the effects on earth's global climate resulting from future Maunder Minimum cycles that may

occur. There has been recent speculation among the scientific community that the Sun may be entering an extended period of low activity, identical to the Maunder Minimum (Figure 1) that occurred in the late 17$^{th}$ century. This is indicated by the extended length of the current 11-yr solar sunspot cycle (Feulner & Rahmstorf, 2010). Recent work in studying the effects from future Maunder Minimum periods of low solar activity have been carried out by Feulner and Rahmstorf (2010).

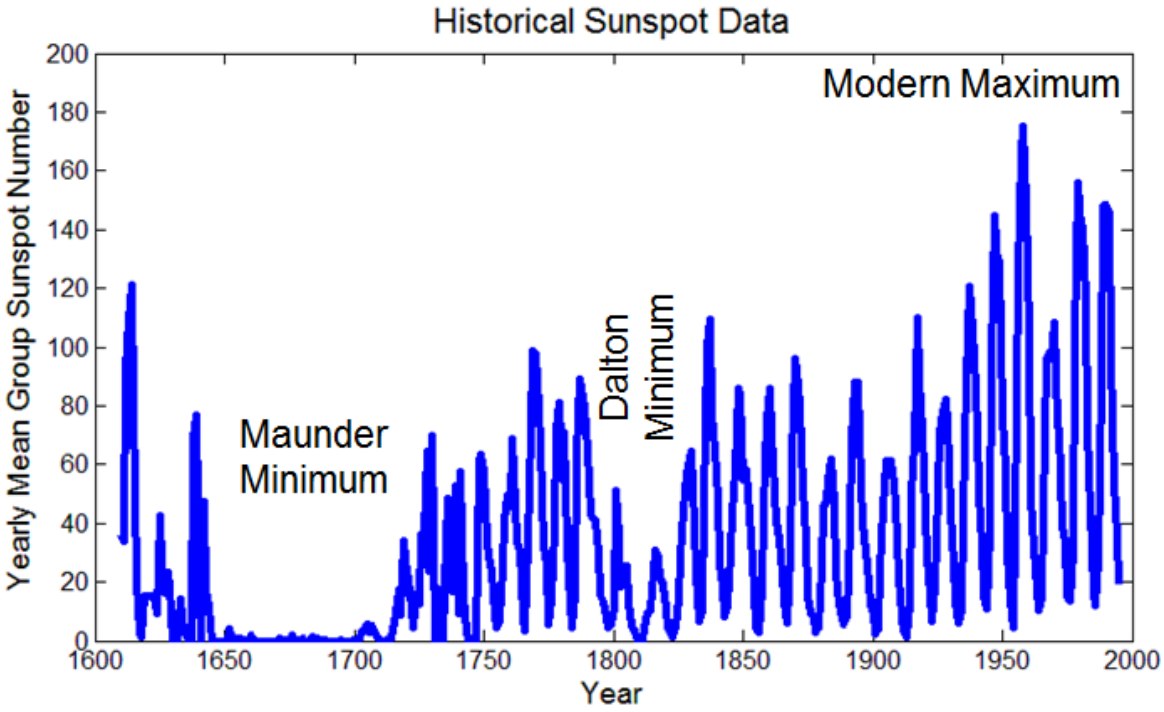


Figure 1. Plot of historical sunspot data over 400 years. The plot shows the yearly mean Group Sunspot Number, which is calculated by taking the average of all the monthly means. Note the two periods of low solar activity between the year 1650 and 1720 (Maunder Minimum) and during the early 1800s (Dalton Minimum). Both the Maunder Minimum and Dalton Minimum shows yearly mean group sunspot numbers well below the modern maximum. Both periods of reduced solar activity are known to correlate with periods of colder climate on the Earth. Plot derived from NOAA National Geophysical Data Center.

They find only a small change of -0.3℃ in the year 2100 when compared to a model using normal solar activity of recent decades. This temperature offset is much smaller than the temperature change computed from climate models that assume current

greenhouse gas emission rates extrapolated to the year 2100. This work will improve on climate model simulations carried out by Feulner and Rahmstorf (2010) by extending the models out to the year 2200. Different climate models will be produced using NASA's GISS GCM-II model to determine how much future periods of low solar activity can offset the effect of global warming as a result of greenhouse gas emissions into earth's atmosphere. The effects on regional climate as a result of small changes in solar irradiance will be examined over several centuries. Regional temperature changes over the continents and oceans due to periods of low solar activity has been explored by Shindell et al. (2001). The authors find evidence for regional climate change over a century due to slight variations in solar irradiance, similar to the results found by Feulner and Rahmstorf (2010). Both of the studies mentioned previously found significantly colder temperatures over the continents, even though the average global temperature change was much smaller. The work carried out in this study will use an updated version of the GISS GCM-II model to improve on climate models produced by Feulner and Rahmstorf (2010) and Shindell et al. (2001). The climate models will be extended over several centuries to determine long-term climatic variations due to periods of low solar activity. In a study by Douglass and Clader (2002), they note a linear trend in the sensitivity of temperature to small changes in the solar irradiance. The sensitivity to the variation in solar irradiance was approximately two times that expected from a standard Stefan-Boltzmann radiation balance assumption with no feedback. Extending the simulations to several centuries should be carried out to determine whether such a linear trend in the data continues over longer time spans, or whether a non-linear trend is observed. Climate model simulations involving a variation in solar irradiance can help

determine whether observed correlations between the total solar irradiance and climatic change require an unrealistic change in solar irradiance, or whether the climatic variation is more sensitive to radiative forcing than is currently accepted.

Another study to be carried out using the GISS GCM-II is to determine whether or not there are correlations between the length of a solar sunspot cycle and temperature anomalies. An important question to be answered is whether there is an amplification in the response to variations in total solar irradiance, as a result of a positive feedback mechanism.

Another positive-feedback mechanism to be explored using global climate model simulations is the albedo-temperature feedback (Gorodetskaya et al., 2006). The feedback mechanism operates as follows: assume there is an initial change, such as reduced solar activity, that results in a colder climate. The climate cooling results in an increase in the amount of snow and ice cover on the earth. Since the albedo (reflectivity) of snow and ice is higher than the surrounding terrain, less solar radiation is absorbed at the surface of the earth. This results in greater cooling, which results in the formation of more snow and ice at the earth's surface. Since there is a decrease in the amount of absorbed heat over the increased areas of high-albedo snow and ice, the resulting temperature drop becomes greater than the initial cooling. This illustrates an example of what is known as a positive feedback mechanism (Figure 2). The goal of examining the albedo-temperature feedback mechanism in global climate models is to determine the degree of amplification of the total cooling by this feedback process. The reverse process (Figure 3) can also be examined using global climate models, in which an initial increase in warming reduces the total surface area of ice and snow. This increases the amount of solar radiation that is

absorbed by the newly exposed land or ocean, resulting in further warming. An interesting question to be answered by modeling the albedo-temperature feedback is to determine how sensitive earth's climate is to the positive feedback mechanism.

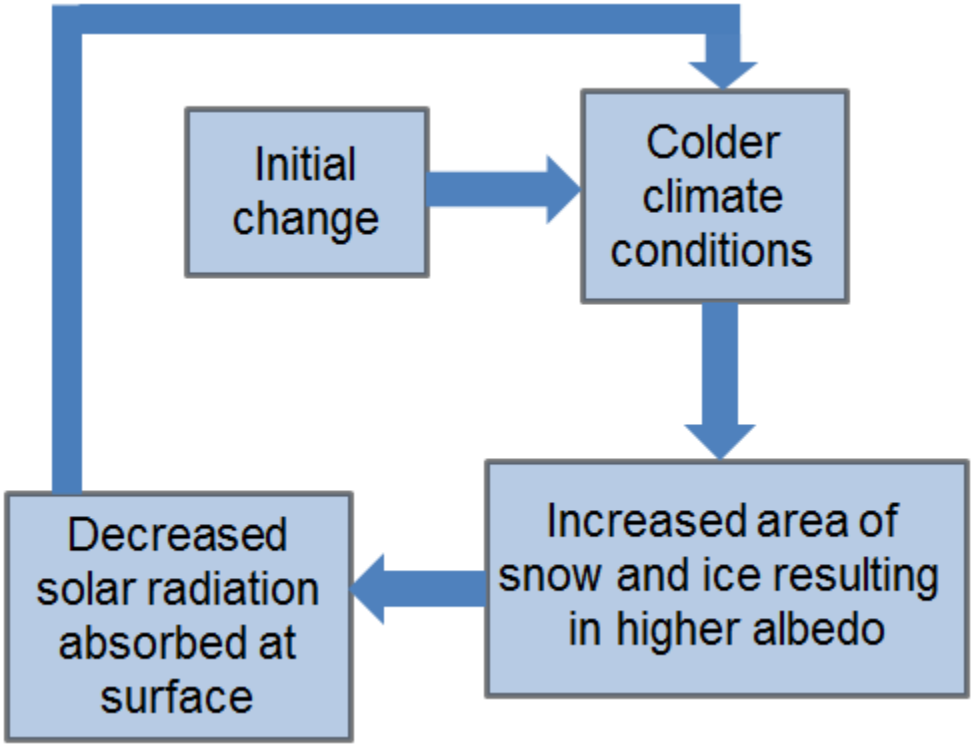


Figure 2. Albedo-temperature positive feedback process. As a result of initial climate cooling due to a reduction in solar activity over long time spans, the total surface area of ice and snow increases, resulting in a decrease of solar radiation that is absorbed by high-albedo ice and snow at the surface of the earth. This causes a further amplification of climate cooling.

When the amount of sea ice increases and the amount of snow increases over snow-free regions of the continents, as a result of an initial temperature drop, the surface reflectivity (albedo) can increase upwards of 80-95% (Koenderink, J. J., et al. 1992). The regions of continents that were previously covered with high-albedo snow will then absorb less radiation emitted by the sun. The same holds true for ice-covered regions of seas and oceans. More solar radiation will be reflected back to space, resulting in further

cooling. This Albedo-Temperature feedback has profound consequences on earth's climate on centennial scales.

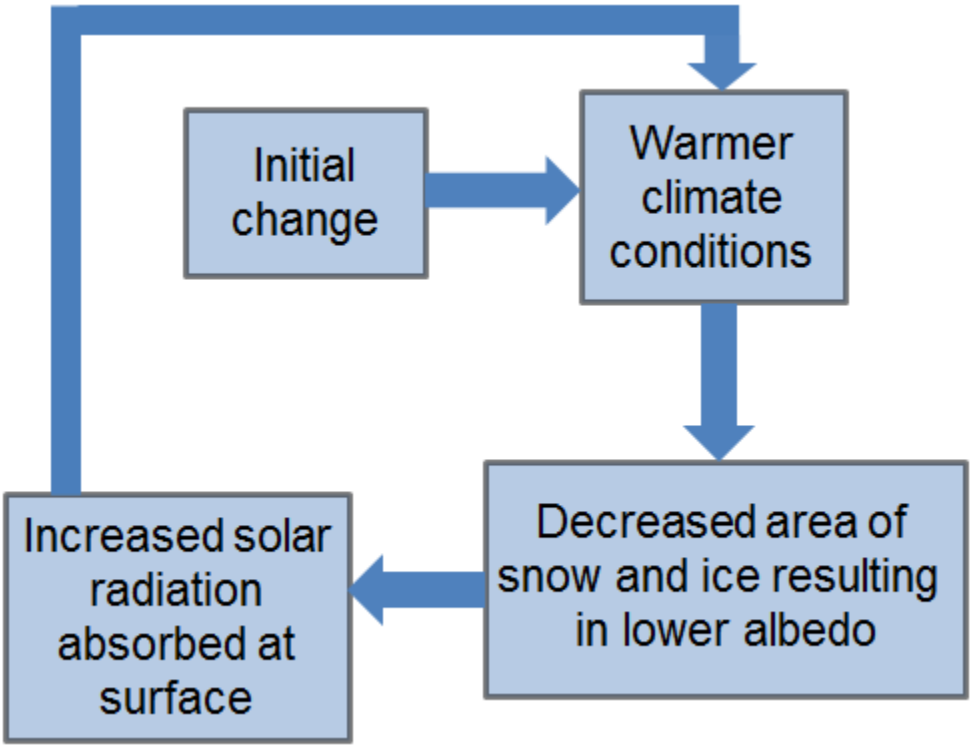


Figure 3. Inverse of the albedo-temperature feedback process. An initial change towards higher temperature induced by an increase in solar activity or greenhouse gas emissions results in a warming climate. The warmer temperatures decrease the total area of snow and ice resulting in lower reflectivity (albedo) at the earth's surface. This results in increased solar radiation absorbed by continents and oceans not covered by snow and ice, resulting in an amplification of warmer climate conditions.

**Greenhouse Gas Forcing**

One of the major forcing on Earth's climate is due to both natural and anthropogenic emissions of greenhouse gases (Bruhl, 1993; Evans et al., 1999; Hansen et al., 1997;). Greenhouse gases, such as $CO_2$, $CH_4$, $N_2O$ (Figure 4), and others, are good absorbers and emitters of infrared radiation in earth's atmosphere. These molecules are able to absorb and emit infrared radiation because they vibrate at the frequency of the infrared radiation. In other words, the greenhouse gas molecule is able to convert the

infrared photon into one or more excited vibrational states. The greenhouse gas molecules (Figure 3) all have dipole moments (resulting from an asymmetric distribution of electrons) that effect the electric field of the radiation. For example, the water molecule, $H_2O$, has an electron-poor region that results in a partial positive charge and a partial negative charge as a result of an electron-rich region due to the oxygen atom – i.e. the oxygen atom is more electronegative than the two hydrogen atoms. Greenhouse gas emissions lead to warming of the atmosphere due to the so-called greenhouse effect. The greenhouse effect can be explained as follows: incoming visible solar radiation is not absorbed by the atmosphere – i.e. the atmosphere is said to be transparent to incoming visible solar radiation. Infrared radiation is emitted from the surface of the earth at a peak wavelength (from Wien's displacement law) of approximately 10 microns because it is substantially cooler than the sun. The greenhouse gas molecules (Figure 4) absorb this radiation and re-emit at longer wavelengths (downward to the earth's surface) in the infrared portion of the electromagnetic spectrum. In other words, the atmosphere is opaque to the longer wavelength radiation (although a small amount of the infrared radiation escapes to space), which results in warming of the planet's atmosphere.

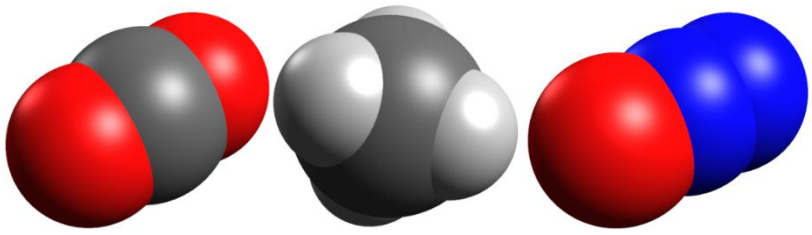

Figure 4. Greenhouse gas molecules used in EdGCM. From left to right: $CO_2$, $CH_4$, and $N_2O$. All three molecules have dipole moments, making them good absorbers of infrared radiation. The greenhouse molecules shown here have been rendered using Van der Waals Spheres, where blue represents nitrogen, red represents oxygen, grey represents carbon, and light grey represents hydrogen atoms.

The most important greenhouse gases in earth's atmosphere are carbon dioxide, methane, nitrous oxide and chlorofluorocarbons (CFCs). Even though water vapor ($H_2O$) produces the strongest greenhouse effect in earth's atmosphere of any individual gas (Held et al., 2000), the short cycling lifetime of water vapor (a few days) in the atmosphere means that it has a negligible contribution to the greenhouse effect in earth's atmosphere. The greenhouse gas with the strongest contribution to the warming of earth's atmosphere is carbon dioxide, followed by methane, and then nitrous oxide and chlorofluorocarbons (CFCs). It is important to note that the total Greenhouse Warming Potential (GWP) of a greenhouse gas depends on its abundance, the strength of its greenhouse effect, and its resident lifetime in the atmosphere. For example, carbon dioxide ($CO_2$) has a higher global warming effect than methane ($CH_4$), even though methane has a much higher GWP strength (21 to 25 over 100 years). This is due to a much lower abundance of methane in earth's atmosphere, relative to carbon dioxide. Furthermore, methane's shorter lifetime offsets its total contribution as a greenhouse gas. Both nitrous oxide and CFCs have very potent GWPs (298 to 310 and 3800 to 10900 over 100 years, respectively). However their total contribution to radiative forcing is very small as a result of the trace abundances of these gases in earth's atmosphere (concentrations of 1774 ppb for $CH_4$ and 319 ppb for $N_2O$, relative to $CO_2$ with an atmospheric concentration of about 380 ppm) (Ewings, 2007). The effect of phasing out CFCs resulted in their lower abundance over time. What makes carbon dioxide ($CO_2$) the most powerful greenhouse gas is its very high abundance relative to the other greenhouse gases in the atmosphere. However, future global warming could cause melting of the

arctic permafrost layers and the release of methane (from stored methane clathrate) into the atmosphere, increasing the positive feedback mechanism and further amplifying global warming (Shakhova et al., 2008; Hauglustaine et al., 1994; Biastock, A., et al. 2011; Archer, D. et al. 2009; Krey, V. et al. 2009). An illustration of the methane-clathrate feedback mechanism is shown in Figure 5.

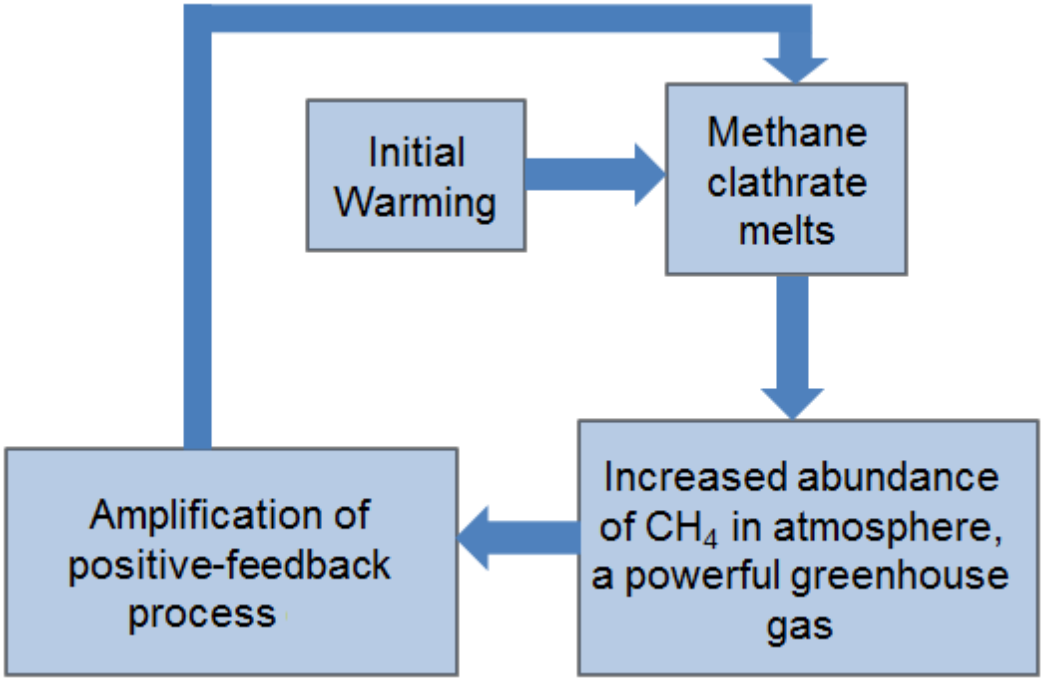


Figure 5. Positive feedback process due to melting methane clathrates in permafrost.

The amplification in global warming due to the greenhouse effect is shown in Figure 6.

A moderate greenhouse effect on an the earth is necessary to make the planet's surface habitable for human life. Without a greenhouse effect the planet's temperature would be too cold for comfortable conditions. We can illustrate the effect of not having a moderate greenhouse effect by using a simple energy balance requirement to obtain the equilibrium temperature at the planet's surface.

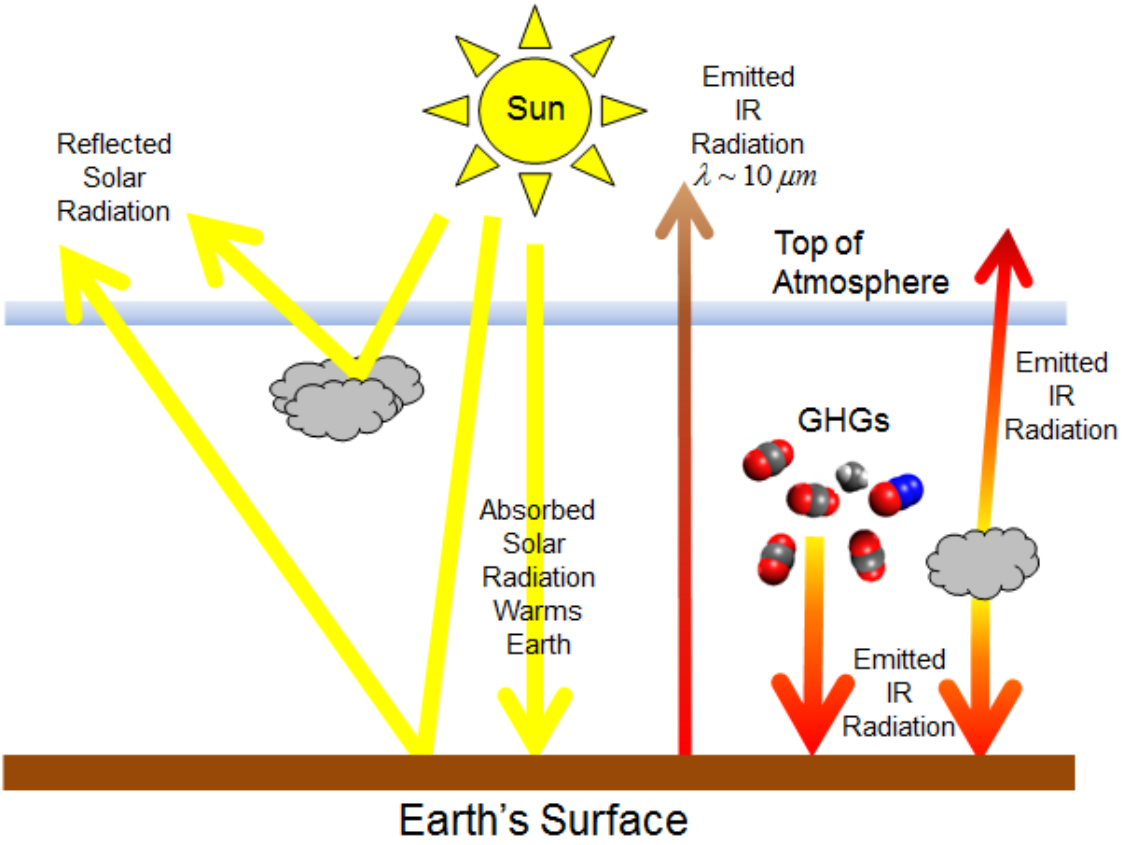


Figure 6. Illustration of the greenhouse effect. The atmosphere is transparent to incoming solar radiation. Some solar radiation is reflected back into space from the surface and clouds, and about one half of the solar radiation is absorbed by the surface of the earth and warms it. The earth's surface emits longer wavelength radiation back to space, with a peak emission wavelength of about 10 microns (in the infrared portion of the electromagnetic spectrum). The atmosphere is mostly opaque to infrared radiation. A small amount of IR radiation escapes to space, but most of the long-wavelength radiation is absorbed and re-emitted by greenhouse gas molecules (GHGs) and clouds. The net effect is the warming of the surface of the earth and the lower portion of the atmosphere.

The equilibrium temperature of a planet can be derived from the energy balance condition (energy received = energy emitted).

$$
\begin{aligned}
&E_{in} = E_{out} \\
&E_{in} = S_0 \pi R_{\oplus}^2 \left(1 - A\right) \\
&E_{out} = \sigma T^4 \left(4\pi R_{\oplus}^2\right) \\
&\Rightarrow T^4 = \frac{S_0 \left(1 - A\right)}{4\sigma}
\end{aligned} \quad (1)
$$

In these equations, $S_0$ is the power per unit area (or irradiance) generated by the Sun at the top of Earth's atmosphere, $R_{\oplus}$ is the radius of the Earth, $A$ is Earth's albedo, $T$ is the equilibrium temperature of Earth, and $\sigma$ is the Stefan-Boltzmann constant. The energy absorbed and emitted by the planet is denoted by $E_{in}$ and $E_{out}$, respectively. The solar irradiance at the mean distance of Earth from the Sun (1 AU) is calculated as

$$
S_0 = \frac{L_{\odot}}{\left(4\pi r^2\right)} \sim \frac{3.85 \times 10^{26} W}{4\pi \left(1.496 \times 10^{11} m\right)^2} \sim 1370 W / m^2 \quad (2)
$$

and assuming the Earth's average albedo is ~0.30 (Wielick, B. et al. 2005; Goode, P. R., et al. 2001), the equilibrium temperature is calculated as

$$
T = \left[\frac{S_0 \left(1 - A\right)}{4\sigma}\right]^{1/4} = \left[\frac{\left(1370 W / m^2\right)\left(1 - 0.3\right)}{4\left(5.67 \times 10^{-8} W / m^2 K^4\right)}\right]^{1/4} = 255 K \quad (3)
$$

The actual temperature at the Earth's surface is 288 K. The difference is due to a moderate greenhouse effect that provides an extra 33 K of atmospheric warming. For the planet Venus, the solar irradiance is approximately

$$
S_0 = \frac{L_{\odot}}{\left(4\pi r^2\right)} \sim \frac{3.85 \times 10^{26} W}{4\pi \left(1.496 \times 10^{11} m \times 0.72 AU\right)^2} \sim 2640 W / m^2 \quad (4)
$$

which yields an equilibrium temperature for Venus of approximately

$$T = \left[ \frac{\left(2640 W/m^2\right)\left(1-0.6\right)}{4\left(5.67\times10^{-8} W/m^2K^4\right)} \right]^{1/4} = 260\,K \quad (5)$$

260 K for an assumed albedo of 0.60 (due to cloud cover). The large difference between the calculated equilibrium temperature and the observed temperature of 740 K on Venus is evidence for a runaway greenhouse effect. One of the major objectives of long-term climate modeling is to determine why the climate of Venus is so different from Earth's, even though the two planets have similar physical characteristics (e.g. mass, radius, density) . Climate modeling experiments could provide valuable clues as to why Venus underwent a runaway greenhouse effect early in the planet's evolution, and whether Earth faces a similar future due to increased global warming (both natural and anthropogenic induced). The currently accepted scenario for the extreme divergence in climate between the Earth and Venus can be explained in terms of the distribution of carbon on the planets. Both planets have roughly the same abundance of carbon (Schuiling, R. D. et al. 2006). However, on Earth the carbon dioxide ($CO_2$) is mostly incorporated into organic sediments and carbonate rocks. In contrast, most of the carbon dioxide on Venus is tied up in the planet's atmosphere. This illustrates the important relationship between the role of life on the distribution of $CO_2$ and regulation of climate. Using the energy balance calculation described earlier in this section, if we assume the both Venus and Earth absorb all incident radiation from the Sun (albedo = 0), the equilibrium temperatures of the planets would be 328 K and 278 K, respectively (note: if the albedo is assumed to be nonzero for both planets, the actual temperature differences between the two planets would be lower due to higher reflectivity). The resulting difference between the two

equilibrium temperatures for Earth and Venus amounts to 50 K, while the difference in the observed temperatures for Earth and Venus is approximately 450 K. The Earth has only a moderate greenhouse effect, relative to the runaway greenhouse effect on Venus (Kasting, 1988; Rasoonl et al., 1970). For both planets, the temperature will increase due to the greenhouse effect and is limited by thermal equilibrium between the IR emission and incoming solar radiation. For an earth-like planet whose atmospheric temperature is below the saddle point (i.e., the critical threshold) for a negative feedback mechanism to be maintained, an earth-like environment will exist. However, if the planet's atmosphere reaches the critical threshold, positive-feedback mechanisms will result in a runaway greenhouse effect pushing the planet's environment towards that encountered on Venus (Figure 7).

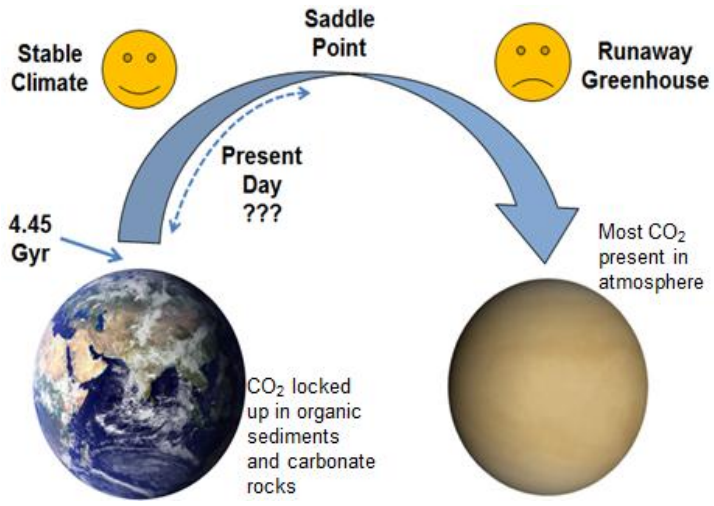


Figure 7. Critical threshold to initiate a runaway greenhouse effect. As the Sun's luminosity increases over time the earth's climate has been moving towards the critical threshold for a runaway greenhouse effect.

A current topic of research centers on whether increasing $CO_2$ emission from natural and man-made sources could accelerate earth's climate towards the critical saddle point for a

runaway greenhouse effect to occur. Another critical question in climate science is whether or not an increase of $CH_4$ emission from methane clathrates, stored in permafrost in the arctic region, could push Earth over the critical saddle point within the next few hundred years. Since we do not currently know how close earth's climate may be to the critical "saddle point", a sharp increase in methane (a far more powerful greenhouse gas in terms of GWP than $CO_2$) emission into the atmosphere in combination with increasing $CO_2$ emissions, may accelerate earth's climate towards the critical saddle point.

To explore the runaway greenhouse effect, this work will carry out a hypothetical experiment in which the earth is moved to the location of Venus, where the incident solar irradiation is about twice that of earth. This initial change will lead to climate warming, and it is suspected that this would result in a positive-feedback mechanism involving water vapor. An increase in the amount of water vapor present in the planet's atmosphere as a result of climate warming should lead to increased greenhouse trapping of infrared radiation. This should lead to further amplification of climate warming by means of a positive feedback as illustrated in Figure 8.

In the above scenario, a runaway greenhouse effect is suspected to occur as a result of breakdown of the negative feedback mechanism that stabilizes the planet's climate. As long as the outgoing infrared flux is sufficient, the surface temperature remains stable. When the atmospheric temperature increases (in this case, as a result of locating the earth to the orbit of Venus), an increase in the concentration of water vapor in the atmosphere occurs. The increase in water vapor content in the atmosphere leads to the breaking of the negative feedback process that is responsible for stabilizing the planet's climate. The objective of the earth-to-Venus orbit experiment is to determine

whether the GISS GCM-II can estimate the temperature at which the negative feedback mechanism (stabilizing) is broken, resulting in a runaway greenhouse effect. The scenario described above assumes that there are no clouds present in the planet's atmosphere, and neglects effects due to water vapor condensation and cloud formation.

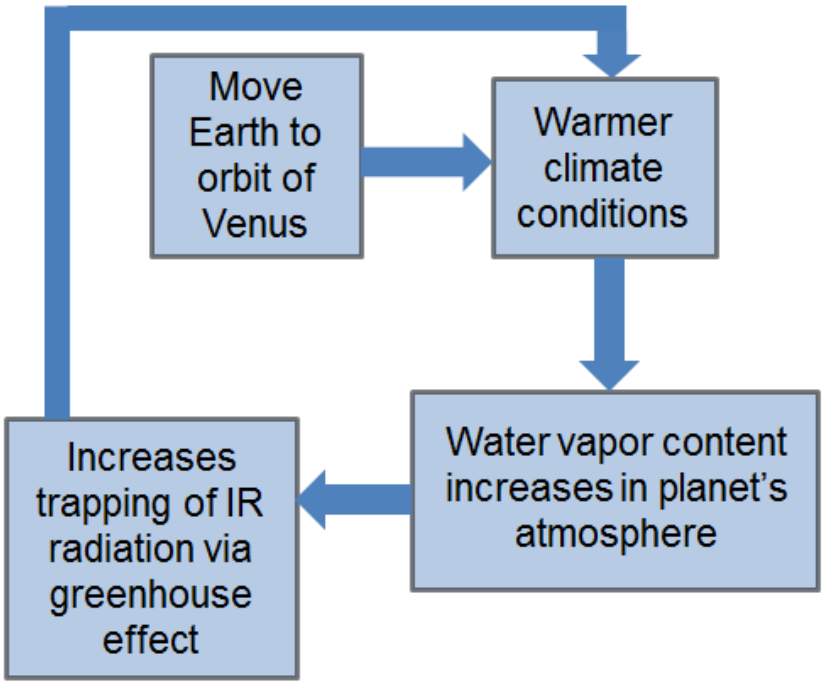


Figure 8. Positive feedback mechanism involving water vapor. Positive-feedback process due to water vapor in the atmosphere for the hypothetical experiment described above. Moving the Earth to the location of Venus results in an initial change in climate to warmer conditions. This increases the amount of water vapor in the planet's atmosphere, leading to amplification of the greenhouse effect. The stronger greenhouse effect leads to higher temperatures, resulting in further climate warming. During cooling, this feedback mechanism works in reverse.

However, the experiment described here will use the GISS GCM-II, which includes the effects of water vapor condensation and cloud formation. This can lead to more complicated effects, such as changes in the planet's albedo, due to cloud cover.

Studying climates on planets with similar physical properties as earth is critical to understanding the future climate on Earth. Determining whether a runaway greenhouse

effect occurs over astronomical time scales as governed by the slow increase in solar luminosity over the next few billion years, or whether the effect can be accelerated by steep increases in greenhouse gas emissions (from natural and man-made) over several centuries is a question that remains to be answered.

The planet Venus represents a terrestrial planet located at the inner boundary of the so-called habitable zone, the zone around a host star where liquid water can exist at the surface of a planet. This corresponds to a temperature range of approximately 273 K to 373 K. However, heliocentric distance is not the sole parameter for determining the habitable zone of an earth-like planet. The habitable zone also depends on the type of atmosphere the planet has. To investigate the inner and outer boundaries of the habitable zone for a planet with an initial atmosphere similar to earth, the GCM-II global climate model will also be used to carry out another hypothetical simulation that involves placing the Earth at the current orbit of Mars. This has the effect of essentially reducing the amount of solar insolation by a factor of one-half that of the present-day earth,

$$S_0 = \frac{L_\odot}{\left(4\pi r^2\right)} \sim \frac{3.85\times10^{26}\,W}{4\pi\left(1.496\times10^{11}\,m\times1.52\,AU\right)^2} \sim 593 W/m^2 \tag{6}$$

for an assumed heliocentric distance of 1.52 AU.

Unlike Mars, which has a tenuous atmosphere of carbon dioxide, it is of interest to study the climate of an earth-like planet located at the heliocentric distance of Mars. Climate models will be simulated over a few hundred years to determine the effects of a reduced solar irradiance for a planet with Earth's present atmosphere. If time permits, simulations will be carried out using an increase of greenhouse gases to determine whether an earth-like planet can sustain a habitable climate at the orbit of Mars. Results

of the simulations may be of interest to scientists conducting research on the terraforming of Mars over short timescales using strong greenhouse gases, such as CFCs (chlorofluorocarbons).

## The Effect of Vegetation on Planetary Albedo

The type and total area of vegetation in a local region can affect the albedo of that region (O'Halloran et al., 2011). For example, in the arctic there are two different types of vegetation, spruce forest and circumarctic tundra. The change in albedo is the result of the interaction of local snow fall and the type of vegetation. Snow fall over regions that are covered with tundra produce high albedo because the snow covers most of the tundra, while snow that falls over a region of spruce forest will leave most of the darker forest exposed. In this case, the albedo will be significantly lower than that over the tundra region since the exposed trees absorb most of the solar radiation. As the climate cools, more of the tundra vegetation replaces the forest. As a result there is an increase in the surface albedo leading to more solar radiation being reflected. This, in turn, leads to further climate cooling – i.e. a positive feedback mechanism known as the vegetation-albedo feedback is established (Figure 9).

## The Effect of Orbital Parameters on Planetary Climate

Both obliquity (axial tilt) and orbital eccentricity have an effect on the climate of an earth-like planet (Kasting, 1997). The obliquity determines how much insolation a planet receives from its host star as a function of its orbital cycle (Lissauer et al., 2011). If a planet's obliquity were zero, there would be no (or little) change in the amount of solar

energy from one orbit cycle to another. As the inclination increases, for example, from 24.5 degrees (for present-day Earth) to 45 degrees, the amount of solar energy

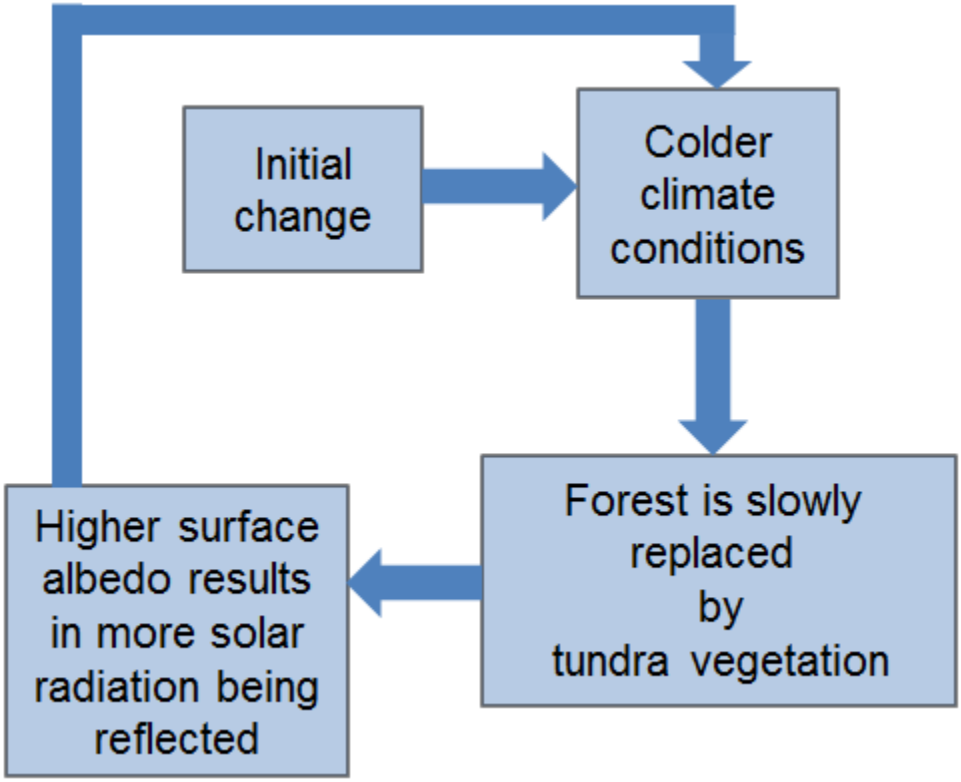


Figure 9. The positive vegetation-albedo feedback process. Illustration of the vegetation-albedo positive-feedback process. As more tundra vegetation replaces forest due to an initial cooler climate, the surface albedo increases. This results in more solar radiation being reflected, and a further decrease in temperature. This positive-feedback mechanism can work in reverse during periods of warmer climate.

would increase due to the extra amount of daylight hours in Earth's northern hemisphere during the summer season. The opposite would be true for Earth's southern hemisphere, where the number of nighttime hours would increase. A reduction in the number of daylight hours during the winter season reduces the overall amount of solar irradiance absorbed by the planet. This leads to colder climate, especially at higher latitudes. In other words, higher axial tilts have the effect of amplifying seasonal climate on earth-like planets. This research will produce hypothetical models of earth's climate using different

obliquities to study the effect of seasonal temperatures. It is important to note that the obliquity variation effects climate at higher latitudes more so than at equatorial regions. The GISS GCM-II climate model allows one to place variations on the planet's obliquity and eccentricity to determine the resulting climate.

By studying how the obliquity of an earth-like planet effects the planet's global climate, limits may be placed on habitable conditions on hypothetical earth-like worlds that are currently being discovered with space-based observatories such as NASA's Kepler mission. Placing limits on the habitability conditions on earth-like planets as a function of obliquity is important because it has been suggested that earth-like planets need a large moon to stabilize their obliquity (ref needed). For example, Earth's own moon stabilizes the planet's obliquity, minimizing the variation in axial tilt (Lissauer et al,. 2011; Laskar et al., 1993). This has the effect of minimizing climatic variations that could lead to unsuitable environments for various forms of life to survive on the planet. Earth's obliquity varies from 21.5 to plus or minus a few degrees over a timescale of approximately 41000 years (Williams, D. M., et al. 2003; Laskar, J. et al. 1993). It is thought that the variation in axial tilt may be responsible for ice ages (need ref). Because Mars does not have a relatively large moon like Earth, there is no stabilizing effect of its obliquity. The larger variation in obliquity from about 14.9 to 35.5 degrees (Ward, 1973) over a longer timescale of 120000 years has long-term implications for Mars's climate. At the high end of this obliquity range (Figure 10), the planet should undergo warm summers and higher humidity as a result of a higher sun angle. In contrast, for the low obliquity limit, the planet should have cooler summers and lower humidity due to low sun angles (Figure 10). This work will use the GISS GCM-II climate model to produce

global climate models of an earth-like planet over this obliquity range at the distance of Mars. It is of interest to determine the effect on climate over this obliquity range at the distance of Mars for a planet with abundant oceans and vegetation, in contrast to present-day Mars which is devoid of oceans and vegetation. Results of the simulations will provide information about the habitability of earth-like planets at the outer edge of the Sun's habitable zone.

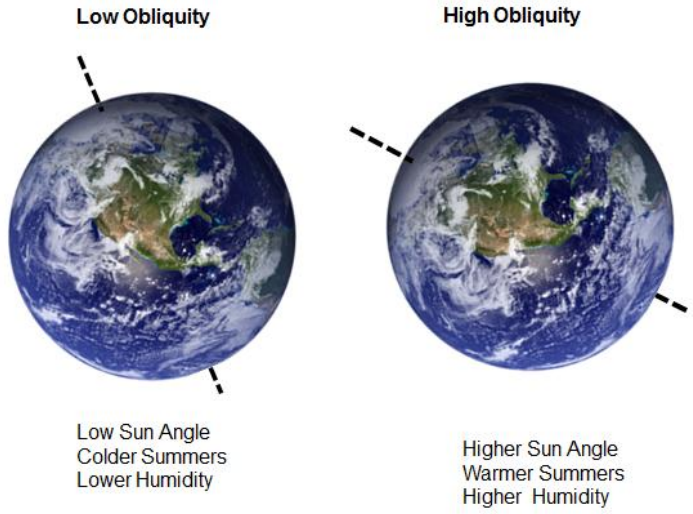


Figure 10. High and low obliquity for an Earth-like planet. Planets with high obliquities will have seasonal climates with more extreme conditions. In the case of lower axial tilt, a planet will tend to have colder summers with lower humidity as a result of the lower sun angle and vice versa for planets with high obliquities.

The eccentricity of a planet (deviation from a perfectly circular orbit) also has an effect on its climate, though not as strong of an effect as that due to the planet's axial tilt (obliquity). As the eccentricity of an earth-like planet approaches zero (for a circular orbit) the more uniform the planet's climate variation will be. In contrast to a planet's axial tilt affecting the polar climate, the eccentricity of a planet will change the climate over all latitudes of the planet (Williams, 2002). For earth-like planets with high eccentricities (>0.2), there will be two extreme cases where the planet is far away from its

host star (Figure 11), and two opposite cases where the planet is much closer to its star (Figure 11). This can be seen by analyzing the equation for an ellipse in terms of the semi-major axis, *a* and semi-minor axis, *b*

$$e = \frac{\sqrt{a^2 - b^2}}{a} \quad (7)$$

where *e* is the orbital eccentricity of the planet. It is assumed that the mean irradiation over one orbital cycle on the planet will scale as $(1\text{-}e^2)^{-1/2}$ for a constant semi-major axis, where *e* is the eccentricity of the planet's orbit.

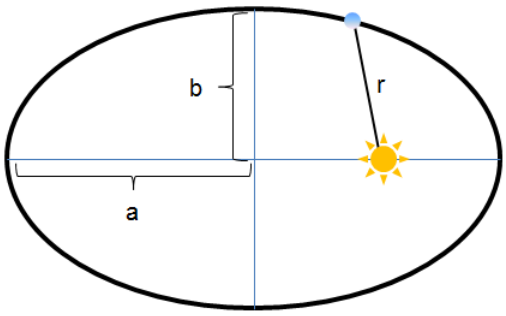


Figure 11. Diagram of an elliptical orbit. The difference in solar irradiance due to the high eccentricity of the planet's orbit over a complete orbital cycle, introduces a climatic change over the cycle. The planet is represented by the filled blue circle and the host star lies at one of the foci of the ellipse. The parameter *r* represents the planet's current radial distance from the star as it moves in its orbit.

The orbital eccentricity and obliquity of a planet can combine to produce a complex change in the climatic pattern of an earth-like planet. The obliquity and orbital eccentricity of the planet can be varied in the GISS GCM-II to study the effects of these parameters on a planet's climate. Earth-like planets on high orbital eccentricities may have marginally habitable conditions. The GISS GCM-II can be used to sample a wider range of habitability conditions that may arise on earth-like planets discovered by current or future observatories. An important question to explore is how fast the climate on an

earth-like planet would respond as a result of the planet's high eccentricity. Global climate models produced with the GISS GCM-II in this work will be limited to several hundred years due to computational time constraints.

## Theory Behind Global Climate Models

Global climate models use numerical methods to solve a set of equations describing the dynamics, thermodynamics and radiative transfer of the climate system. Three dimensional models, such as the GISS GCM-II used in EdGCM (Chandler et al., 2005), use atmospheric chemistry, composition, terrain and ocean models, in addition to the dynamical equations to produce models of Earth's climate system. Complex climate modeling involves dividing the atmosphere into individual 3-D boxes, with each individual box having its own localized climate. The atmosphere in each of the grid cells interacts with the air in other cells, both horizontally and vertically (Figure 12). The same applies for water in ocean grid boxes. Each individual ocean box interacts vertically and horizontally with other ocean boxes within the finite grid. Currents, temperature, and salinity is modeled within each of the ocean boxes, and their interaction is also modeled. The influence of vegetation and terrain is also included in these complex climate models.

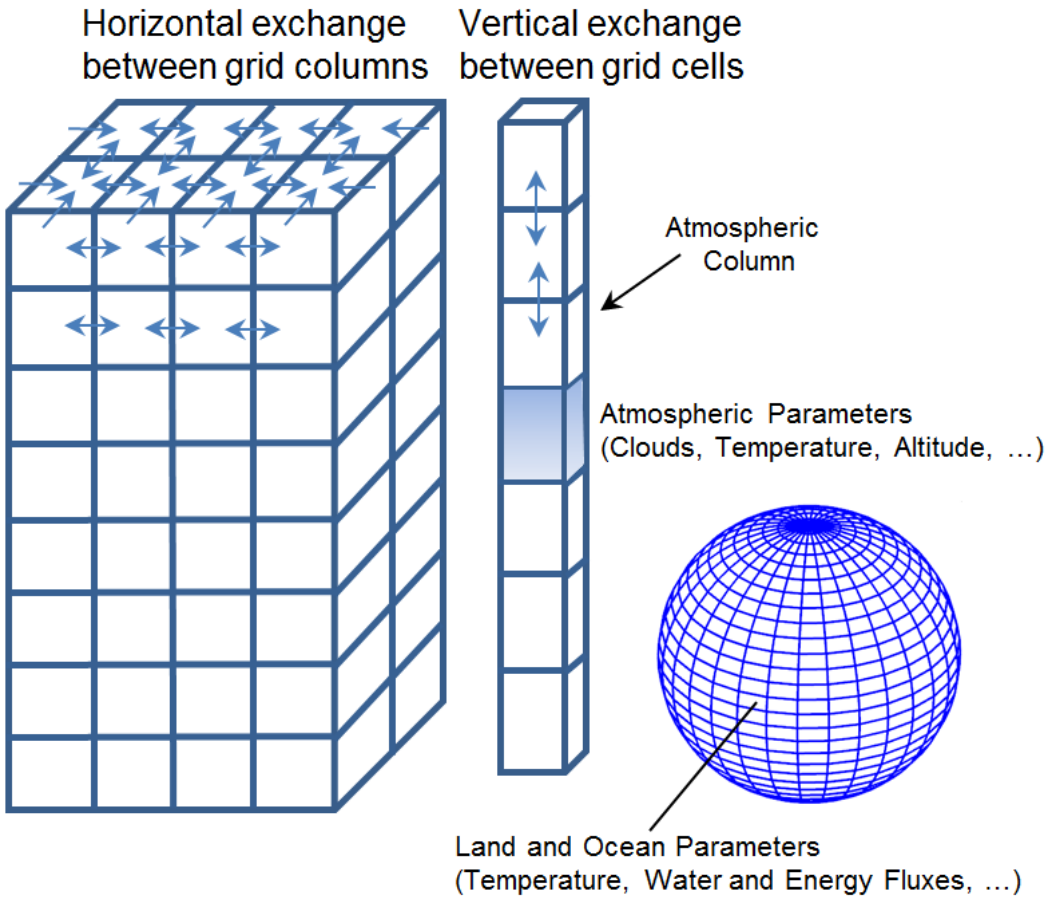


Figure 12. 3-D climate model concept over a finite grid. Climate model parameters (temperature, air currents, clouds, humidity, altitude, …) are computed for each local grid cell, and are vertically and horizontally exchanged between grid cells as governed by the set of climate model equations. The same principle applies at the surface of the earth, where each grid cell has its own local climatic conditions. Interchange between local grid cells is again governed by the climate model equations.

Global climate models essentially model the planet's energy balance among four basic components comprising the model (Hansen et al., 1983; Hansen et al., 1988; Henderson-Sellers et al., 1988; Ghil, 1984). The atmospheric component describes the transport of heat and water across the planet, and is dependent on aerosols and clouds in the atmosphere. The absorption, reflection and scattering of solar radiation by clouds, aerosols, greenhouse gases, determine the energy balance in earth's atmosphere. The atmospheric component evaluates the energy balance, including the re-emission of long-

wave radiation from greenhouse gases, clouds, and the planet's surface using radiative transfer theory. The atmospheric component of the model must taken into account the effects of finite cloud thickness, the distribution of clouds in 3-D (both horizontally and vertically). The details of the earth's topography (land versus oceans), the distribution of snow and ice, as well as vegetation and vegetation type are handled by the land component. Soil, bodies of water, snow/ice, vegetation and the carbon reservoir is modeled by the land component of the model. The ocean component of the model simulates the mixing and movement of ocean currents, in addition to biogeochemistry. The ocean component is critical to the overall climate model since most of the heat and carbon in the climate system is stored in the earth's oceans. The absorption of solar radiation is regulated by the sea ice component. In addition, the sea ice component of the climate model governs the exchange of heat between the atmosphere and seas. Water exchange between the atmosphere and seas is also included within the sea ice component of the climate model. The interaction between model components and their variables including fluxes of momentum, water and heat are modeled on a 3-D grid, with individual cells representing different geographical locations on the planet. The dynamical equations model the coupling between of the individual components with the global climate model. The dynamical equations govern the overall circulation of the atmosphere and eddy circulation patterns on a smaller scale. The details of the equations used in global climate models will be covered later in this chapter.

The degree of detail (or resolution) of the global climate model depends on the size of the individual grids within the model. The grid size is a function of the amount of computing power available to solve the dynamical equations. Less computing power is

required for a large grid spacing, but at the cost of less detail in the results of the climate model. A common rule of thumb used is for every doubling of the grid resolution, ten times more computational power is required.

**Global Climate Model Equations**

The physical equations that govern the behavior global climate models are given by (Henderson-Sellers, 1985; Hansen, *et al*., 1983) ,

$$
\begin{aligned}
&1)\ \frac{\partial \vec{V}}{\partial t} = -\left(\vec{V}\cdot\nabla\right)\vec{V} - \frac{1}{\rho}\nabla p - \vec{g} - 2\vec{\Omega}\times\vec{V} + \nabla\cdot\left(k_m\nabla\vec{V}\right) - \vec{F}_d \\
&2)\ \rho c_p \frac{\partial T}{\partial t} = -\rho c_p\left(\vec{V}\cdot\nabla\right)T - \nabla\cdot\vec{R} + \nabla\cdot\left(k_T\nabla T\right) + C + S \\
&3)\ \frac{\partial \rho}{\partial t} = -\left(\vec{V}\cdot\nabla\right)\rho - \rho\left(\nabla\cdot\vec{V}\right) \\
&4)\ \frac{\partial q}{\partial t} = -\left(\vec{V}\cdot\nabla\right)q + \nabla\cdot\left(k_q\nabla q\right) + S_q + E \\
&5)\ p = \rho R_d T
\end{aligned}
\qquad (8)
$$

where pressure, temperature, humidity and winds are computed at every local grid cell in the model. In the above equations, $\vec{V}$ is velocity, $T$ is temperature, $p$ is pressure, $\rho$ is density, $q$ is specific humidity, $g$ is gravitational acceleration, $\Omega$ is angular rotation velocity of earth, $\vec{F}_d$ is drag force of earth, $\vec{R}$ is radiation vector, $C$ is conductive heating, $c_p$ is heat capacity at constant pressure, $E$ is evaporation, $S$ is latent heating, $S_q$ is phase-change source, $k$ are diffusion coefficients, and $R_d$ is the dry air gas constant. The equations of conservation of momentum (eq. 8, number 1), conservation of energy (eq. 8, number 2) and conservation of mass (eq. 8, number 3) govern the global climate as a result of radiative heating at the equatorial regions, and radiative cooling near the planet's polar regions. The equations describe the dynamics of the earth's

atmosphere on large scales. Analytical solutions are not possible due to the inherent nonlinearity of the equations, so numerical methods are used to solve the equations over a finite 3-D grid. The equation of conservation of $H_2O$ (eq. 8, number 4) describes the effects due to heating from condensation in the atmosphere and cooling due to evaporation of water vapor from the surface of land and oceans. The equation of state (eq. 8, number 5) is based on the ideal gas law, and is used in climate models to describe how temperature, pressure and density change with location in the atmosphere. The equation of state is a function that relates temperature, pressure and density and is required to determine the thermodynamic state of a fluid medium (earth's atmosphere). Individual atmospheric gases and/or mixtures of atmospheric gases obey the ideal gas equation.

The heat that is exchanged in climate models is defined as internal energy associated with the molecular motion of air and water molecules and atoms. Therefore, the speed of molecular and atomic motions are directly associated with the amount of heat. Numerical climate codes obey the first law of thermodynamics, which demands energy conservation when heat energy is transformed to and from other forms of energy. In other words, this means that when there is a change in the internal energy of a system, it represents the amount of heat that is gained by the system minus the amount of work performed by the system. In mathematical form, this can be expressed as

$$dU = Q - W \quad (9)$$

where $dU$ represents the change in internal energy, $Q$ the heat added to the system, and $W$ the work done by the system. For example, a gas will undergo both an expansion (the work) at the same time its temperature increases (i.e. an increase in its internal energy)

when the gas gains heat energy. There is a relationship between the temperature, heat, and internal kinetic energy of molecules in air and water, expressed mathematically as

$$Q = c_M m \Delta T \quad (10)$$

where $c_M$ is the specific heat (the amount of heat required per unit mass of material needed to increase the temperature by 1℃), $m$ is the mass, $Q$ the heat added to the system, and $\Delta T$ is the change in temperature. There are several ways the air temperature changes in climate models. Heat may be transferred by the conduction of air molecules or water molecules in oceans. However, over large spatial scales, conduction is not very efficient at transporting heat. Convective transport can occur, mainly in the troposphere, and causes vertical mixing. It involves the transport of heat mainly by the mass motion of a fluid medium. In other words, water or air that is warm will typically diffuse away from the source of the heat, transporting energy. Convection can occur within the oceans resulting in vertical transport. Near the Earth's tropical regions, convection is an efficient mechanism for transporting heat energy. In contrast, convection is inefficient at the planet's polar regions. Air is horizontally transported via the process of advection. When cold air is replaced with warmer air, it is known as warm air advection, and when warm air is replaced with colder air, it is called cold air advection. Advection is similar to convection, in that both processes are efficient at transporting heat from one region of the planet to another. Radiative processes involve the transfer of heat energy via the emission of electromagnetic waves. Radiative transport of heat from the Sun to Earth is the primary driving force by Earth's weather and climate. The Earth's surface cools via radiative cooling. Latent heat involves a phase change of water with the release or absorption of heat (per unit mass) energy. Latent heat is an efficient mechanism for the

global transport of energy. It plays a key role as an important source of energy for changing the climate and weather patterns on Earth. In numerical climate models, when ice melts to a liquid or sublimes to a vapor (a phase change), the surrounding environment loses heat energy. When vapor undergoes a phase change to a liquid via condensation, or when ice freezes (a phase change), the surrounding environment gains heat energy. Heat energy is also released to the surrounding environment as a result of deposition, a phase change from a vapor to ice. When a parcel of air undergoes a change in pressure, temperature, or volume without the loss or gain of heat energy, the process is said to be adiabatic. Adiabatic processes often occur when air rises or descends, and plays a key role in the vertical motion of air within the troposphere. The role of the oceans in climate models is vital in maintaining the Earth's (or other Earth-like planets) habitability. The large amount of evaporation that occurs over the oceans helps maintain habitable temperatures as the planet's surface loses heat to the atmosphere. Approximately half of the solar insolation that reaches the planet's surface is lost through the process of ocean evaporation.

The non-linear partial differential equations describe the resulting change in temperature patterns, the difference in mass flow, and general circulation patterns that tend to equalize the differences. The general flow is modified by the rotation of the earth as noted by the presence of the Coriolis term $\left(2\vec{\Omega}\times\vec{V}\right)$ in the momentum equation (eq. 8, number 1). Other effects including latent heat releases and topographic features also modify the general flow. Most of the inertia (mass) lies in the earth's oceans, which cover approximately 70% of the planet's surface. Ocean circulation is forced by wind stresses, contrasts in ocean salinity and temperature, and changes in ocean basin topography. A

strong coupling exists between the ocean and atmosphere, and plays a critical role in climate modeling.

In contrast to the earth's oceans, the land has relatively little reaction mass (i.e. small inertia), even though it occupies only about 30% of the planet's surface. There is coupling between the land and atmosphere as determined by the albedo and surface terrain (e.g. vegetation vs. tundra vs. desert regions), water cycling (e.g. evaporation), and cryospheric components (e.g. amount of snow and ice coverage).

The fundamental climate model equations (eqs. 8) treat the earth's oceans and atmosphere as a fluid medium, and they describe the physical laws that govern the bulk motion of these fluids. The equation of momentum conservation (eq. 8, number 1) is based on Newton's Second Law and the Navier-Stokes equations. The equation of momentum conservation involves the sum of the pressure gradient force, the Coriolis effect, effective gravity and friction (Figure 13). It characterizes the hydrodynamical motion of a fluid medium (air) over the earth's surface. Although the horizontal component of the pressure gradient is very small relative to the vertical component, it plays a critical role in climate because of its involvement in characterizing air circulation over localized regions of the planet. The pressure gradient term in the momentum equation describes the way in which the gradient pressure force acts on air – i.e. the production of wind. The viscous frictional force acts in a direction opposite to the wind flow, and the gravitational force acts in a downward direction towards the surface of the planet.

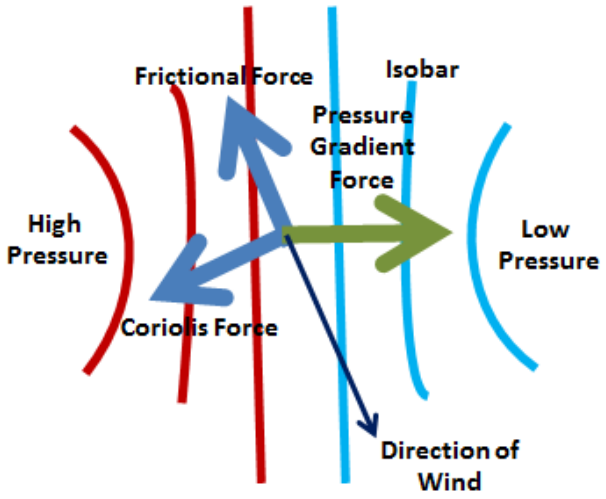


Figure 13. Factors involved in the equation of conservation of momentum. The wind essentially flows from a region of high pressure to low pressure, and the Coriolis effect acts perpendicular to the frictional force. The pressure gradient $(\nabla p)$ describes the direction of the most rapid change in pressure for a given localized region. It is important to note that the pressure gradient force points from regions of high pressure to those of low pressure, but the pressure gradient has an orientation that is opposite to the pressure gradient force. An isobar is a line of constant pressure, and is represented by red and cyan lines in this diagram.

Equation 3 is known as the continuity equation, which describes the mass motion of a fluid (air). For example, in Earth's northern hemisphere the continuity equations plays a role in governing how convergence occurs in the region of low pressure, and how divergence occurs near a high pressure region. Both convergence and divergence occur as a result of frictional forces that induce ascending or descending air flow, respectively. Mathematically, the diverging air flow around high pressure regions implies that $\vec{V} \cdot \nabla > 0$, which results in $\partial\omega / \partial p < 0$ - i.e. a vertical compression occurs - where $\omega = dp / dt$. Convergence at the surface around a low pressure region implies that $\vec{V} \cdot \nabla < 0$. This results in $\partial\omega / \partial p > 0$ - i.e. there is a vertical stretching that occurs. The velocity of vertical air is computed by integrating the continuity equation (mass

conservation) from a given reference pressure to another pressure level within earth's atmosphere.

Changes in geopotential height are caused by temperature changes, which are governed by the first law of thermodynamics. Equation 2 is based on the thermodynamic energy equation, which describes how the expansion and contraction of air results in an increase or decrease in temperature, respectively. The energy equation describes how convection and turbulence within the atmosphere affects the exchange of mass with the environment. A simple scenario that illustrates how the energy equation governs climate can be described as follows. Consider a given amount of heat energy input into the climate system. This leads to a change in the air temperature as governed by the first law of thermodynamics. A hydrostatic balance is established, resulting in a change of air pressure. This leads to air motion according to the principle of geostrophic balance. The resulting air motion then leads to the establishment of a thermal wind balance, and the cycle repeats. This process is governed by the first law of thermodynamics, which states that the total energy must be conserved when heat (energy) is converted into other forms of energy. Mathematically, this is equivalent to the change in internal energy as a result of the addition of heat added to a closed system minus the work done by that system, $\Delta U = Q - W$, where $Q$ is the heat added to the system, $W$ the work done by the system, and $\Delta U$ the change in internal temperature, which is related to the temperature. Thus, when heat is added to gases in earth's atmosphere, there will be expansion of the gas (or gases) and a resulting increase in the temperature of the gases – i.e. an increase in internal energy. The temperature of an atmosphere can be changed in two ways. Non-adiabatic (by adding/removing heat to/from an air parcel. Adiabatic processes involve changing the

air temperature without the addition or removal of heat to or from an air parcel. For example, expanding air will cause a temperature rise, and compressed air will cool.

The heat transfer by mass motion of air or water (oceans) is known as convection. When the heated air or water moves away from the heat source, it carries energy with it. Convective heat transfer is efficient in the atmosphere over the tropical regions of the earth, but is not very efficient in the polar regions. Conduction (heat transfer by molecular collisions) is not very efficient in earth's atmosphere since it is considered to be a poor conductor and has a low thermal conductivity. On large spatial scales within earth's atmosphere, heat transfer by conduction can be neglected in global climate models. When heat is horizontally transported within earth's atmosphere, it is known as advection. As with convection, the process of advection depends on mass motion of air to transport heat (energy) from one region to another. Advection within the atmosphere typical occurs when cold air replaces warm air or warm air replaces cold air. Advection can be thought of as one form of convection in climate models.

Energy is redistributed across the Earth's surface by three different processes. The first process involves the transfer of heat energy from the surface of the planet to its atmospheric layers by convection and conduction. This process is known as sensible heat. Energy then flows from the topical regions of the planet to the polar regions via advection. This sets up the atmospheric circulation pattern on the planet. The polar regions of the planets receive warm air from the tropic regions, while the equator receives cooler air from the polar regions as a result of the circulation pattern. A phase transition from frozen and liquid water to its vapor phase, results in the global redistribution of the vapor via the latent heat flux. The vertical and horizontal circulation of water vapor in the

atmosphere to colder regions results in its condensation to a liquid phase through rain and snow. The condensation releases heat energy that is contained within the water vapor. The large area of oceans in the tropical regions of the planet absorb copious amounts of radiation energy from the Sun. The heat energy increases the temperature of the ocean water, and through the process of convection and conduction, transfers it down into lower layers of the ocean. Ocean currents then transfer the heat to the polar regions from the equatorial regions of the planet. The distribution of heat energy at the planet's surface is given by the sum of the sensible heat, the surface heat flux into the oceans of land, and the latent heat. The amount of net radiation being distributed to each of these three components is governed by the specific heat of the surface terrain (ocean or land), the conductive and convective properties of the surface terrain (e.g. oceans, forests, deserts, …), diffusion properties of the atmospheric layers overlying the surface, and the distribution of water and ice/snow on the surface of the planet.

Radiation plays a major role in earth's climate by transferring heat (energy) via emission of electromagnetic waves. When greenhouse gases in earth's atmosphere absorb infrared radiation emitted from earth's surface, heating results. When earth emits radiation back to space it results in cooling. The radiation emitted by the sun provides the main source of energy that drives weather and climate on earth. The equation of radiative transfer used in climate models describes energy conservation – i.e. the balance between energy loss due to absorption and scattering of radiation and gain of energy due to emission within the atmosphere.

In summary, most global climate models involve the solution of a set of differential equations subject to initial conditions and boundary conditions of the model.

The climatic system can be described by a set of state variables that include those for the atmosphere (temperature, pressure, wind, humidity) and those for the oceans (sea temperature, salinity, velocity, …). The 3-D model is characterized by a set of dynamical equations including the equation for energy transport (heat transport), the equation of continuity or mass (water, tracers), the momentum equation (turbulence, wind stress), expressed in terms of the state variables. The numerical solution of the set of climate equations is subject to boundary and initial conditions, which specify the solar forcing, greenhouse gases, and aerosol/volcanic emissions, and other conditions. Within the planet's atmosphere, the interaction between the dynamics (the horizontal transport of momentum, heat, and water) and physics (the parameterizations of sub grid-scale processes, such as radiation, convection, cloud formation, precipitation, and other processes) control the outcome of the climate model. Large-scale (typically >1000 km) processes are well-resolved in global climate models, but small-scale (sub grid-scale) processes that redistribute quantities vertically are uncertain in climate models, and are therefore parameterized. Small scale process include phenomena such as thunderstorms, cumulus convection, boundary layers and micro turbulence on spatial scales ranging from about one cm to a several kilometers and temporal scales ranging from seconds to days. Large-scale phenomena include planetary waves down to cloud clusters. These resolved phenomena have spatial scales ranging from hundreds of kilometers to over 1000 kilometers, and temporal scales ranging from hours to years.

## Boundary Conditions, Initial Conditions and Climate Forcing

Boundary conditions are a set of fixed conditions that do not vary as a result of global climate model calculations. The topography and distribution in land mass and oceans are the most important boundary conditions in a GCM. The distribution of continental ice sheets, vegetation classes, and the spatial extent of fresh bodies of water also represent important boundary conditions to the global climate model.

Another form of auxiliary data needed for climate models is a set of initial conditions – i.e. the initial state of the climate model. Initial conditions include (but not limited to) atmospheric parameters such as the initial temperature, pressure and humidity for every location in the planet's atmosphere. The initial conditions are typically based on observed data, but they can also be theoretical to study the effects of climate on various changes in atmospheric parameters and orbital parameters of the planet. Small changes in the initial conditions can result in a broad distribution of resulting climate models, and this distribution can be used to place a rough estimation on the model's accuracy.

In addition to initial conditions, Global Climate Models (GCMs) apply a set of climate forcing that are a critical component of the model (Hansen et al., 1984). Greenhouse gases are one of the best known examples of a climate forcing, and are a major focus of current research in future climate prediction. A major question in climate modeling is whether or not greenhouse gas emissions as a result of anthropogenic factors is the cause of the increase in global temperatures during the late 20$^{th}$ century and early 21$^{st}$ century. In contrast to boundary conditions specified in the climate model, climate forcing need not remain fixed, but may vary as a function of time and space. Global climate models usually specify greenhouse gas trends with time as simple mathematical

functions, such as a doubling of carbon dioxide emission with time, or an exponential increase in methane gas as a result of release from methane clathrates trapped under the Antarctic ice (Table 1). Other examples of climate forcing involve the increase in trace greenhouse gases, such as chlorofluorocarbons and nitrogen oxides. Climate forcing can also include dust and sulfuric acid droplets ejected into the earth's atmosphere as a result of volcanic activity. Volcanic activity can have short- and long-term impacts on earth's global climate. Short- and long-term variation of solar irradiance that are associated with sunspot cycles are another class of climate forcing that are accounted for in global climate models. Anthropogenic forcing, such as aerosol droplets produced by industrial

**Table 1. Historical Trend of Greenhouse Gas Emissions.**

| Greenhouse Gas | 1850 | 1958 | 2008 | 2100 |
|---|---|---|---|---|
| Water Vapor ($H_2O$) | 1%[1] | 1%[1] | 1%[1] | 1%[1] |
| Carbon Dioxide ($CO_2$) | 285.2 ppmv | 314.9 ppmv | 385.6 ppmv | 970.0 ppmv[2] |
| Methane ($CH_4$) | 0.791 ppmv | 1.224 ppmv | 1.766 ppmv | 3.413 ppmv[2] |
| Nitrous Oxide ($N_2O$) | 0.2754 ppmv | 0.2908 ppmv | 0.3219 ppmv | 0.4600 ppmv[2] |
| CFC-11 | 0.000 ppbv | 0.0076 ppbv | 0.245 ppbv | 0.045 ppbv[3] |
| CFC-12 | 0.000 ppbv | 0.0296 ppbv | 0.528 ppbv | 0.222 ppbv[3] |
| Ozone ($O_3$) | 10-15 ppbv[1] | 70 ppbv[1] | 70 ppbv[1] | 10-15 ppbv[1] |

[1] Concentrations are highly variable on a seasonal and spatial basis; ozone concentrations given for troposphere only.
[2] As per IPCC scenario A1F1 (IPCC 2000).
[3] The CFC gases are among those phased out of production under the terms of the Montreal Protocol (1990), so their concentrations are projected to decrease over the course of the 21st century (IPCC 2000).
*Source*: The *EdGCM Workshop Guide*: NASA Climate Modeling and Data Applications Workshop.

pollution are under study in current climate modeling. The focus of current climate models is to determine the combined effects from all these climate forcing to better understand how the planet's climate changes over time and the effect on the biosphere.

## Climate Feedback Mechanisms

In contrast to the previously described climate forcing, the effects on global climate models due to climate feedback mechanisms is more pronounced. This is due to the large number of feedback mechanisms that occur at the same time, which either amplify or dampen the origin forcing. The planet's global cooling and warming are dominated by three main climate feedback mechanisms. The *ice-albedo* feedback, the *water vapor* feedback, and the feedback due to cloud cover.

The greenhouse effect due to carbon dioxide emissions from both natural and anthropogenic sources is minor compared to the positive feedback that results. The earth's atmosphere is relatively transparent to incoming visible solar radiation, but opaque to the infrared radiation that is emitted as a result of absorption by carbon dioxide. The positive feedback amplifies that effect of warming as a result of the $CO_2$ greenhouse effect. In other words, the initial effect of the forcing is amplified. The net result is an increase in evaporation of water from the ocean surfaces, mainly in the tropical regions on earth. This increases the content of water vapor in the planet's atmosphere. Water vapor has a very strong greenhouse warming potential, and further increases the temperature of the planet's atmosphere resulting in more water vapor being produced in the atmosphere. The so-called runaway greenhouse effect sets up a positive feedback loop within the global climate model. As a result of the initial $CO_2$ and increased water vapor abundance in earth's atmosphere, another positive feedback

mechanism occurs as higher quantities of sea ice begins to melt. The melting sea ice reduces the total surface area of ice on the planet, which results in a decrease in the planet's albedo due to the reduced area of ice and snow. This results in a higher absorption of incident solar radiation by the planet's surface with less radiation being reflected back to space. This second feedback operates along with the first feedback mechanism to raise the planet's temperature even further.

The third major feedback mechanism is the most complex of the three feedbacks, and is a key subject of climate model research. The cloud feedback mechanism has caused controversy in that not all global climate models agree on whether or not the effect produces an amplification or a dampening of the original forcing. Because high clouds are colder and tend to re-emit energy to space at a temperature which is lower than the planet's surface temperature, they tend to trap heat. In contrast, clouds that are located lower in the planet's atmosphere tend to reflect more solar radiation back to space – i.e. they increase the planet's overall albedo. In global climate models there is a connection between the greenhouse effect and overall cloud content in the atmosphere. As the planet's temperature rises due to an increase in greenhouse gas emissions, it becomes more difficult for clouds to condense at lower altitudes within the atmosphere. In other words, the temperature becomes too high in the lower atmosphere for clouds to condense as a result of cooling and a positive feedback towards warming occurs. However, the negative feedback that occurs as a result of less clouds forming at high altitudes may mitigate or offset the positive feedback due to the lower number of clouds at low altitudes. The oceans act to absorb a significant amount of $CO_2$ greenhouse gas in the atmosphere. The effect of the Earth's oceans on the radiation energy imbalance can be

estimated by considering the amount of heat energy stored by the oceans over the last 20 years (1990 to 2010). Levitus et al. (2012) gives a total heat content of the oceans of ~$1.5\times10^{23}$ J. This yields a total absorbed energy flux equal to $1.5\times10^{23}$ J divided by the number of seconds in 20 years ~ $1.5\times10^{23}$ J/$6.31\times10^{8}$ s ~ $2.38\times10^{14}$ W. It should be noted that this energy flux represents a lower limit because the deeper layers of the ocean are neglected. Levitus et al. assumes that the measured energy is approximately 90% of total energy of the planet. Therefore, given the surface area of the planet,

$$4\pi R_{\oplus}^{2} = 4\pi\left(6378000\,m\right) = 5.1\times10^{14}\ m^{2} \quad (11)$$

the amount of irradiance (or flux) that is absorbed per unit area is given by

$$F = \frac{2.38\times10^{14}\,W}{4\pi R_{\oplus}^{2}} = \frac{2.38\times10^{14}\,W}{5.1\times10^{14}\,m^{2}} \approx 0.47\,W/m^{2} \quad (12)$$

Assuming the net radiative forcing as estimated by the Intergovernmental Panel on Climate Change (IPCC) is equal to ~1.5 W/m$^2$, the planet's oceans absorbs and stores approximately 31% of the planet's radiative energy imbalance. Even if the planet's total radiative forcing were to be stabilized at current levels, the difference, 1.5 W/m$^2$ – 0.47 W/m$^2$ ~ 1 W/m$^2$ would result in a continued warming of the planet, until a new equilibrium (radiative balance) is established. It is not currently known how long it would take to reach this equilibrium.

Most global climate models tend to agree that the sign of the combined cloud feedback is positive, but with a higher variation and uncertainty in the resulting models. Future global climate models using higher resolution grids will help determine the effects on planetary climate due to the combined cloud feedback mechanism.

One of the main goals of climate modeling is to determine how sensitive a planet's climate system is to different types of forcing. The "sensitivity" of a planet's climate is based on the change in global mean temperature that occurs over the equilibrium time scale for both the planet's atmosphere and oceans as a result of climate forcing mechanisms. For example, the temperature rise due to a doubling of carbon dioxide emissions (i.e., the sensitivity of the planet's climate) is predicted to be in the range of 2 to 4 degrees Celsius based on many different climate model results (IPCC, 2001).

## The Habitable Zone Boundaries for Earth-like Planets

One of the main goals of this work is to explore the climate of an Earth-like planet (including Earth) at the inner and outer boundaries of the Sun's habitable zone. It is of interest to determine if present-day Earth can maintain a climate suitable for habitation by humans over several hundred years when hypothetically placed at the inner and outer boundaries of the habitable zone. The simulations will simulate Earth's climate at the location of the Sun's inner boundary of the habitable zone (near the orbit of Venus) and the outer boundary (near the orbit of Mars). The climate models will use Earth's current orbital eccentricity and obliquity as a reference baseline. Several alternative climate models will be conducted using a wide range of orbital eccentricities and planetary obliquities (axial tilt) to determine the effects on climate over several hundred years. The main objective of the climate model simulations is to determine whether or not there is a significant change in the planet's climate over a few hundred years (short-term) as a result of the change in solar insolation at the inner and outer HZ boundaries.

The stellar habitable zone is an annulus region around a host star within which water (which is required by life as we know it) remains in a stable liquid phase (from 273 K to 373 K) (Figure 14). However, a calculation of the precise location of a star's habitable zone (HZ) is more complex. The location of the HZ boundaries also depends on the nature of a planet's atmosphere, such as percentage of cloud cover which can increase planetary albedo and the greenhouse effect which can provide additional warming of the planet. For example, the equilibrium temperature of the Earth is about 255 K, but its actual temperature is near 288 K. The difference is due to Earth's greenhouse effect, and if it were not for this additional greenhouse warming factor, climatic conditions would be harsh for humans on Earth.

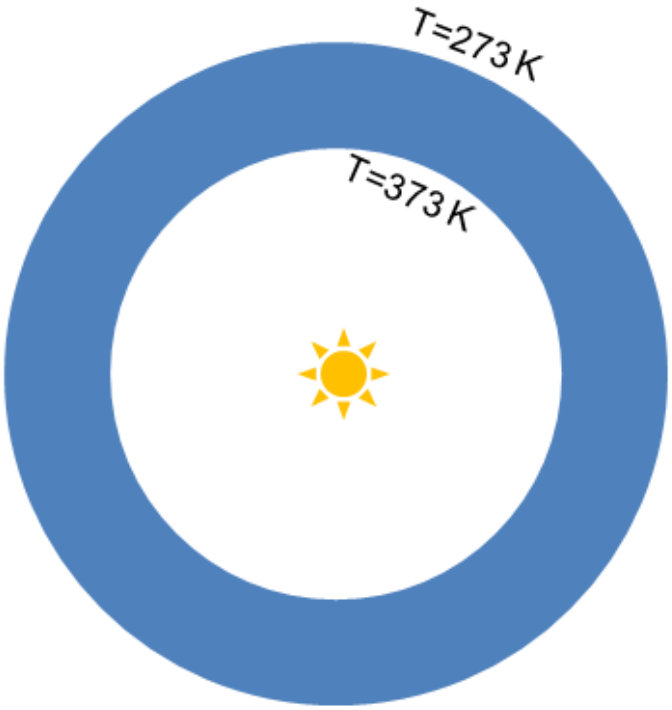


Figure 14. The Sun's habitable zone. The inner boundary is set by the boiling point of water, and the outer boundary is determined by the freezing point of water. The actual location of a planet's habitable zone is more complex, and depends on various factors such as the amount of greenhouse warming, clouds, albedo, mass, and other contributing factors.

As a star evolves (ages), its luminosity increases as hydrogen is fused into helium within the star's core. The increase in temperature and pressure occurs faster in stars that have higher mass and lower metallicity. In response to the changes in the star's core, there is a steady increase in luminosity and changes in effective temperature to maintain equilibrium. Therefore, the HZ will migrate outward as the star ages and luminosity increases. In the 3-D climate model simulations presented in this work, the change in solar luminosity due to stellar evolution will be negligible since the time span of the simulations is only a few hundred years.

It is of interest to note that is is possible for a planet, such as Venus, to have an "effective albedo" that plays a key role in determining its location in the HZ. For Venus, the effective albedo is very negative relative to the Earth. This is the result of a runaway greenouse effect operating on Venus. The effective albedo for Mars lies in the normal range and is larger than Earth's.

A simple calculation of the stellar HZ can be made based on the energy equilibrium (energy in = energy out) condition. The energy the reaches the planet and the planet's cross section can be expressed as

$$\frac{L_*}{4\pi a^2},\ \pi R_p^2 \quad (13)$$

where $a$ is the semi-major axis of the planet's orbit, $R_p$ is the radius of the planet, and $L_*$ is the luminosity of the host star. The fraction of energy absorbed by the planet is expressed in terms of its average albedo, $A$, as $(1-A)$. Thus the amount of energy that is absorbed by the planet is given by

$$\frac{L_*}{4\pi a^2} \times \pi R_p^2 \times (1-A) \quad (14)$$

i.e. the product of the energy that reaches the planet, the planet's cross section, and the fraction of energy absorbed. The amount of energy radiated by the planet is given by

$$4\pi R_p^2 \times \sigma T_p^4 \quad (15)$$

The energy balance assumption can then be expressed as

$$\frac{4\pi R_*^2 \sigma T_*^4}{4\pi a^2} \pi R_p^2 (1-A) = 4\pi R_p^2 \sigma T_p^4 \quad (16)$$

where $T_*$ is the effective temperature of the host star, and $R_*$ is the radius of the star. It can be seen from the energy balance equation that the luminosity of any source can be expressed as

$L = 4\pi R^2 \sigma T^4$, which is just the product of the total surface area of the source and the Stefan-Boltzmann law. The energy balance condition can be used to obtain the equilibrium temperature of the planet

$$T_{eq} = \left[ \frac{(1-A_b) L_*}{16\pi a^2 \sigma} \right]^{1/4} \quad (17)$$

where *a* is the semi-major axis of the planet's orbit, $A_b$ is the planet's Bond albedo, $L_*$ is the luminosity of the host star, and $\sigma$ is the Stefan-Boltzmann constant. A more convenient expression involving the use of common units for estimating a planet's equilibrium temperature is

$$T_p = 278 \frac{1}{\sqrt{a(\mathrm{AU})}} \left( \frac{L_*}{L_\odot} \right)^{1/4} (1-A)^{1/4} \ ^\circ\mathrm{K} \quad (18)$$

Solving for the planet's semi-major axis, *a*, in this equation leads to an expression that can be used to calculate the inner and outer boundaries of the HZ by setting the temperature to 373 K and 273 K.

$$a = \sqrt{\frac{(1-A_b)L_*}{16\pi\sigma T^4}}$$
$$= \sqrt{\frac{(1-0.306)\times 3.845\times 10^{26}\ J/s}{16\pi\times 5.67\times 10^{-8}\ J/(s\,m^2\,K^4)\times(273.15K)^4}} = 1.30\times 10^{11} m = 0.867\ AU$$
$$= \sqrt{\frac{(1-0.306)\times 3.845\times 10^{26}\ J/s}{16\pi\times 5.67\times 10^{-8}\ J/(s\,m^2\,K^4)\times(373.15K)^4}} = 6.95\times 10^{11} m = 0.465\ AU \quad (19)$$

The minimum and maximum distances using the Earth's real albedo are unrealistic considering neither one is outside of the Earth's real orbit. The maximum distance offers a more realistic distance for the HZ. However, the minimum distance is inside that of Venus and therefore is probably not realistic. This calculation indicates that other factors must change the range of the inner and outer boundaries of the HZ. For example, using an effective albedo of -0.7, the range is calculated to be

$$a = \sqrt{\frac{(1-A_b)L_*}{16\pi\sigma T^4}}$$
$$= \sqrt{\frac{(1+0.7)\times 3.845\times 10^{26}\ J/s}{16\pi\times 5.67\times 10^{-8}\ J/(s\,m^2\,K^4)\times(273.15K)^4}} = 2.03\times 10^{11} m = 1.36\ AU$$
$$= \sqrt{\frac{(1+0.7)\times 3.845\times 10^{26}\ J/s}{16\pi\times 5.67\times 10^{-8}\ J/(s\,m^2\,K^4)\times(373.15K)^4}} = 1.09\times 10^{11} m = 0.73\ AU \quad (20)$$

This range for the HZ (0.73-1.36 AU) lies just inside the orbit of Mars and just outside the orbit of Venus. This would be a good number to use for a "zone of interest" and places the Earth somewhere in the middle of the HZ.

To illustrate the dramatic effect that a planet's average albedo has on its habitable environment, one can calculate its equilibrium temperature for an albedo of zero (typical of a piece of black charcoal, and for an albedo assuming a cloud coverage similar to Venus (0.750). The calculations assume the planet is located at 1 AU from a solar type star.

$$T_{\oplus} = \left[ \frac{(1-0.306) \times 3.845 \times 10^{26}\ J/s}{16\pi \left(1.496 \times 10^{11}\ m\right)^2 \times 5.67 \times 10^{8}\ J/\left(s\, m^2\, K^4\right)} \right]^{1/4} = 255\, K$$

$$T_{0} = \left[ \frac{(1-0.0) \times 3.845 \times 10^{26}\ J/s}{16\pi \left(1.496 \times 10^{11}\ m\right)^2 \times 5.67 \times 10^{8}\ J/\left(s\, m^2\, K^4\right)} \right]^{1/4} = 279\, K$$

$$T_{0.750} = \left[ \frac{(1-0.750) \times 3.845 \times 10^{26}\ J/s}{16\pi \left(1.496 \times 10^{11}\ m\right)^2 \times 5.67 \times 10^{8}\ J/\left(s\, m^2\, K^4\right)} \right]^{1/4} = 197\, K \quad (21)$$

The average temperature of Earth is 288 K, so the difference between its equilibrium temperature (using an average albedo of 0.306) and actual temperature represents the *greenhouse warming factor*.

$$\Delta T_g = T_{avg} - T_{eq} = 288\, K - 255\, K = 33\, K \quad (22)$$

If Earth had an albedo of zero, it would allow its temperature to be within habitable conditions suitable for humans (279 K). On the other hand, if Earth had a very high albedo (0.750), its temperature would fall well below that suitable for human life (197 K). These simple calculations show the significance of planetary albedo on habitability.

More realistic calculations based on climate models of early Mars, present-day Earth, and Venus (Selsis et al., 2007) result in the following empirical scaling relations to

compute the inner and outer boundaries of the habitable zone for different spectral class stars

$$
\begin{aligned}
r_{in} &= \left(r_{in\odot} - a_{in}T_* - b_{in}T_*^2\right)\left(\frac{L_*}{L_\odot}\right)^{1/2}\left(1-e^2\right)^{-1/4} \\
r_{out} &= \left(r_{out\odot} - a_{out}T_* - b_{out}T_*^2\right)\left(\frac{L_*}{L_\odot}\right)^{1/2}\left(1-e^2\right)^{-1/4} \\
a_{in} &= 2.7619\times10^{-5}\,AU/K,\; b_{in} = 3.8095\times10^{-9}\,AU/K^2 \\
a_{out} &= 1.3786\times10^{-4}\,AU/K,\; b_{out} = 1.4286\times10^{-9}\,AU/K^2 \\
T_* &= T_{eff} - 5700\,K \\
r_{in\odot} &= 0.72\,AU,\; r_{out\odot} = 1.77\,AU
\end{aligned}
\tag{23}
$$

where *e* is the eccentricity of the planet's orbit, and the inner and out bondaries for the HZ of our solar system, $r_{in\odot}$ and $r_{out\odot}$ were derived using computer models of Venus and early Mars (Selsis et al., 2007), and $T_{eff}$ is the effective temperature of the host star, given by the relationship between stellar luminosity, $L_*$, radius, $R_*$, and effective temperature, $T_{eff}$.

$$
T_{eff} = \left(\frac{L_*}{4\pi\sigma R_*^2}\right)^{1/4}, \quad L = 4\pi R_*^2\sigma T_*^4, \quad R_* = \left(\frac{4\pi\sigma T_*}{L_*}\right)^{1/2} \tag{24}
$$

To calculate the locations of the inner and outer boundaries of the habitable to high accuracy, one must consider in detail the factors governing planetary habitability. These include, but are not limited to reflectivity (albedo), cloud cover percentage, atmospheric composition, the strength of the greenhouse effect, assumptions about water loss from the atmosphere and surface of the planet, and internal density and thus the mass of the planet. Kane and Gelino (2011) have developed parabolic equationn fits between the stellar flux at the HZ boundary in units of the solar constant (1368 W/m$^2$), *S*, and the effective

temperature of the host star, $T_{eff.}$ Given the star's luminosity, $L$, the HZ boundaries are then calculated using the inverse square law.

$$r = \left(\frac{L}{S}\right)^{1/2}$$

$$S = 2.286\times10^{-8}T_e^2 - 1.349\times10^{-4}T_e + 1.786 \quad \text{Recent Venus}$$
$$S = 4.190\times10^{-8}T_e^2 - 2.139\times10^{-4}T_e + 1.268 \quad \text{Runaway greenhouse}$$
$$S = 1.429\times10^{-8}T_e^2 - 8.429\times10^{-5}T_e + 1.116 \quad \text{Water loss}$$
$$S = 5.238\times10^{-9}T_e^2 - 1.424\times10^{-5}T_e + 0.4410 \quad \text{First CO2 condensation}$$
$$S = 6.190\times10^{-9}T_e^2 - 1.319\times10^{-5}T_e + 0.2341 \quad \text{Maximum greenhouse}$$
$$S = 5.714\times10^{-9}T_e^2 - 1.371\times10^{-5}T_e + 0.2125 \quad \text{Early Mars} \qquad (25)$$

The temperature of the planet's surface can be estimated from the energy balance condition (energy absorbed by the planet is equal to the energy emitted), assuming 100% heat redistribution, and the case of inefficient heat redistribution

$$T_p = \left[\frac{L_*(1-A)}{16\pi\sigma r^2}\right]^{1/4} \quad \text{100\% heat redistribution}$$
$$T_p = \left[\frac{L_*(1-A)}{8\pi\sigma r^2}\right]^{1/4} \quad \text{inefficient heat redistribution}$$
$$r = \frac{a(1-e^2)}{1+e\cos\theta} \qquad (26)$$

where $\theta$ is the true anomaly of the planet in its orbit, and $r$ is given by the solution to the differential equation fo the two-body problem – the polar equation for an elliptical orbit. Note that the equilibrium effective temperature of a planet has a temporal dependence due to its orbital eccentricity.

In a runaway greenhouse, the greenhouse effect is amplified by water vapor, thereby increasing the planet's surface temperature. If the flux from the host star is high enough there will be a rapid evaporation of surface water. In turn, water is soon

photodissociated in the planet's upper atmosphere and the hydrogen escapes to space, resulting in a high D/H ratio. In the parabolic equations (eqs. 25 for *S*), an "Early Mars" model assumes that solar flux is at the star of the main sequence phase of the Sun when liquid water was believed to exist on Mars.

In contrast, a "Recent Venus" model assumes that Venus formed with water (perhaps oceans). The solar flux about 1 Gyr ago when oceans may have existed, or flowing water on the surface forms the basis for this model.

The "Maximum Greenhouse Effect" model is based on the maximum distance at which a planet's surface temperature of 273 K can be sustained by a $CO_2$ atmosphere with no clouds, and the "First $CO_2$ condensation" model (for 273 K surface temperature) is the distance at which $CO_2$ clouds start to form (condense).

The 3-D climate models presented in this work will expand upon current analytical studies of planetary climate at the boundaries of the habitable zone of a solar-type star. The high-fidelity climate models will include the effects of solar forcing, greenhouse gas warming, planetary albedo (due to clouds and land) and variation in orbital parameters, all of which play a role in determining the actual location of the planet's habitable zone. In contrast to semi-empirical methods typically used to describe the habitable zone boundaries, the approach used in this work is based on the NASA GCM-II 3-D climate model. The 3-D model treats Earth's climate as a coupled atmosphere, land, and ocean system.

# CHAPTER II

# METHODOLOGY

## Basic Approach and Objectives of the Study

The approach used in this research consists of two main scientific objectives. The first objective will investigate the effects of linear and non-linear trends of several greenhouse gases on the effect of earth's climate over ~200 years (2005-2200). The effects on earth's climate resulting from a variation in solar irradiance over the timespan of the 3-D climate model simulations (200 years) will also be explored. Numerical climate models will include the effect of a solar minimum, similar to the Maunder Minimum, which is thought to have initiated the so-called "little ice age". The goal will be to determine if such a period in low solar activity could account for a period of lower temperatures over the continents, according to the EdGCM version of the NASA GCM II climate model. In addition to models which use greenhouse gases with varying trends over a few hundred years, additional models will be produced with different orbital parameters for Earth. The orbital parameters that can be changed within the EdGCM climate model are the earth's orbital eccentricity, the planet's obliquity (axial tilt), and orbital inclination (the angle of the earth's orbit with respect to the ecliptic plane). The results from a series of different 3-D climate models using different orbital parameters and greenhouse gas forcing will support future studies of earth-like planets that are

currently being discovered in other solar systems by NASA's Kepler mission. However, in its present form, EdGCM has an extremely limited capability to model Earth-like planets outside of the Solar System. The series of 3-D climate models will provide a starting point for research on planetary habitability of hypothetical earth-like planets in different solar systems. Such planets are expected to have a wide range of different greenhouse gases, solar irradiance, and orbital parameters. The effect on planetary habitability can be examined by carrying out a sequence of 3-D climate models over a phase space consisting of different greenhouse emission trends, orbital parameters (eccentricities, inclinations, obliquities), and solar irradiance variation.

The second main objective of this work is to determine the extreme limits of habitability of an earth-like planet using Earth as a reference. The aforementioned series of 3-D climate models are based on earth's current location within the habitable zone of the star. The next sequence of climate models to be produced will be based on the inner and outer boundaries of the habitable zone – defined as the region where water can exist in a stable liquid phase. The approach used will involve placing the earth at the inner and outer boundaries of the sun's habitable zone. The inner boundary will be located at 0.72 AU, approximately the semi-major axis of Venus. The outer HZ boundary will be located at 1.77 AU, slightly beyond the orbit of Mars. These two boundary locations are based on models from Selsis et al. (2007), described earlier in this work.

At each boundary of the habitable zone a series of climate models will be generated over a wide range of planetary obliquities, orbital eccentricities and inclinations to determine the limits of habitability conditions (those temperatures which carbon-based life as we know it can tolerate) of an earth-like planet. The specific values

for the obliquities used will be 0 (no axial tilt), 23.5, 65 and 90 (each pole of the planet will alternately point towards its parent star during its orbital cycle) degrees. It is of interest to simulate the climatic effects on Earth-like planets over a wide range of obliquities. The Earth is fortunate to have a relatively large natural satellite that stabilizes its obliquity. This results in a climatic pattern that is relatively stable. It is thought that the formation of large moons around other Earth-like planets may be a relatively rare process in comparison to Earth, assuming the formation mechanism of the moon is due to an accident of accretion by a glancing impact of a Mars-sized object (Halliday, A. N. 2000). If Earth had no natural satellite its axial tilt would vary between 0 and 85 degrees (Laskar, Joutel, & Robutel, 1993). Since the formation mechanism for Earth's moon is thought to be a rare event, a majority of Earth-like planets discovered (and future discoveries of Earth-like planets) will have obliquities that vary chaotically over wide values (Figure 15). It is of interest to determine whether these planets with high obliquities can have suitable climates to support advanced life similar to our own. The simulations may help determine whether planets with temperate climates suitable for humans is a rare phenomenon, or common place. It is assumed that climatic patterns on Earth-like planets with very high obliquities (near 90 degrees) (Figure 15) would be severe over different regions of the planet, with large variations in seasonal cycles. The large variation in seasonal cycles should be associated with steep temperature variations over mid- to high-latitude continent regions. For Earth-like planets that are located near the outer boundary of the host star's habitable zone the variation in climate should be less. This is the result of increased amounts of carbon dioxide ($CO_2$) in their atmospheres due to changes in the planet's carbonate-silicate cycle (Williams & Kasting, 1997). The

high efficiency of transport of heat through the atmospheres of Earth-like planets with dense $CO_2$ atmospheres would reduce latitudinal temperature gradients and decrease the strength of seasonal variations. The 3-D climate models produced using the EdGCM will either verify or refute this

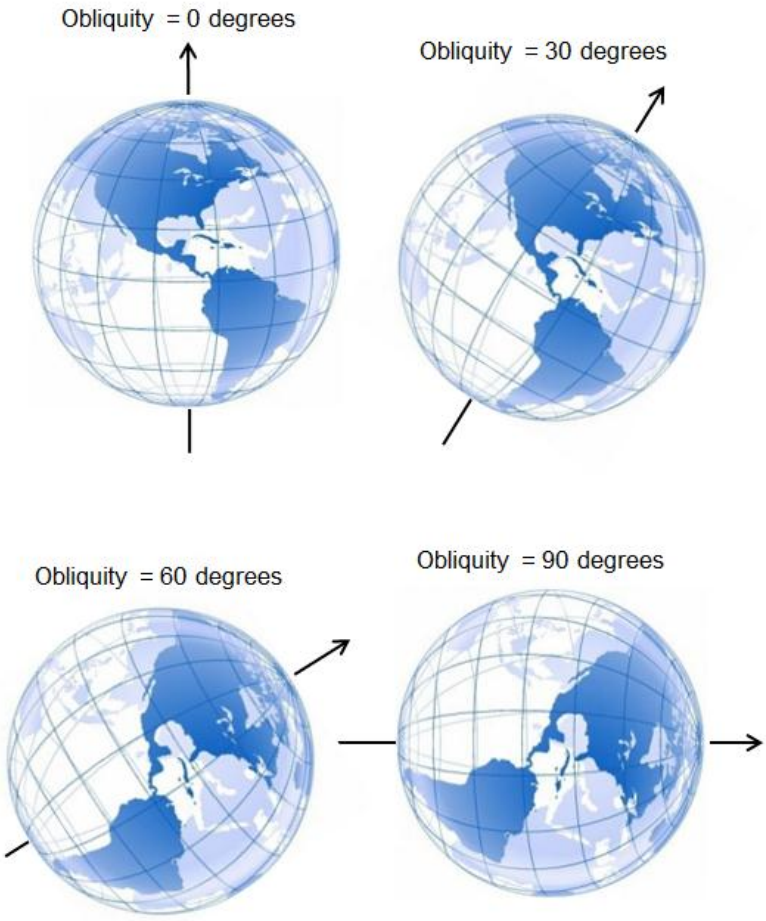


Figure 15. Illustration of varying obliquity. An obliquity of zero degrees would result in very little (or no) seasonal variation on the planet's global climate. As the obliquity increases, the seasonal variations increase, until they reach a maximum when the obliquity is 90 degrees (axial tilt of 90 degrees). As the planet's obliquity increases, the polar region facing the host star experiences increased ice melt, and vice versa six months later when the opposite polar region is facing the star. A decrease in polar ice results in a decrease in the albedo. This leads to an increase in the temperature over these regions, and an amplification of the positive feedback mechanism. As the obliquity increases, an increase in the evaporation rate will occur over the southern hemisphere dominated by oceans during the cycle of the planet's orbit when the southern hemisphere is oriented towards the host star.

assumption. The results of the simulations may help determine whether Earth-like planets located near the outer boundary of the habitable zone can maintain habitable climates, even with high obliquities and dense $CO_2$ atmospheres.

The orbital eccentricities that are used in the simulations are based on the minimum and maximum range of eccentricities of discovered extrasolar planets. The values used for the climate model simulations are 0.0167 (Earth's current eccentricity), 0.2 and 0.3. Higher eccentricity simulations resulted in numerical instability in the climate model code, and could not be run.

The simulations in this study will provide the scientific community with a data archive of 3-D climate models under different orbital, solar irradiance, and greenhouse forcings that earth-like planets will exhibit as they are discovered in greater numbers by future ground-based and space-based observatories. The simulations will also improve upon analytical and semi-analytical methods of investigating hypothetical climates on earth-like planets orbiting solar-type stars. In addition, the three-dimensional climate models produced by the EdGCM (NASA GCM-II) analysis tool will improve upon 1-D and 2-D numerical models produced by the Astrobiology community.

## The Educational Global Climate Model (EdGCM) User Interface

The EdGCM software tool was chosen for this study because it has a user-friendly interface (Figure 14) to a research-grade climate model, allowing many models to be simulated within a reasonable amount of time (several weeks for this study). The interface is the front-end to the Global Climate Model (GCM) developed at the NASA Goddard Institute for Space Studies (Hansen et al., 1983). The GISS GCM uses the equations of conservation of energy, conservation of mass, conservation of momentum

and an equation of state to produce a three-dimensional global climate model. The newly designed interface provides a simple GUI (Figure 16) to the research-grade GCM II climate code. The user has full control over various greenhouse gas trends over time, orbital parameters (eccentricity, obliquity or axial tilt of the planet, inclination of the planet's orbit with respect to the ecliptic, and longitude of ascending node of the planet's orbit), solar irradiance, as well as different paleocontinental configurations. Output

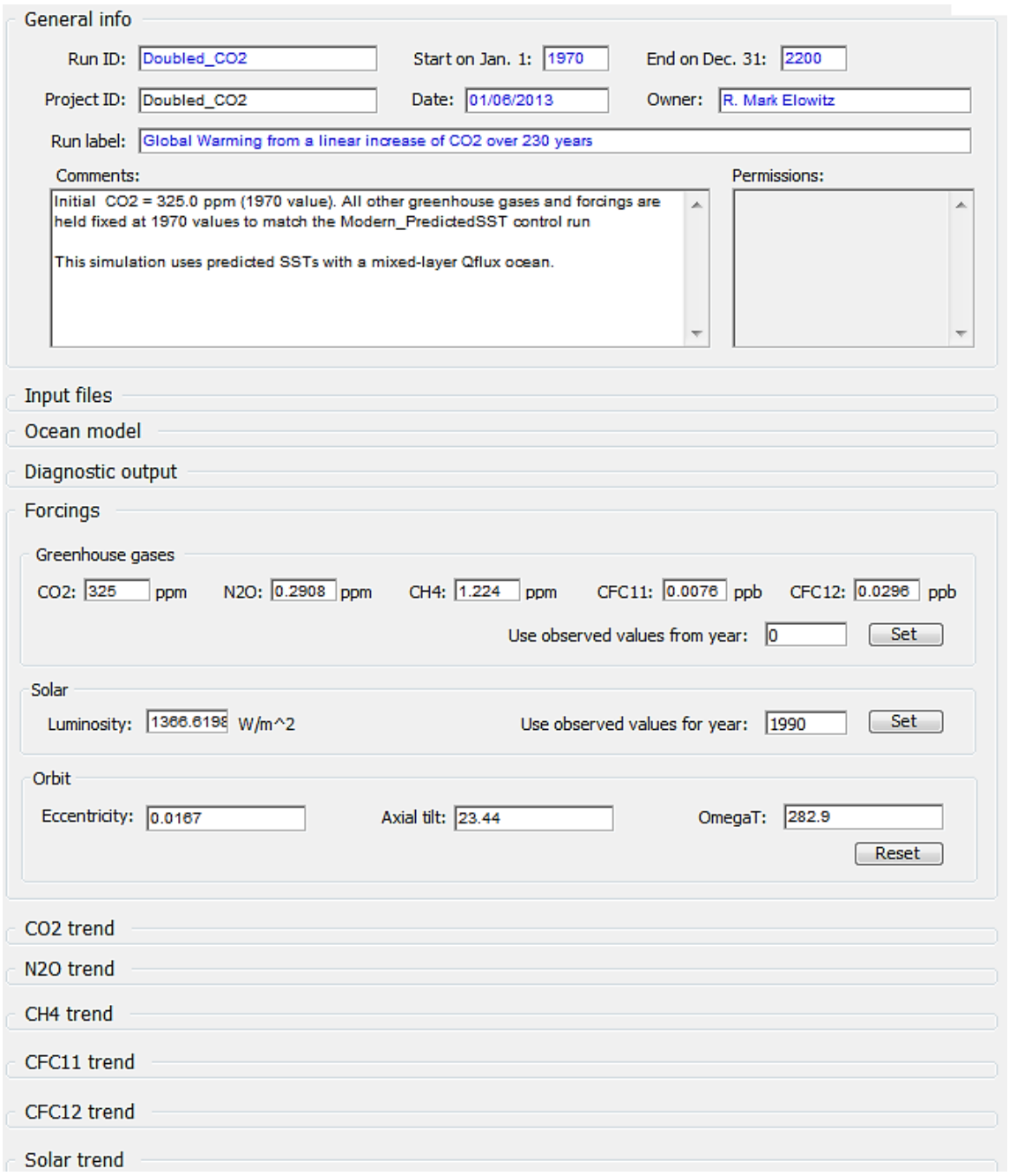


Figure 16. User interface to the NASA GCM-II climate model. The interface allows access to a research grade 3-D climate model (NASA GCM-II). From the main level menu, various greenhouse gas forcings/trends can be set, solar irradiance and solar irradiance trends can also be established, and the eccentricity of the planet's orbit as well as the planet's axial tilt (obliquity) can be specified.

options of the EdGCM software package include the production of time series plots for various climate variables, global map visualizations for different climate variables to help determine variations in regional climate as a function of time, and numerical data for all climate variables used within the EdGCM computer code.

A secondary objective of this research is to fully evaluate the EdGCM software package by comparing selected climate models with observational data obtained by satellites used to conduct global meteorological studies of Earth. An assessment will be made as to whether or not the EdGCM software package would make a useful contribution to scientific and technical classes given as part of the UND Space Studies curriculum. Lessons learned from analysis of 3-D climate models produced by EdGCM in this work will lead to suggestions for improvements and/or modifications to the EdGCM tool.

# CHAPTER III

# RESULTS AND ANALYSIS OF CLIMATE MODEL SIMULATIONS

## EdGCM: Initial Conditions for Model Climate Simulations

The EdGCM is the front-end user interface to the NASA GCM-II global climate model. It allows the user to specify the initial greenhouse gas abundances for a given time, the initial solar irradiance (flux), and the initial orbital parameters for an Earth-like planet. The user is also able to set up trends for each of the five major greenhouse gases (carbon dioxide, methane, nitrous oxide, and two different chlorofluorocarbon species, commonly denoted as CFCs). The single or multiple trends over specified time periods may be set up for each greenhouse gas, including constant, stepwise, linear, exponential, or a user-defined trend contained in an external data file. For example, the user may set up a linear trend in carbon dioxide emission over a particular interval of time, followed by an exponential increase in carbon dioxide over a second interval of time. Transient variations in greenhouse gas emissions are also possible. In addition to trends in greenhouse gases, the user may also set up trends in the solar irradiance over a specified period of time. The same type of trends (linear and nonlinear) can also be established for the solar irradiance. This is useful for analyzing the effects of solar irradiance variations on global climate. An example model is provided in this work where a "maunder minimum" (a prolonged sunspot minimum) is established over a timespan of

approximately 50 years. It is of interest to see if the GCM-II 3-D climate model can produce the cold winters in parts of Europe and North America that is thought to be due to prolonged periods of minimum sunspot activity. The EdGCM interface also allows the user to change the land and vegetation distribution, but these will not be changed in this work since the climate models are only being computed over ~200 years. These geographical boundary conditions are only important for paleoclimate simulations, and will not be discussed further in this work.

There are three orbital parameters that can be set for a particular climate model. These include the orbital eccentricity, axial tilt (obliquity) of the planet, and longitude of perigee. This research will carry out climate model simulations using the orbital eccentricity and obliquity to study the effects of global climate and to place limits on the habitability of Earth-like planets. Planets with high eccentricities or high/low obliquities should exhibit extreme climate variations as a function of time (or orbit cycle).

The simulations performed in this research include a model using a linear trend in greenhouse gas emissions based on current estimates of increase of these gases in Earth's atmosphere (IPCC). The second simulation is based on a linear trend in greenhouse gas emissions, followed by an exponential increase. For example, if temperatures were to rise to the point at which methane is released from clathrates under the arctic permafrost, it could introduce an exponential rise in methane (Biastock et al. 2011; Archer, D. et al. 2009; Krey, V., et al. 2009). It is of interest to explore the effects of such a rise in methane (a powerful greenhouse gas in comparison to carbon dioxide) over timescales of approximately 200 years. The third simulation will explore the effects of a prolonged period of solar irradiance on Earth's global climate. It is of interest to determine whether

the GISS GCM-II 3-D climate model can reveal any evidence of colder climates over parts of North America and Europa. The next few simulations will explore the effect of placing the Earth at the inner and outer boundaries of the habitable zone. This is done by computing the solar irradiance at the two boundaries, and specifying that solar irradiance as the initial input to the climate model. It is of interest to explore the effects of relocating the Earth to the inner and outer habitable zone (discussed earlier in this work) on the overall global climate. It is of interest to determine whether the Earth (or similar planet) could remain habitable for humans over timescales of approximately 200 years. The final simulations will introduce more complex factors, such as variations in the orbital eccentricity and obliquity of an Earth-like planet. It is of interest to see the effect of climate variations over a range of eccentricities and obliquities. For these simulations the Earth will be located at its present position within the habitable zone, and the eccentricity and obliquity will be varied. The simulations will assume current trends in greenhouse gas emissions and solar irradiance. Future work should include variations in orbital eccentricity and obliquities for the inner and outer boundaries of the habitable zone, but due to the CPU time involved in computing the 3-D models over ~200 years, these more complex models will not be performed in this research.

## EdGCM: Description of Climate Model Output Data

The main output from EdGCM is in the form of global maps showing the temperature distribution across the planet (minimum, maximum, and mean), albedo, net heating at the planet's surface, net radiation of planet, and a multitude of other climate variables that can be displayed as maps. For the simulations carried out in this work, the output presented is the annual average of the minimum, maximum, and mean surface air

temperature distribution across the planet. The planet albedo, surface albedo, neat heating at the surface of the planet, net radiation from the planet, and total cloud cover is also presented in order to describe correlations between temperature and these climate model variables. To reduce the amount of noise in the climate model data, the maps displayed in this work are the average of five years. For each simulation, average maps are shown for the year ranges 2005-2009, 2096-2100, and 2196-2200. These ranges were chosen to look for changes over the ~200 year simulation.

The scientific results shown in the global climate maps are based on a three-dimensional grid system within the GCM-II code. Each individual grid is divided into an 8 degree latitude by 10 degree longitude area. The atmosphere is divided up into nine separate layers in the vertical direction, and two ground layers. Within each three dimensional grid cell, the equations of momentum, mass and energy conservation are solved to generate the global climate model output shown in the maps.

**Results of the Greenhouse Gas Forcing Models**

The first simulation assumed a linear increase in carbon dioxide ($CO_2$) of approximately 2.1 ppm per year, based on an initial abundance of 379.0 parts per million (ppm) (Figure 17 top pane). The simulation was run over the time interval ranging from 2005 to 2200. A linear trend for methane ($CH_4$) was used based on the latest estimates from the IPCC AR4 2007 working group on climate. An initial value of 1.774 ppm was used, and an increase in the concentration of methane of approximately 0.99% per year (~0.018 ppm/yr) was used in the simulation (Figure 17 middle pane). An initial value of 0.319 ppm (for the year 1999) was used for nitrous oxide ($N_2O$), and a linear trend based on an estimate of approximately 0.12% per year (~0.0004 ppm/yr) by the IPCC AR4

2007 working group on climate was assumed (Figure 17 bottom pane). The two chlorofluorocarbon species (CFC11 and CFC12) were held at a fixed level of 0.00025 and 0.00053 ppb, respectively.

The solar irradiance was fixed at 1366.62 $W/m^2$ in this simulation so that only the effects from greenhouse gas forcing is analyzed. The orbital parameters for present-day Earth were used, with an orbital eccentricity of 0.0167 and an axial tilt (planetary obliquity) equal to 23.44 degrees.

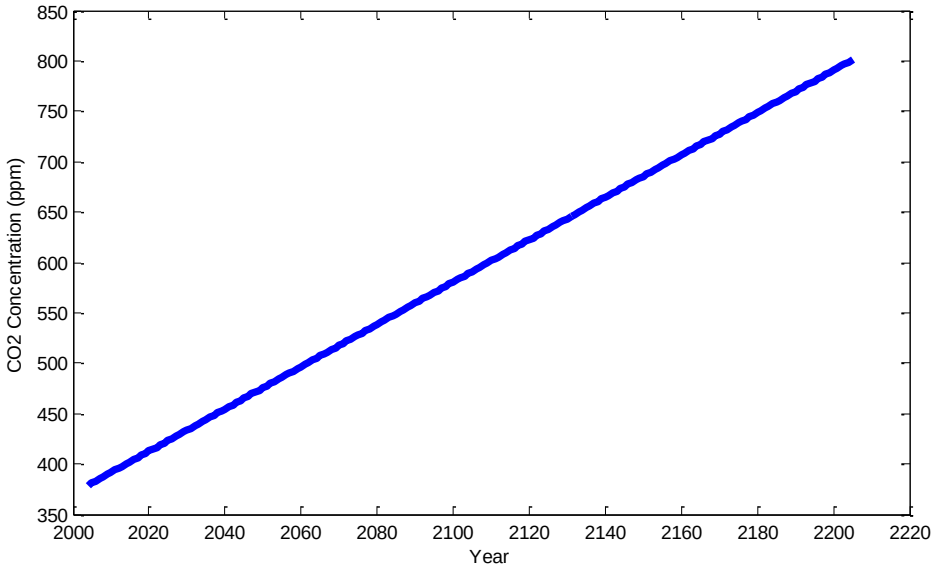

Figure 17 Cont

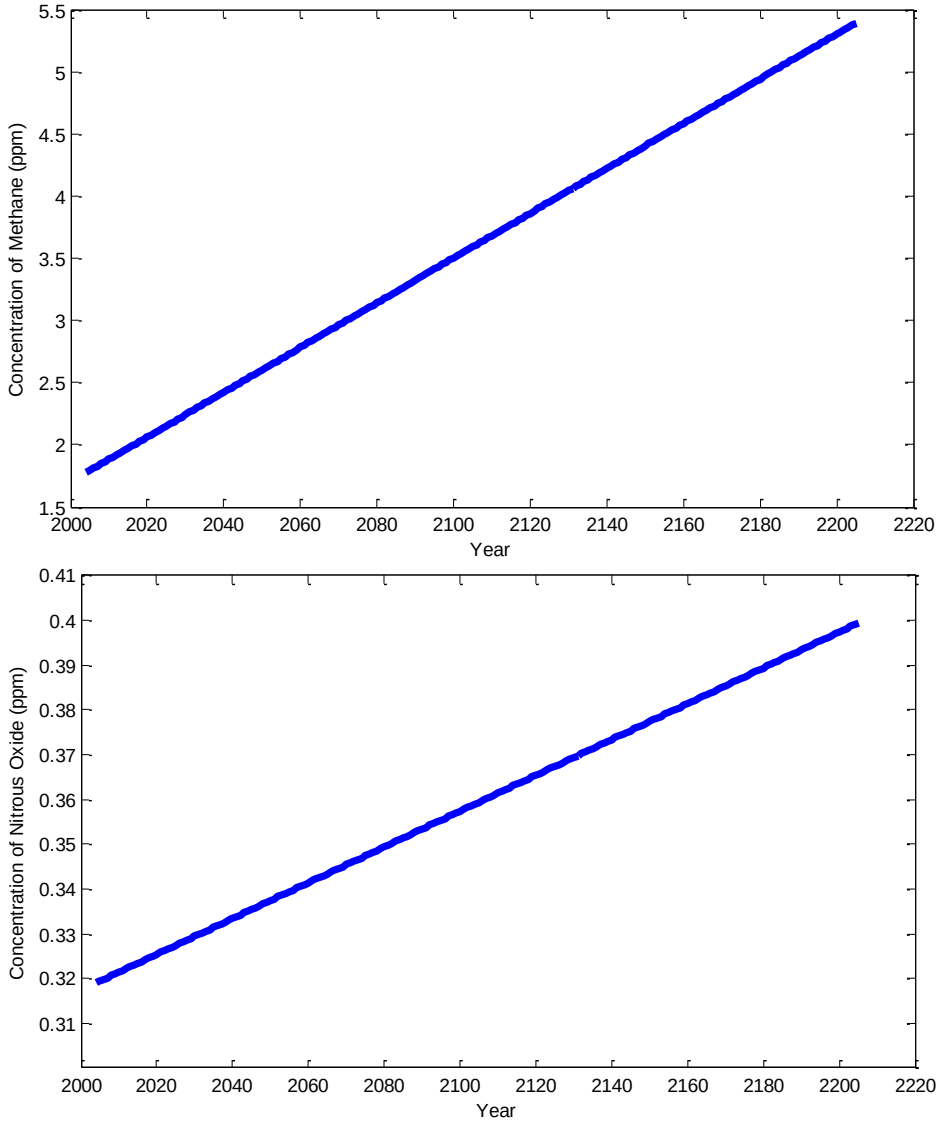


Figure 17. Linear trends in greenhouse gas emissions. Top: A linear trend in carbon dioxide emission over the ~200 year simulation period. An initial value of 379.0 ppm concentration is assumed with an increase of 2.1 ppm per year from 2005 to 2200, to a maximum value of 801.1 ppm. (Middle): An initial value of 1.774 ppm methane concentration is assumed with a linear increase of 0.018 ppm per year from 2005 to 2200, to a maximum value of 5.392 ppm. (Bottom): A linear trend nitrous oxide ($N_2O$) emission over the ~200 year simulation period. An initial value of 0.3190 ppm was used for the concentration of nitrous oxide emission with an increase of 0.0004 ppm per year over approximately 200 years. The maximum value for nitrous oxide at the end of the simulation run was 0.3994 ppm.

The following global maps show the results from the simulation based on the current estimates of increasing greenhouse gas emissions, fit to a linear trend with time.

The estimates are based on predictive analysis carried out by the Intergovernmental Panel on Climate Change (IPCC). It is important to note that these climate model results represent only one possible model out of a multitude of possible models based on both linear and nonlinear trends in
greenhouse emission.

The average global surface air temperature average over five years (2005-2009) is shown in Figure 18. There is a clear latitudinal temperature gradient present, with the highest temperatures seen over the equatorial region of the Earth and cooler temperatures observed over the polar regions. There is an interesting asymmetry in temperature between the north (arctic) and south polar (Antarctica) regions on the Earth. This is partly due to the fact that Antarctica is approximately three kilometers above sea level, and that the temperature decreases with height in the atmosphere within the troposphere. Another explanation for the observed north-south polar zone asymmetry in temperature is the result of warm ocean temperatures being transferred within the icepack contained within the arctic polar region. This process results in a warmer climate of the north polar region, in contrast to the south polar region where the process is less efficient. The last reason we see the asymmetry in temperature for the north and south polar zones is the result of the orbital motion of the Earth around the Sun. During the south polar winter, the Earth is near (or at) aphelion (where Earth is at its maximum distance from the Sun). This occurs during July when the Antarctic region is experience its winter season. During the Antarctic summer season, the Earth is near (or at) its perihelion, when the planet lies near (or at) its minimal distance from the Sun. This orbital motion due to Earth's orbital

eccentricity has a minor contribution to the colder climate at the south pole, but the first two effects dominate the cause of the arctic-Antarctic temperature asymmetry.

Figure 19 shows the maximum temperature distribution over the Earth. The map shows a five year average of the annual minimum temperature over the years 2005 to 2009. The north-south polar asymmetry in temperature is similar to that of the mean temperature shown in Figure 18. The maximum temperatures are located in two localized region in North Africa and the equatorial region shows the warmest climate. The two local regions in North Africa show a maximum temperature (annual average, averaged

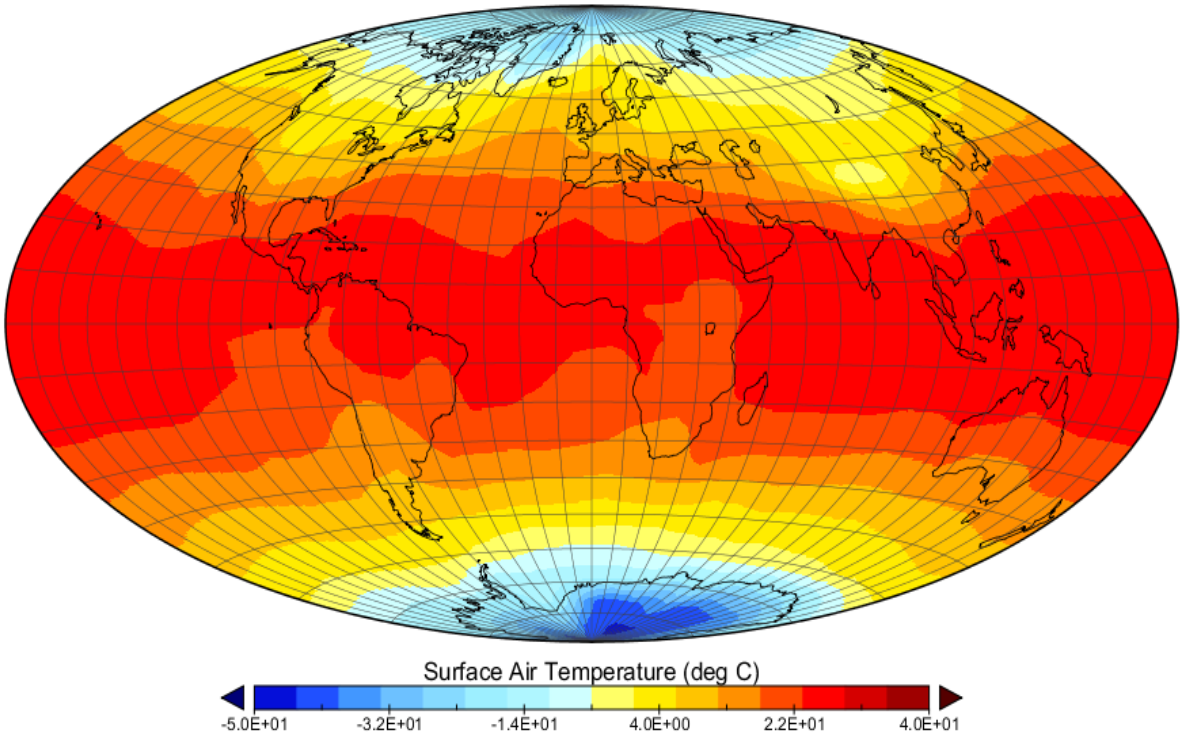


Figure 18. Surface air temperature for linear greenhouse emissions. Global temperature distribution near the the surface of the Earth as modeled by EdGCM. The map shown is a Hammer projection. The data is average over five years (2005-2009) to reduce noise in the data. Note the temperature gradient across latitude, ranging from hottest over the equatorial regions, and coolest at the polar regions.

over five years from 2005-2009) of approximately 310 K or 98.3 degrees Fahrenheit (F).

Most of the United States experiences an average annual temperature ranging from 50 to

80 F. The most interesting feature of the maximum temperature map is the hot spot over Western Africa. This is significant because hurricanes that affect North America originate from hot air that rises upward. Columns of hot air move out over the Atlantic ocean, where the moisture content of the air increases due to the warm ocean temperature. The warm moist air moves westward over the Atlantic as it feeds off of the ocean's energy. The moist warm air combined with the effects due to the Coriolis force, result in counterclockwise rotation of forming hurricanes over the Atlantic ocean.

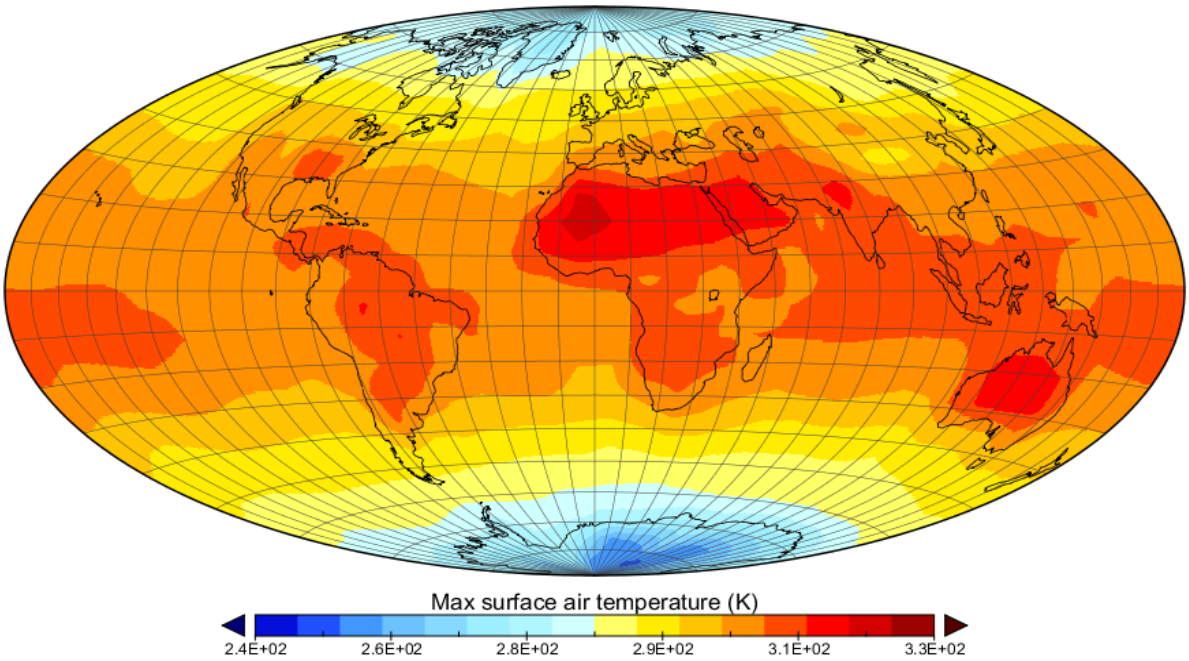


Figure 19. Maximum surface air temperature for linear GHG emissions. Maximum annual air temperature averaged over the years 2196-2200 as modeled by EdGCM. Note the hot spots over West and Northwest Africa. The hot air over Northwest Africa is ultimately responsible for the formation of hurricanes over the Atlantic ocean. The arctic-Antarctic temperature asymmetry is also apparent in agreement with that shown in Figure 18.

The surface albedo (reflectivity) is shown in Figure 20 below. The first apparent observation to note is the high albedo over the north and south polar regions. Snow-covered sea ice has an albedo of 0.95, fresh snow has albedos that range from 0.8-0.85,

and melting snow has albedos ranging from 0.3-0.65. These different albedo produce an average albedo of approximately 0.70 in parts of the arctic and Antarctic regions on Earth. The high albedos of the polar regions contribute to the colder temperatures seen on the global temperatures maps shown in figures 18 and 19 by reflecting more solar radiation back to space. There is an observed correlation between higher albedo and lower temperatures and vice versa as seen on the surface air temperature map and surface albedo (Figures 18, 19, and 20). Most of the continents have surface albedos that range from 20 to 40%. The average surface albedo of Earth is approximately 43%. It is important to note that the surface albedo does not take into account the albedo of planet's average cloud cover, and is therefore not representative of the Earth's total average albedo of approximately 30% (surface plus clouds).

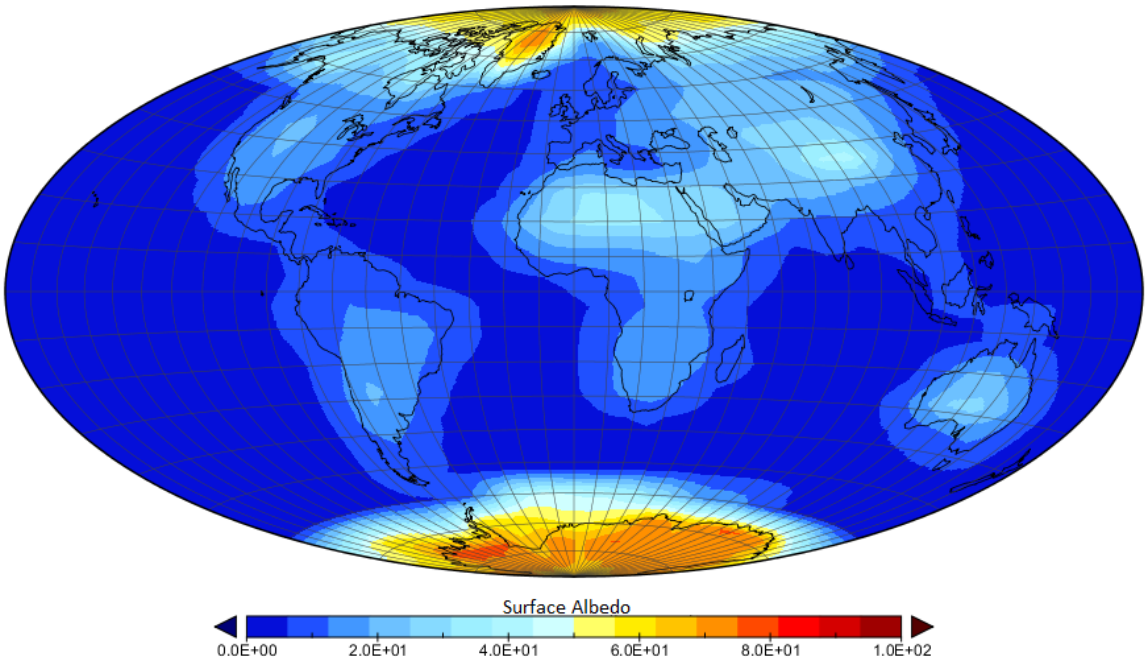


Figure 20. Surface albedo for linear GHG emissions case. Global Hammer projected map showing the surface albedo of Earth, averaged over five years (2005-2009). Note the high surface albedo of the polar regions due to the effects of sea ice and snow covered ice. The continents have albedos that range from 20 to 40%.

The next global map (Figure 21) shows the planetary albedo, including the effects due to cloud cover. The high albedo of the polar regions are apparent as well as the lower albedo observed at the equatorial region of the planet. Water has a very low albedo near 2%, but the higher albedo observed within the ocean regions takes into account the albedo of cloud cover of these regions. There is a gradient in the planetary albedo, ranging from high albedos at the polar regions and high latitudes to intermediate albedos at mid-latitude regions to low albedos at equatorial regions.

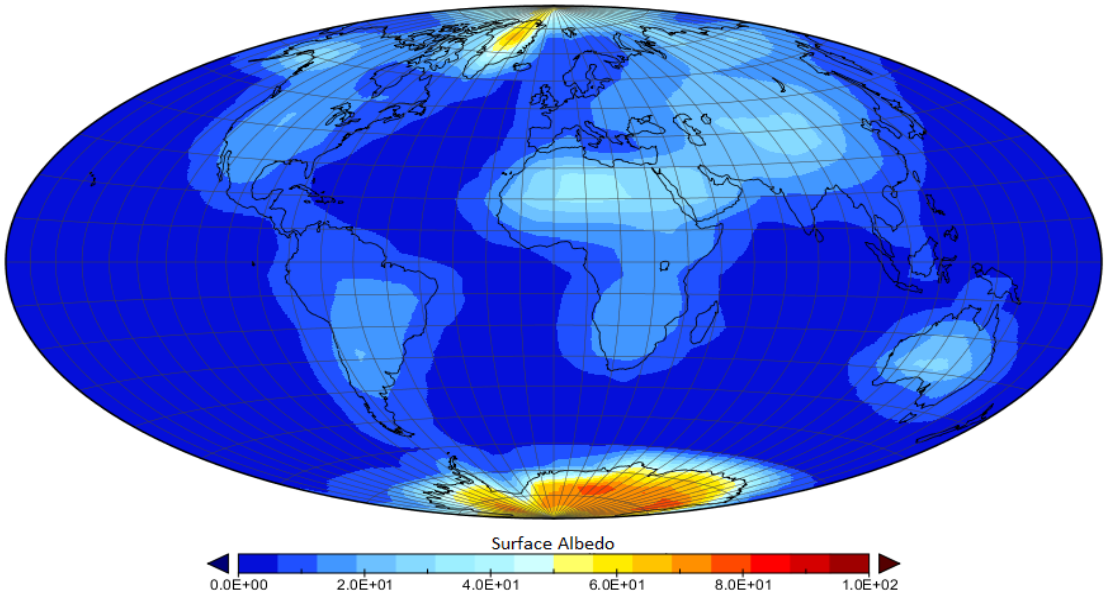


Figure 21. Surface albedo for linear GHG emissions case. Global Hammer projected map showing the surface albedo of Earth, averaged over five years (2196-2200). Note the high surface albedo of the polar regions due to the effects of sea ice and snow covered ice. The continents have albedos that range from 20 to 40%. There is a slight decrease in overall albedo due to 200 years of greenhouse emissions due to melting ice and snow.

The total annual cloud cover averaged over five years is shown in Figure 22. Predicting cloud cover is still one of the major uncertainties associated with climate modeling. Cloud cover plays a major role in determining the overall radiation budget of the Earth's lower atmosphere (troposphere). It is interesting to note that, even though

modern climate models can reproduce the latitudinal temperature profile to high accuracy, they have trouble reproducing the planet's cloud cover to the same accuracy as that of the temperature distribution. One possible explanation to this problem is that most 3-D climate models deal with solving the equations of energy flow. It is a well established fact there is a strong link between temperature and thermal radiation emission from the Earth. The Stefan-Boltzmann law, $F = \varepsilon\sigma T^4$, states that the emitted radiation is directly proportional to the temperature raised to the fourth power. This, in turn, implies that the temperature is proportional to $T^{1/4}$. This means that there is a correspondent proportionality in the error in temperature predicted by climate models. For example, if there is a 10% error in the radiation flow budget determined by the climate model, the Stefan-Boltzmann relation implies an error of only 1/4 × 10 or only 2.5%.

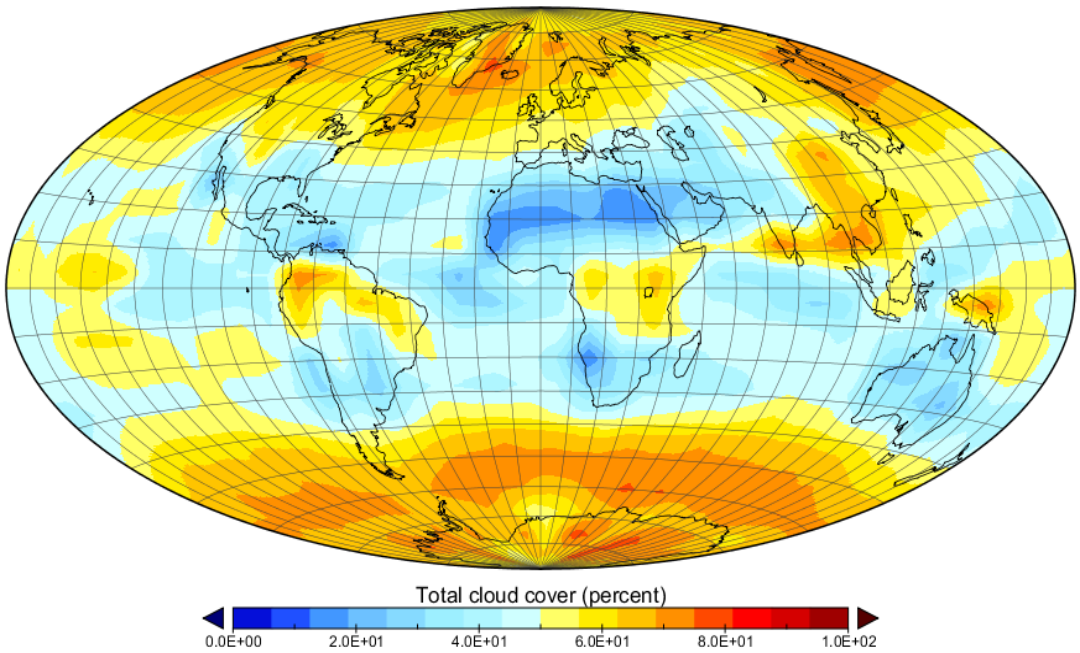


Figure 22. Total annual cloud cover for linear GHG emissions. The total annual cloud cover of Earth averaged over five years (2005-2009). The overall cloud cover of the planet is the greatest uncertainty for most climate models. The latitude grid is divided into sections of 10 degrees. The total cloud cover percentage agrees well with the observed value near 60 degrees south.

The zonal average of the total annual cloud cover is shown in Figure 23. The profile indicates a higher percentage of cloud cover over the planet's polar regions, with a minimum over the equatorial regions.

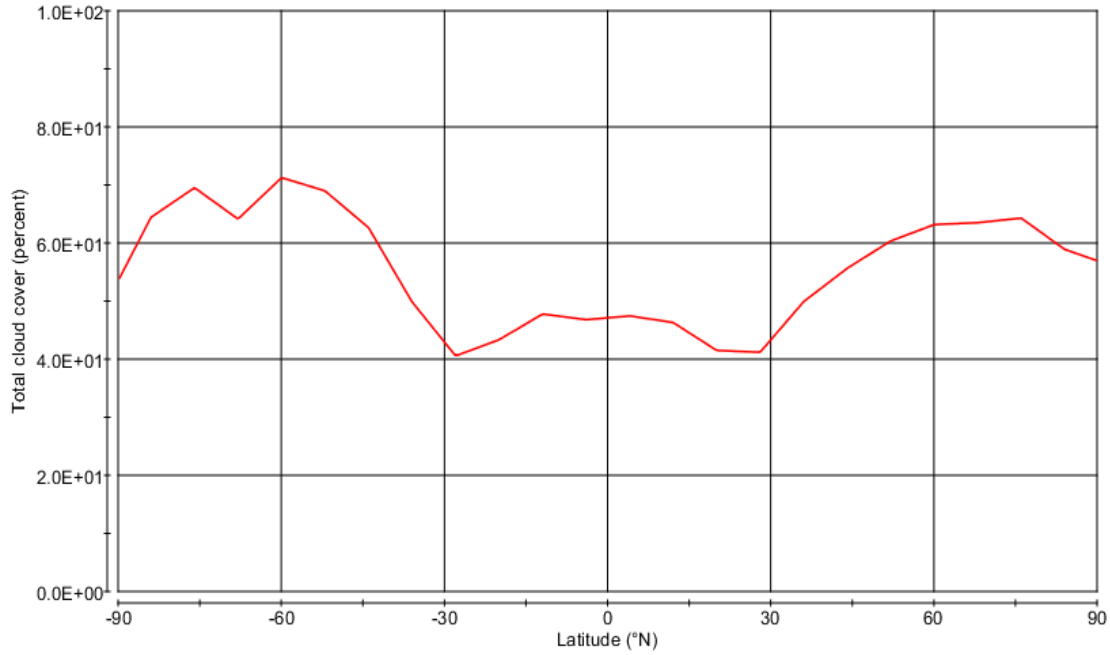


Figure 23. Simulated zonal average of total cloud cover. The zonal average is a five-year average of the total cloud cover of Earth averaged over five years (2005-2009) to reduce inherent noise in the climate model data.

The over all zonal average profile of the cloud cover predicted by the EdGCM model displays a similar shape to the observed profile shown in Figure 24. However, the profile does not agree well with the observed zonal average over the equatorial regions of the Earth. This is not unexpected, as most climate models do a very job at predicting total cloud cover to high accuracy.

The net heating at the surface of the Earth and net radiation of the planet averaged over five years (2005-2009) are shown in Figures 25 and 26. The net radiation of Earth is determined by a balance between energy being emitted by the planet and energy that is

incident on Earth. In other words, the net radiation can be thought of as the total amount of energy that is available to regulate the planet's global climate. The surface of the Earth as well as cloud layers/atmosphere emits heat or thermal radiation. Aerosols, the surface

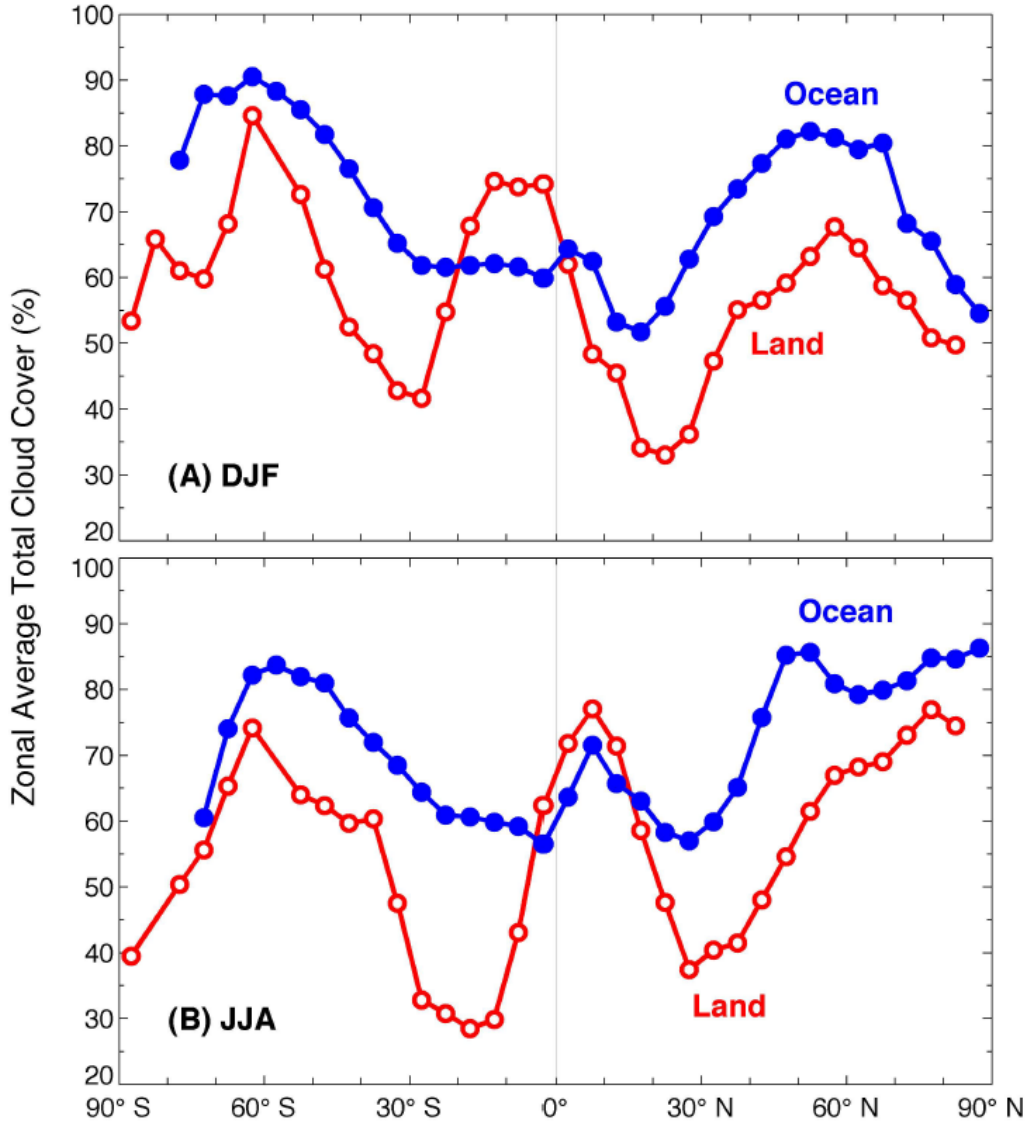


Figure 24. Observed zonal average of the total cloud coverage. Zonal average of the total cloud cover from 1971-1996 over the continental regions, and over the oceans from 1954-1997. Figure from (Hahn et al. (1995) *Journal of Climate* 8: 1429-1446, American Meteorological Society, Boston).

of the Earth, and clouds reflect radiation back to space. A temperature increase or decrease occurs because the average net radiation averaged over the whole planet is not

in perfect equilibrium over the span of an orbital cycle around the Sun. Since ocean water has the ability to hold high amounts of heat, it results in increasing temperatures over the oceans. The most obvious observation from examining the net radiation map

Figure 25. Net heating for linear GHG emissions case.

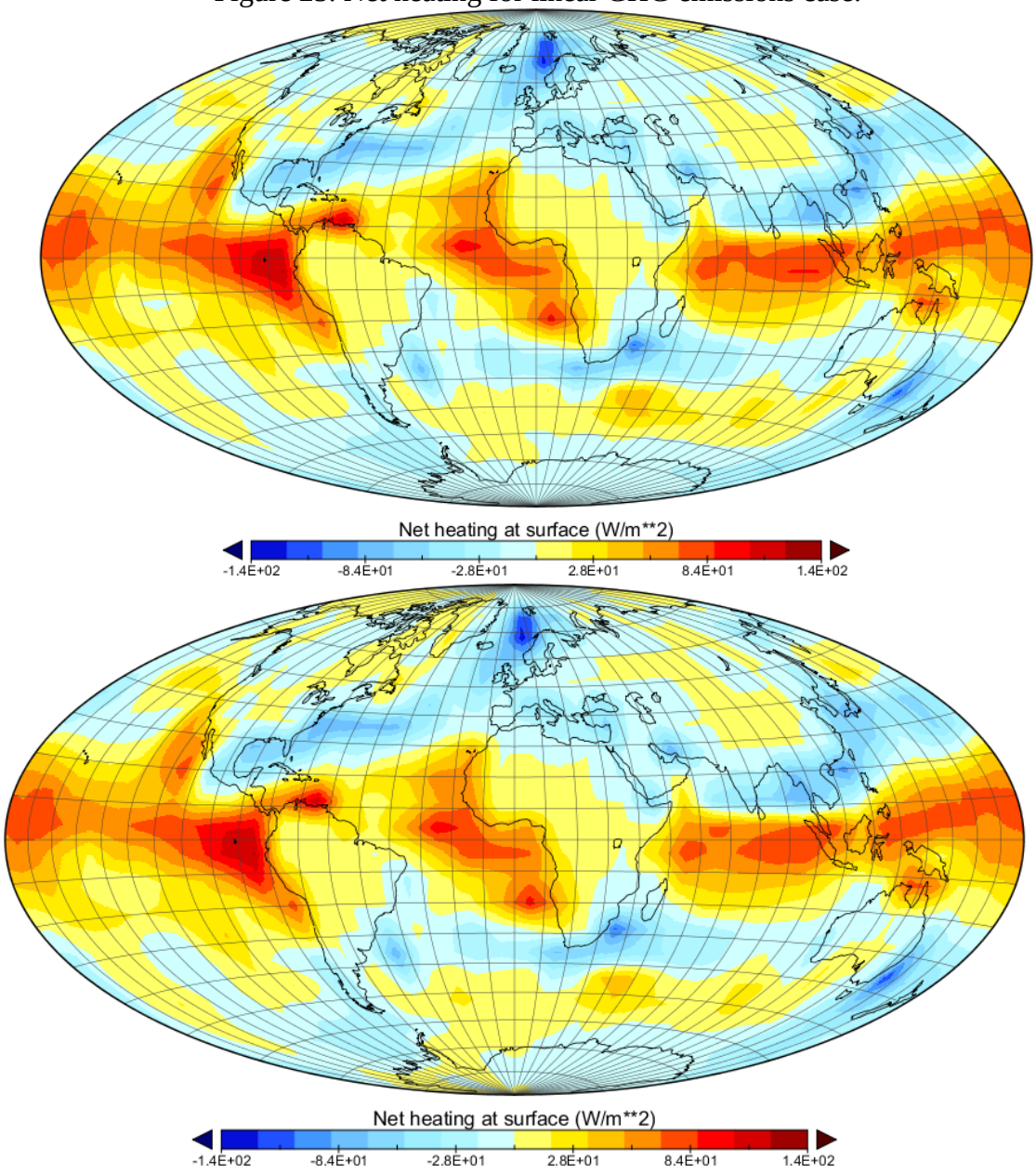

Figure 25 Cont

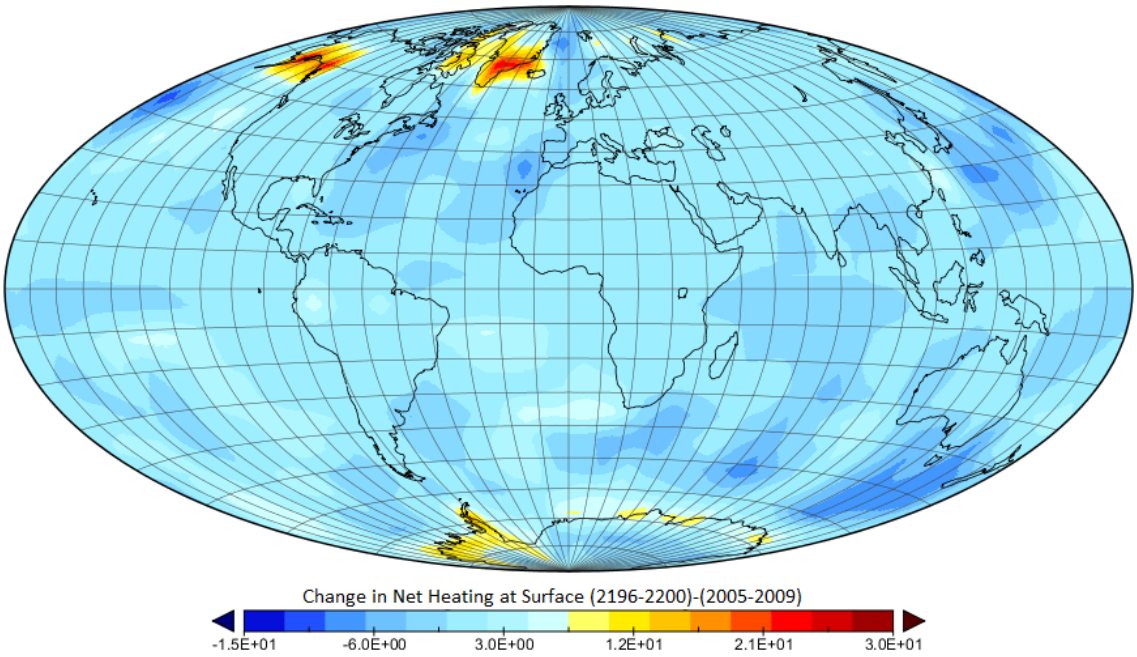


Figure 25. Net heating for linear GHG emissions case. (Top): Annual global net heating averaged over five years (2005-2009) as produced by the EdGCM climate model. Note the positive net heating along the equatorial regions (red colors), and the negative deficit off the coast of Norway (dark blue color). (Middle): Annual global neat heating averaged over five years (2196-2200). Most of the positive net heating at the surface occurs in the oceans. (Bottom): The difference between (2196-2200)-(2005-2009) in the net heating at the planet's surface in $W/m^2$. Most of the planet experiences a positive net heating ranging from 3-5 $W/m^2$, with the exception over Southern Greenland and Southern Alaska, where the change in net heating ranges from 12 to 22 $W/m^2$.

(Figure 26) is a gradient from the equatorial region (with positive net radiation flow) to the polar regions (with negative net radiation flow. It is this imbalance between the equatorial regions of the Earth and the polar regions that is responsible for circulation in the planet's oceans and atmosphere.

The global net heating distribution averaged over five years (2005-2009) shows a similar trend to that for the net radiation of the planet (Figure 26). There is a correlation between the net heating over the equatorial regions and the net radiation (Figure 26). There is an interesting deficit in the net heating seen off the northern coast of Norway.

This cold spot might be the result of the high latitude and significant cooling via evaporation from winds originating from the north polar region. The main cause of the gradient in the net heating over latitude is variations in albedo, and the amount of solar illumination, which changes with latitude. In the equatorial regions of the planet, the amount of solar radiation absorbed is greater than the amount of radiated heat. Oceans absorb solar radiation more efficiently and hold on to heat for longer periods of time than the continents. The slower resistance to temperature change over the oceans is due to the diffusion of the heat absorbed. In other words, it takes the oceans longer to revert back to their original state after warming or cooling. This explains why the climates of locations on or near the ocean tend to be more mild than those over the continents, and why the diurnal and seasonal variations in climate over these regions is minimized. This results in the positive net heating observed along the equatorial zone as can be seen in Figure 25. The high albedos from sea ice and snow over the polar regions results in a net deficit in the net radiation because the amount of solar energy absorbed is less than the amount radiated back to space (Figure 26).

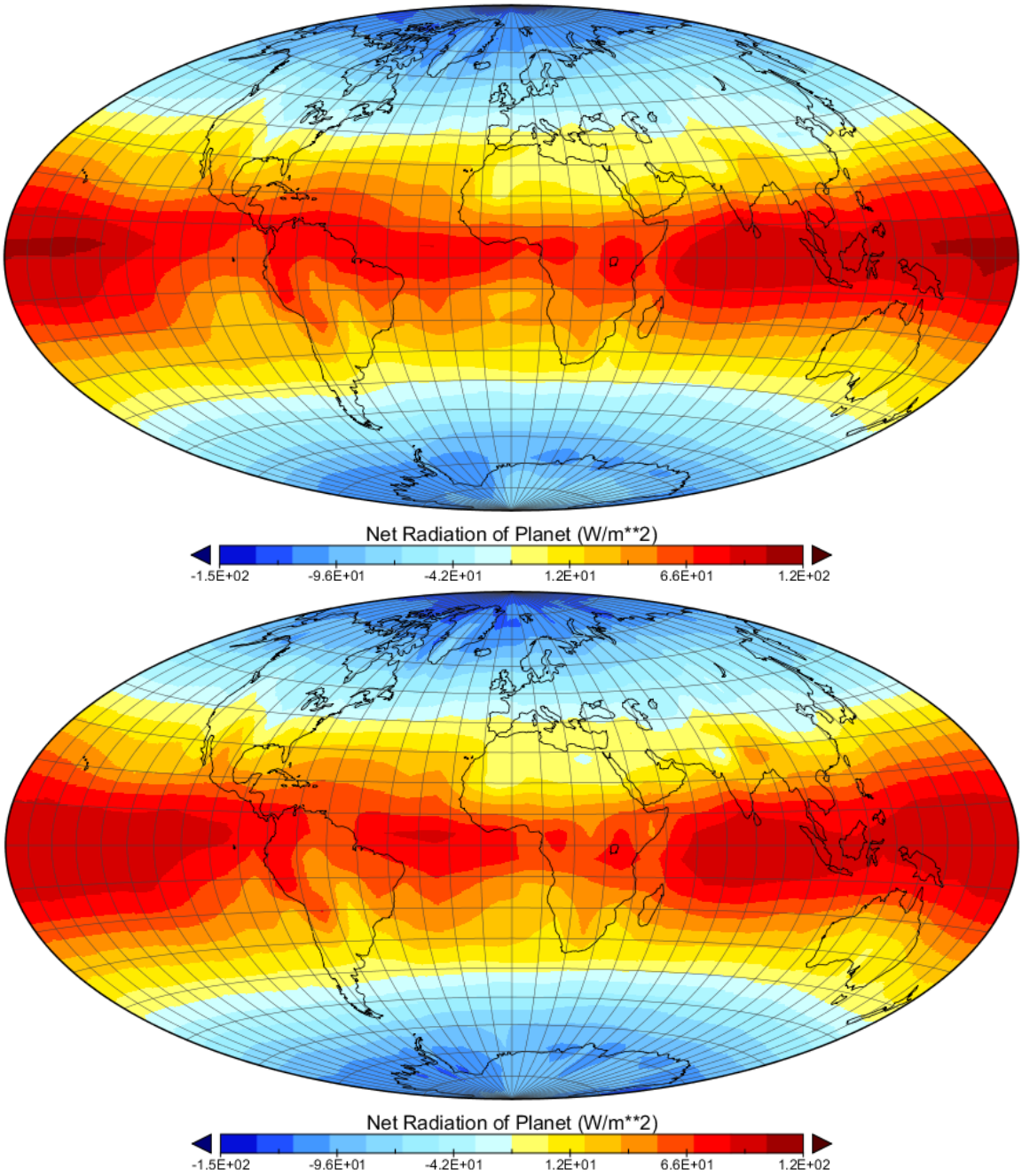


Figure 26. Net radiation for linear GHG emissions case. (Top): Annual global net radiation averaged over five years (2005-2009). Apparent in the map is the gradient in positive net radiation over the equatorial regions (red colors) to net negative radiation (blue colors) towards high latitudes. (Bottom): Annual global net radiation averaged over five years (2196-2200). Most of the net radiation occurs over the oceans (shades of red).

Figures 27 shows the annual surface air temperature averaged over five years to reduce noise in the climate model data. Figure 27 (top map) shows the average over the years 2096-2100. The maximum surface air temperatures occur over the equatorial region, and there is approximately an increase in 5℃ over the hottest equatorial regions, compared to the equatorial regions for the timespan ranging from the year 2005 to 2009. This is most likely due to the current trend in the increase of greenhouse gas emissions (from both natural and anthropogenic sources) over approximately 100 years. If we examine the global distribution of surface air temperatures over the timespan from 2196 to 2200 (Figure 27 bottom map), we see an increase of approximately 4℃ over the hottest regions of the equatorial region. Again, this is probably the result of the linear increase in greenhouse gas emissions (from $CO_2$, $CH_4$, and $N_2O$) over the next 100 years. This warming effect is due to the greenhouse effect acting over 200 years due to a linear increase in greenhouse gases in Earth's atmosphere. The greenhouse effect occurs because molecules such as oxygen and nitrogen have no permanent dipole moment and are thus transparent to incoming visible sunlight and outgoing thermal radiation. However, the three greenhouse gases used in this simulation, carbon dioxide, methane and nitrogen have dipole or temporary dipole moment produced by the molecule's different vibrational transitions. These different modes of molecular vibration allow the greenhouse gas molecule to absorb infrared radiation efficiently. The greenhouse gases are therefore opaque to outgoing long wave (thermal) radiation. A small amount the incoming radiation from the Sun is thus transferred to Earth's atmosphere, after the long wave (thermal) radiation is radiated from the surface of the Earth. One of the long-standing questions in global climate modeling is whether the source of increasing

greenhouse emissions is the result of natural processes or the result of anthropogenic factors.

Figure 27. Surface Air Temperature for the Linear GHG case.

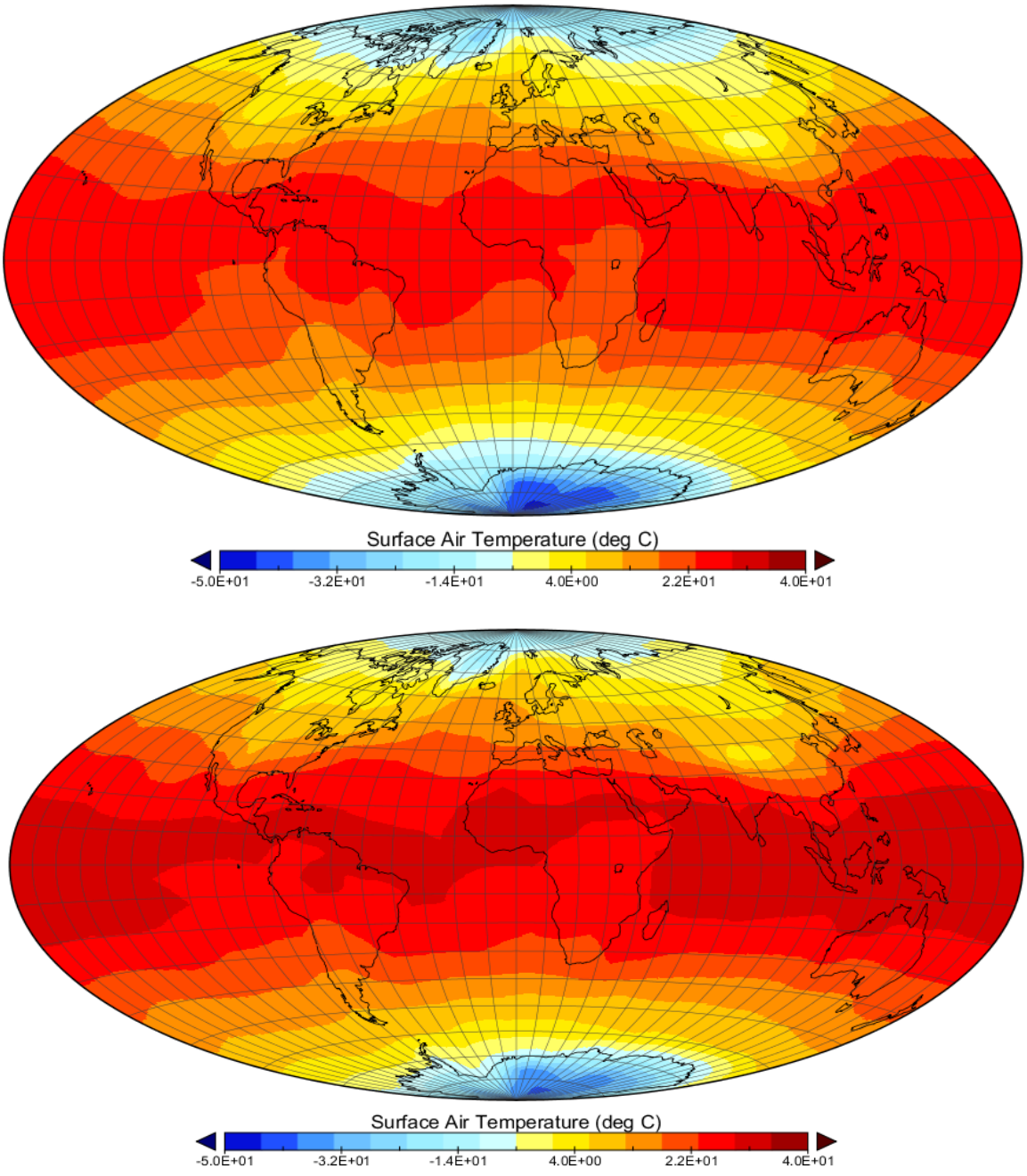

Figure 27 Cont

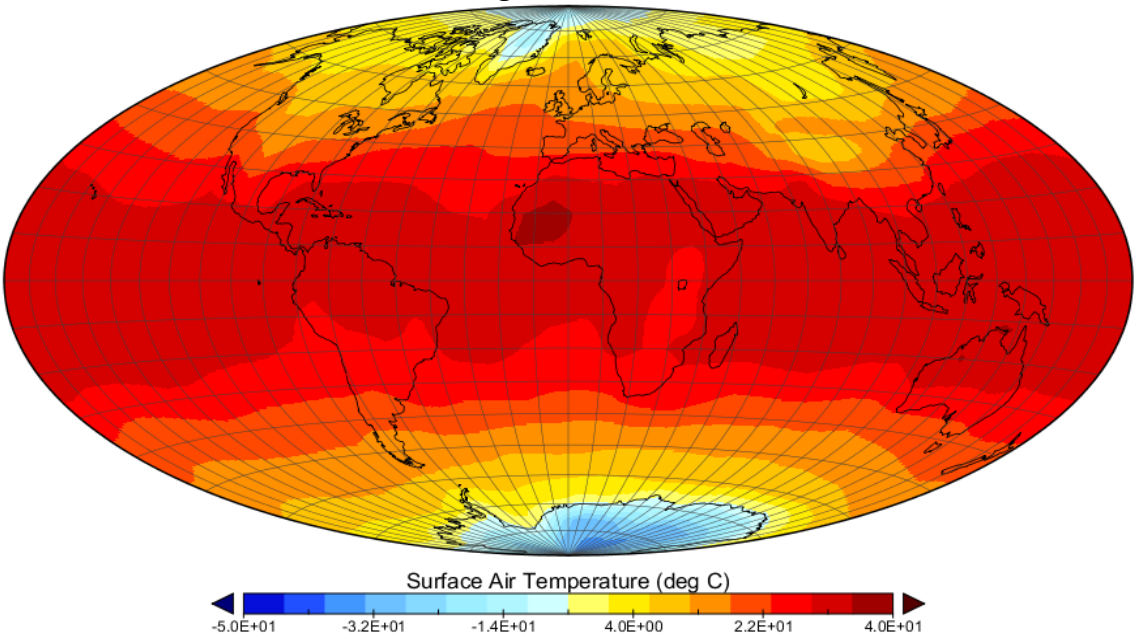


Figure 27. Surface Air Temperature for the Linear GHG case. Five year average of the annual global surface air temperature for the years 2005-2009. Five year average of the annual global surface air temperature for the years 2096-2100 (middle map) and for the timespan 2196-2200 (bottom map). On the top map the darkest red colors correspond to a temperature of 33℃, and the darkest red colors on the bottom map correspond to a temperature of 37℃. Note the warming of the polar region over 200 years of linear greenhouse gas emissions.

The next map (Figure 28) shows the temperature difference between the five-year annual averages of the surface air temperature for (2005-2009) and (2196-2200). The map shows the change in temperature over the Earth due to a linear increase in $CO_2$, $CH_4$, and $N_2O$ over 200 years, based on current estimates from the IPCC 2007 Working Group on Climate. The initial values for $CO_2$, $CH_4$, and $N_2O$ used in the EdGCM simulations were 379 ppm, 1.774 ppm, and 0.319 ppm for the year 2005. The assumed linear increases in the greenhouse gas emissions were 2.10 ppm/yr for $CO_2$, 0.018 ppm/yr for $CH_4$, and 0.0004 ppm/yr for $N_2O$. The key finding in the temperature difference map is the apparent rapid change in temperature over the polar regions of the planet due to 200

years of increasing greenhouse emissions. There is also an increase in temperatures over the land masses, and the ocean show lower temperatures. Heat energy is absorbed by Earth's oceans and transported around the planet. The oceans also act as one of the major sinks of carbon dioxide – it acts to remove carbon dioxide from Earth's atmosphere. The ocean can therefore be thought of as a large heat sink, which delays the effects of climate change due to radiative forcing, as a result of greenhouse emissions. The change in temperature over ~200 years shown in Figure 28 is the result of the combined effect of $CO_2$, $CH_4$, and $N_2O$ on the radiative forcing due to the emission of these greenhouse gases into Earth's atmosphere. It should be noted that this simulation did not include the contribution to the radiative forcing from CFCs, which have a strong GWP (Greenhouse Warming Potential) relative to the other three greenhouse gases.

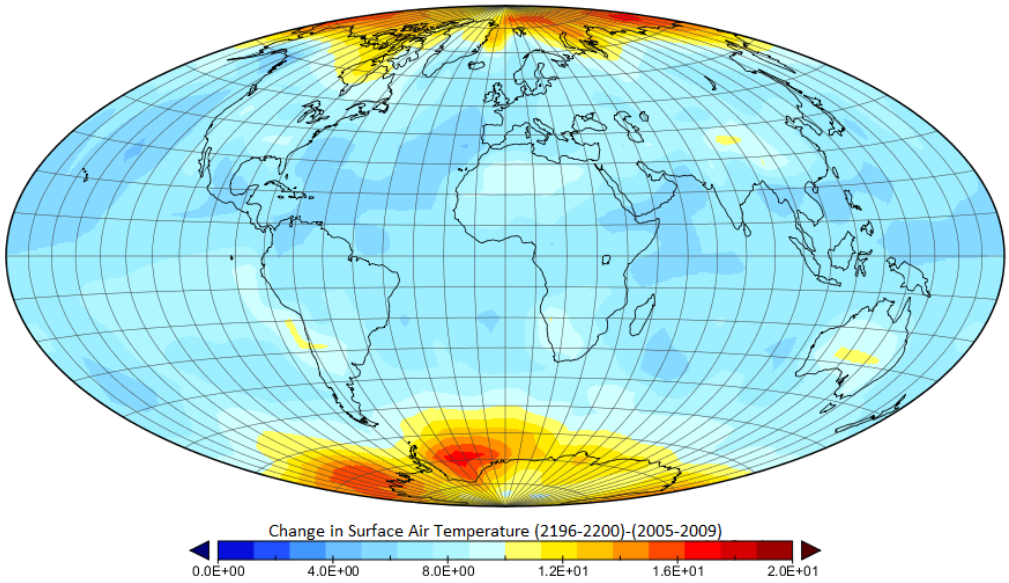


Figure 28. Annual temperature difference for linear GHG case. The five-year average annual temperature difference (2196-2200) - (2005-2009). The simulation assumes a linear increase of 2.10 ppm/yr, 0.018 ppm/yr, and 0.0004 ppm/yr for the three major greenhouse gases, $CO_2$, $CH_4$, and $N_2O$, respectively. The initial values of the three greenhouse gases used in the EdGCM simulation were 379 ppm, 1.774 ppm, and 0.319 ppm for $CO_2$, $CH_4$, and $N_2O$, respectively. The temperature scale at the bottom of the map is in units of Celsius.

An increase in greenhouse gas emissions over the next 200 years could result in the melting of a higher percentage of the Antarctic ice pack and underlying permafrost. There is a concern that the melting of the icepack could trigger a release of methane from clathrates within the permafrost, further amplifying the positive feedback process as a result of a stronger greenhouse effect.

Figure 29 shows the change in surface albedo that occurs over a simulation period of ~200 years. The data was averaged over the years (2005-2009) and (2196-2200). The difference map shows a remarkable correlation between the reduction in albedo at the polar regions (red shades in Figure 29) and the warming at the polar regions seen in Figure 28. This correlation can be explained by sea ice melting which reduces the total

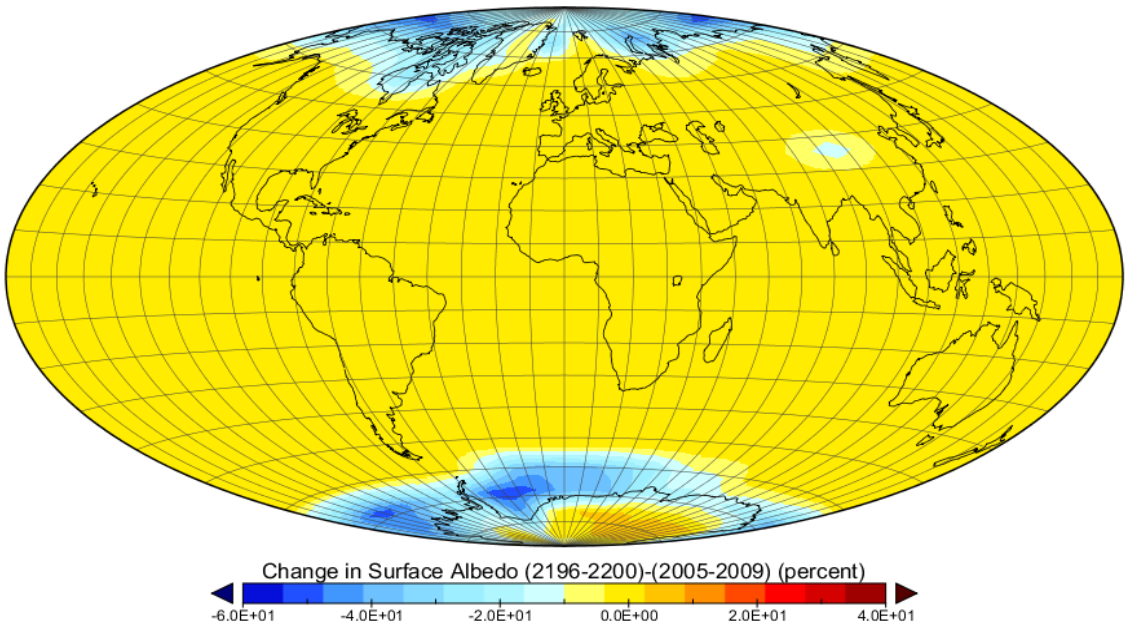


Figure 29. Change in albedo over a 200 year time span. The change in albedo over an ~200 year time period as simulated by EdGCM assuming a linear increase in greenhouse gas emissions. The specific five-year averages are for (2196-2200) and (2005-2009). The Hammer map projection shows a 30-50% decrease in the surface albedo over portions of the polar regions. The decrease in surface albedo correlates with the observed warming at the polar regions (Figure 26).

area of ice and exposes more dark surface area (lower albedo areas). This results in more absorption of solar radiation and an increase in temperature at the polar regions.

The annual global evaporation averaged over five-year periods (2005-2009 and 2196-2200) is shown in Figure 30. An examination of the Hammer projection maps shows that most of the evaporation (the phase change of water from a liquid to a gas) occurs over the seas and oceans, with a maximum occurring in southern India and the South China Sea. Since the process of evaporation requires heat energy, there is minimal evaporation that occurs over the planet's polar regions (shown as shades of blue in Figure 30). The energy is required to break the molecular bonds of the water molecules ($H_2O$), which is why there is far less evaporation that occurs over the north and south polar regions of Earth.

Figure 30. Global map showing evaporation for the linear GHG trend case.

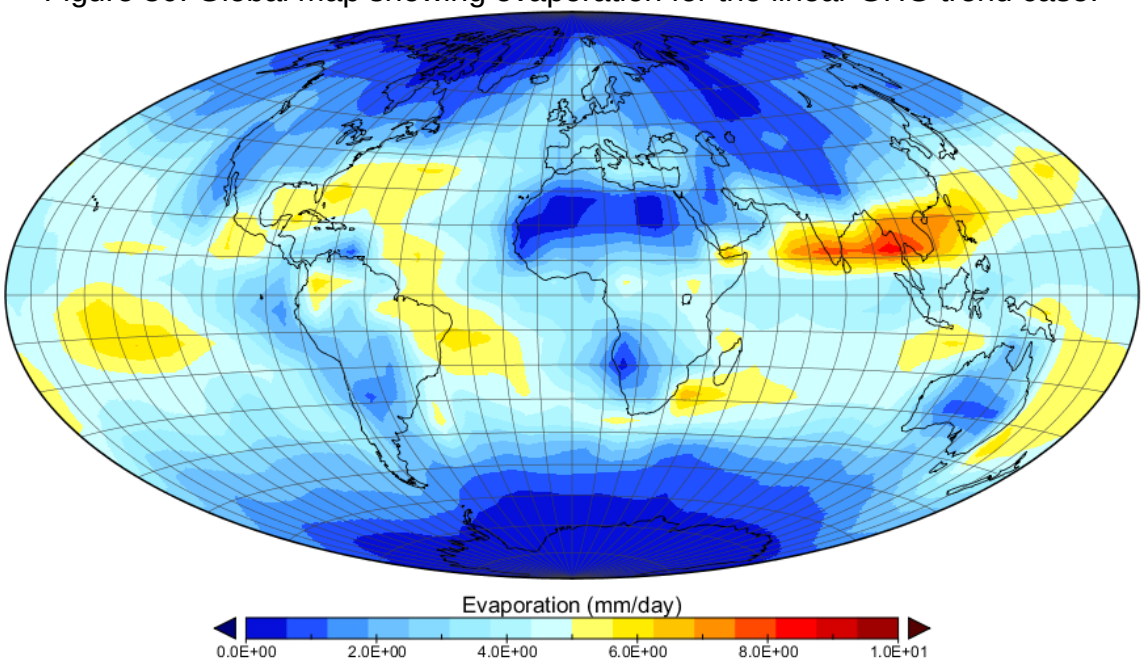

Figure 30 Cont

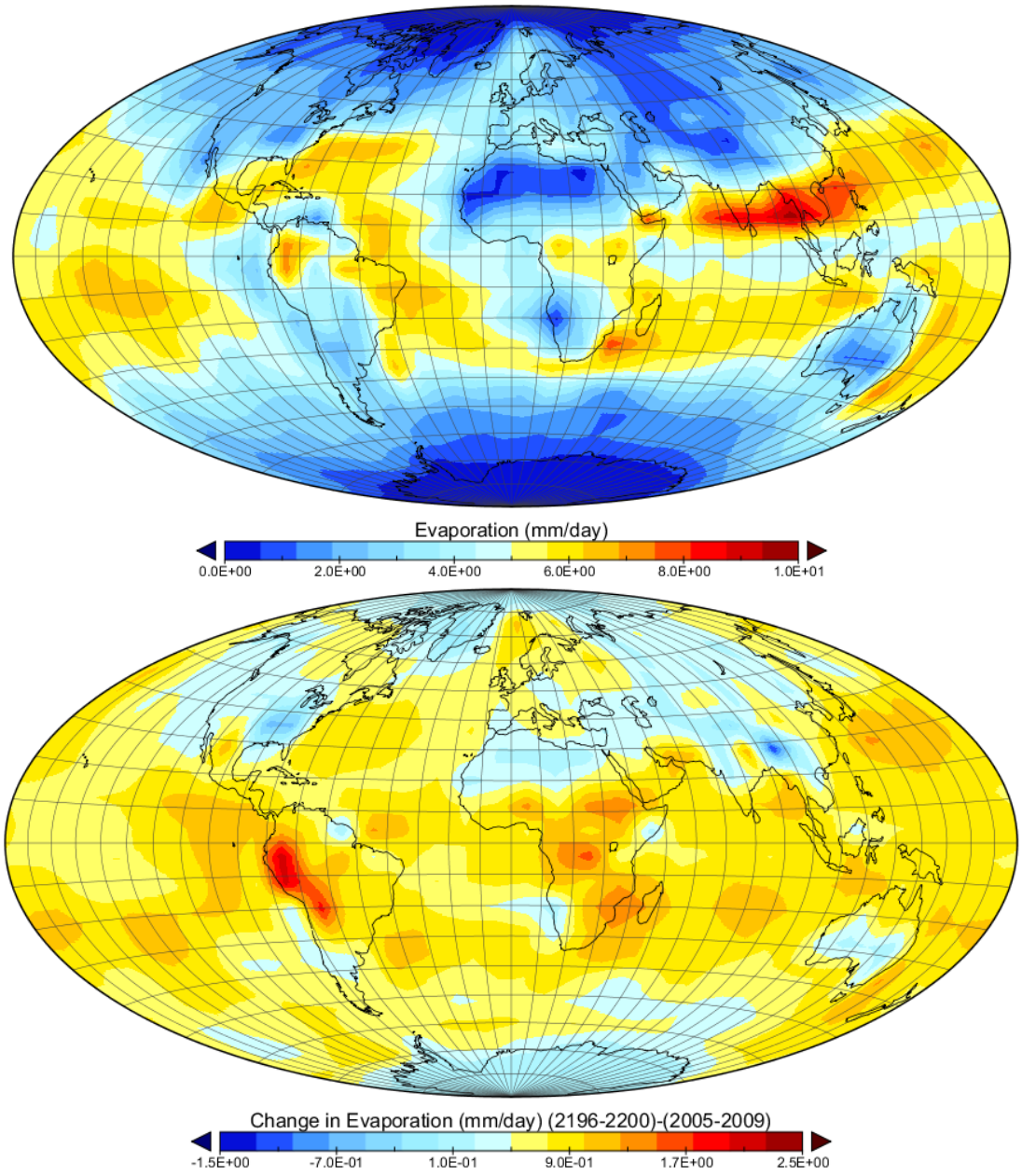


Figure 30. Global map showing evaporation for the linear GHG trend case. (Top): Annual evaporation in millimeters per day averaged over five years (2005-2009) to reduce noise in the data. (Middle): Annual evaporation in millimeters per day averaged over five years (2196-2200). In both cases, most of the evaporation occurs over the oceans, with the maximum occurring in southern India, Cambodia, Vietnam and the South China Sea. (Bottom): The difference in evaporation between (2196-2200)-(2005-2009). Note the increase in the evaporation rate over the oceanic regions.

The large amount of evaporation over southern India, Cambodia, Vietnam and the South China Sea is most likely responsible for the intense monsoon seasons experienced in this region of the world. Current research focuses on what sustains the intense Indian monsoon season, and what role does the heat budget of the ocean play on the monsoon season.

The next simulation results show the effects of radiative forcing resulting from an exponential (non-linear) increase in carbon dioxide emission of the ~200 year simulation period from 2005 to 2200 (Figure 31). The other two greenhouse gases, methane and nitrous oxide were kept at the current trends in the previous simulation.

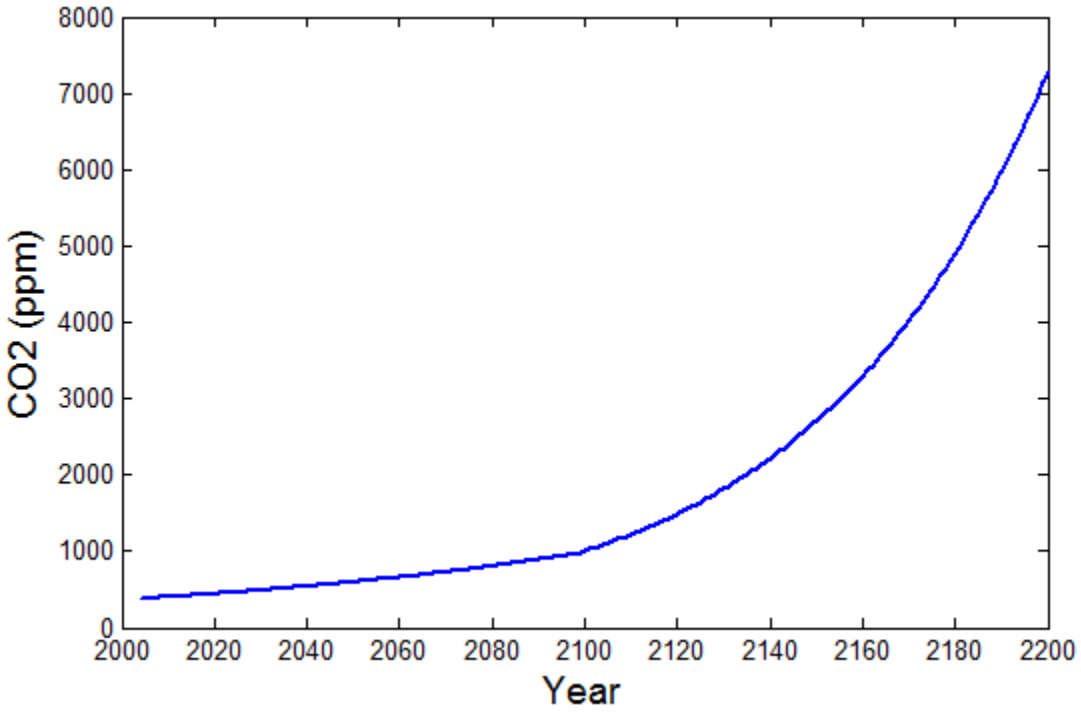


Figure 31. Exponential increase in carbon dioxide. The 2%/yr exponential (non-linear) increase in carbon dioxide ($CO_2$) over the time span 2005 to 2200 (~200 years) used in the EdGCM simulation. The initial value used for $CO_2$ is 380 ppm for the year 2005.

Exponential trends are commonly used in 3-D global climate models to investigate the suspected linear increase in temperature due to an exponential rise in

carbon dioxide ($CO_2$) in the Earth's atmosphere. The results of this simulation performed over approximately 200 years (2005-2200) explore the linear relationship between the exponential increase in $CO_2$ in the atmosphere and the radiative forcing due to the greenhouse gas emission. It is expected that the results will show an proportionate response in temperature rise since radiative forcing is directly proportional to the increase in temperature near the planet's surface. The annual surface air temperature averaged over five year intervals, starting from (2005-2009), (2096-2100), and (2179-2182) are shown in Figure 32. The exponential increase in carbon dioxide over 100 years has resulted in significant temperature changes over the high-latitude and polar regions of the planet. Figure 33 shows a zonal average plot of the difference in temperature between the five-year averages of (2179-2183) and (2005-2009). An examination of the plot shows that the greatest temperature changes are occurring at the polar region of the planet, with minimum to moderate changes occurring at the equatorial regions. This result confirms that changes in global climate tend to occur more rapidly at the Earth's polar regions. These changes at the planet's polar regions are one of the main drivers of global climate changes worldwide since there is a strong coupling between climatic systems. The polar regions also have extremely sensitive ecosystems that drive the various climate feedback mechanisms (reviewed in Chapter I) that effect global climate. The polar regions play a key role in maintaining the Earth's energy budget. The increased albedo due to polar ice and snow allows more solar radiation to be reflected, which protects the other regions of the planet from the effects of global warming. As the carbon dioxide greenhouse gas emissions rise exponential in this simulation, the polar regions lose some of their inherent inertia as a result of an increase in ice and snow melting. As more of the ice and snow

melt there is an increase in the area of lower albedo terrain, which allows more solar radiation to be absorbed by the Earth's surface. This cause an increase in temperatures at the polar regions which, in turn, result in more melting of the polar ice pack and snow – i.e. there is an amplification of a positive feedback mechanism.

The initial five-year annual temperature of Northern Africa is ~30℃ (2005-2009). After 100 years, the five-year annual temperature has risen to ~35℃, and after 200 years, the temperature over the same region has increased to ~40℃. This rise in temperature over 200 years may increase the severity of the Atlantic hurricane season due to the availability of warmer air at the location where Atlantic hurricanes originate from. It is interesting to note that an exponential increase in greenhouse gas emissions leads to a linear increase in the temperature rise with time.

Figure 32. Surface air temperature (°C) maps for an exponential increase in carbon dioxide.

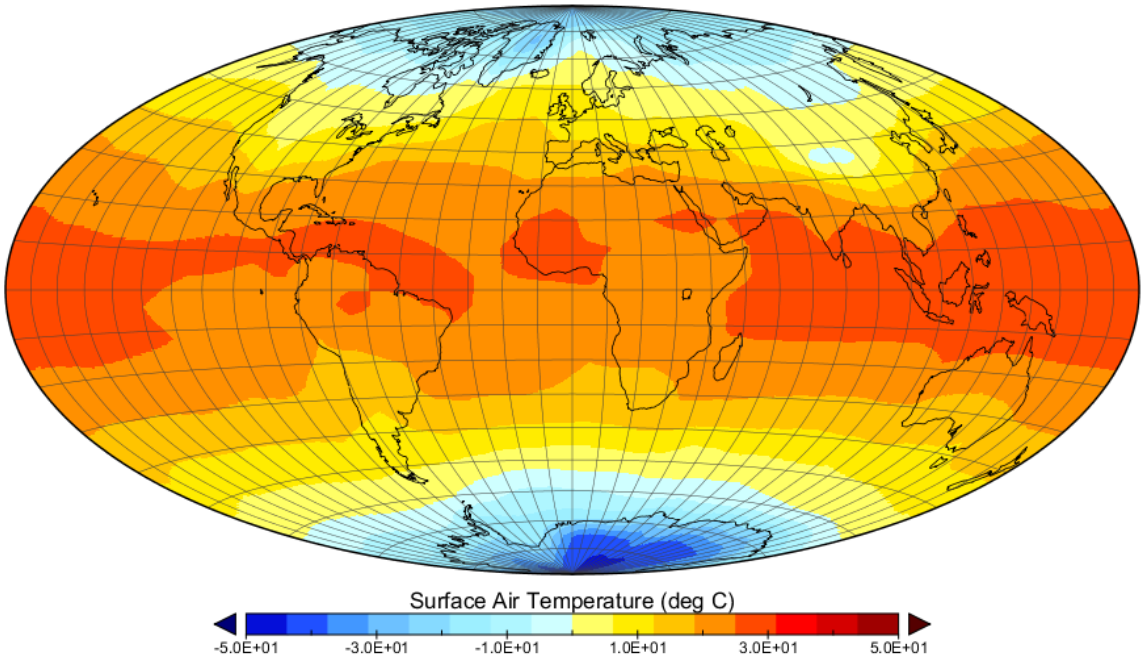

Figure 32 Cont

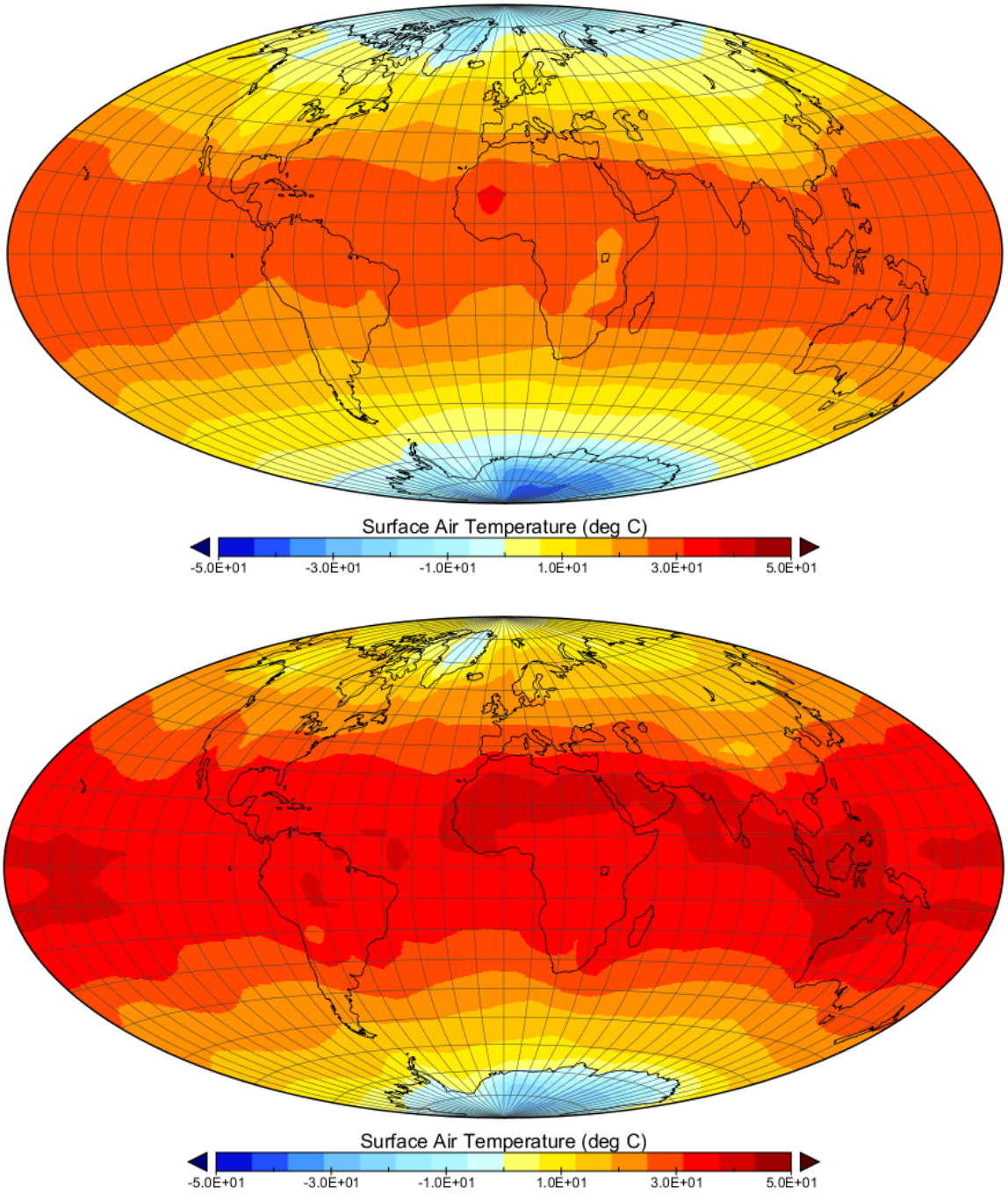

Figure 32 Cont

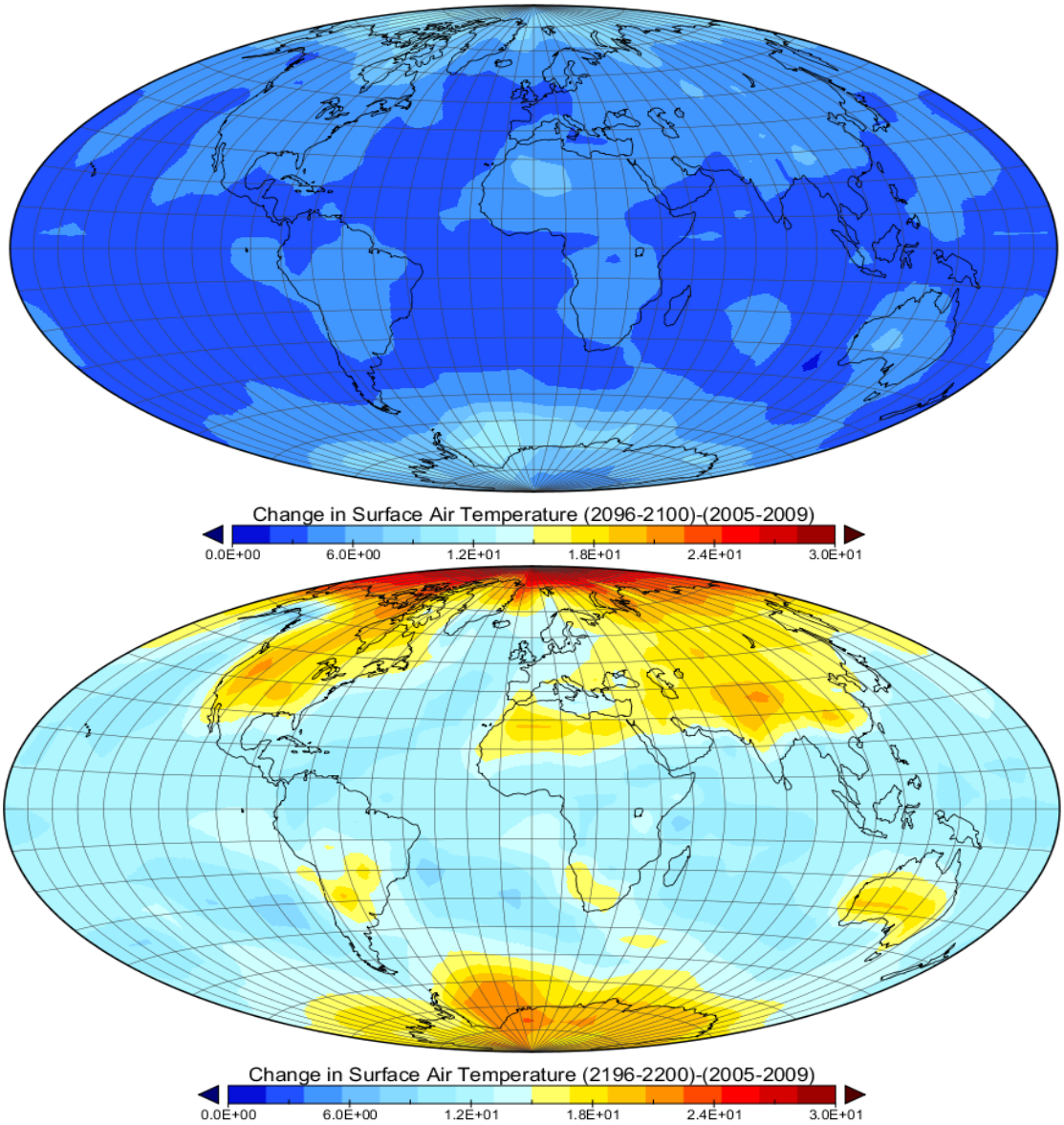


Figure 32. Surface air temperature (°C) maps for an exponential increase in carbon dioxide. The first map projection shows a five-year average of the annual surface air temperature from 2005-2009. The second map projection shows a five-year average of the annual surface air temperature from 2096-2100, and the third map shows another five-year average of the annual surface air temperature from 2196-2200. The fourth map shows the difference in the five-year average of the annual surface air temperature for (2096-2100) - (2005-2009). The fifth map in this sequence shows the difference in the five-year average of the annual surface air temperature for (2196-2200) - (2005-2009). The temperature difference maps illustrate the rapid change of climatic conditions that occur at the planet's polar regions and high-latitude regions, in contrast to the equatorial regions of the planet. In the temperature difference maps, shades of red indicate large temperature differences and shades of blue show relatively small changes in temperature.

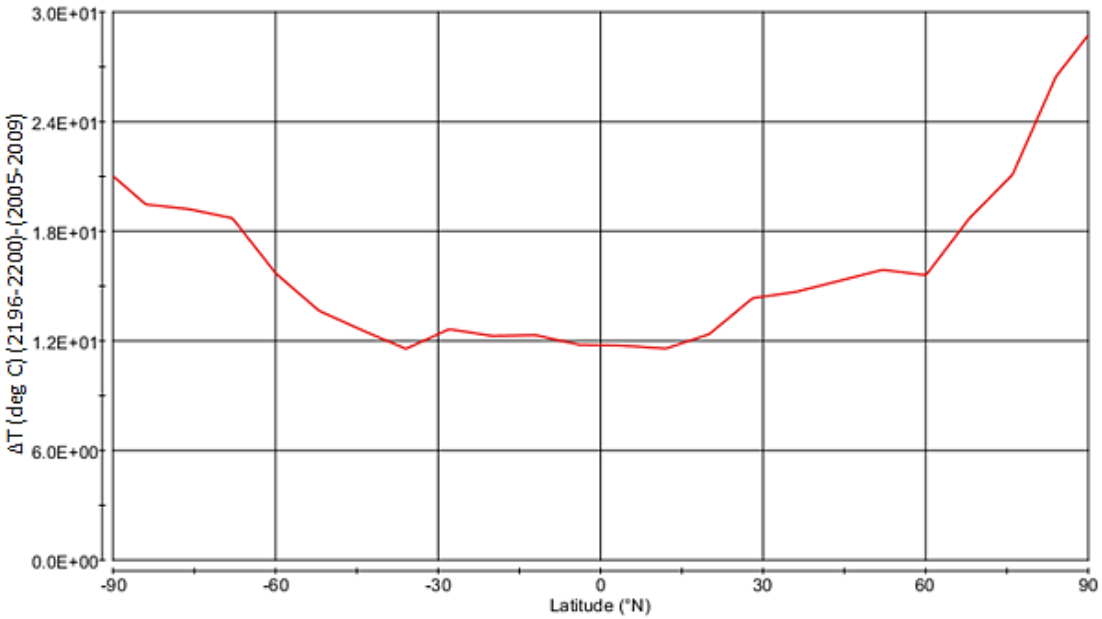


Figure 33. Zonal average distance of surface air temperature for an exponential increase in carbon dioxide. (Top): An alternative way to visualize the results of the 177 year climate model simulation. The plot shows the difference in the zonal averages for (2196-2200) and (2005-2009). Note the large differences that occur at the Earth's polar regions due to an exponential rise in carbon dioxide over the 177 year simulation.

The final results of the exponential trend in carbon dioxide indicate a temperature increase of approximately 4.5-5.0℃ per doubling of the $CO_2$ increase. It is fortunate that there is a linear response to the climate forcing due to an exponential increase in $CO_2$ greenhouse emissions – i.e. the response of the climate forcing becomes progressively smaller as a result of the increasing trend of carbon dioxide emission into the atmosphere. In other words, the same forcing is produced by each doubling of the carbon dioxide emission. For example, if there is an increase in $CO_2$ concentration from 200 to 400 ppmv, the response to the radiative forcing is the same as going from 800 to 1600 ppmv. It is the linear response to $CO_2$ increments that prevents drastic shifts in Earth's global climate that could otherwise render the planet inhabitable. It is important to note that the simulation presented here does not account for the fact that the planet is already in an

energy imbalance state. Therefore, the change in temperature resulting from the $CO_2$ emission may represent a lower limit – i.e. it may underestimate the global warming effect.

The next EdGCM simulation scenario deals with the case where current global warming results in melting of methane clathrates under the permafrost at the arctic region of the planet. As the permafrost under the arctic ice starts to melt in the year 2040, large amounts of methane ($CH_4$) is released. The instability of the methane clathrate leads to the release of methane gas into the atmosphere, and since methane is a potent greenhouse gas (with a GWP of ~25 times that of $CO_2$), its release could lead to an amplification of global warming. The global warming would be due to an amplification of the positive feedback mechanism – i.e. more warming at the arctic region accelerates the release of methane gas from clathrates stored in the permafrost, which further accelerate the positive feedback process (Harvey & Huang. 1995; Prather et al., 2001). Shakhova et al., 2008 estimate that in addition to the methane stored in the artic permafrost, additional amounts are also stored in the Siberian permafrost. The source of the methane stored in the form of clathrates results from the decay of microorganisms from warmer eras in Earth's history (Shakhova et al., 2008). Shakhova concludes from his studies that up to 50 gigatons of methane hydrate could be released into Earth's atmosphere at any given time in the near future, and that it would result in an increase in the methane concentration by a factor of twelve (Shakhova et al., 2008).

In order to explore the consequences resulting from a large release of methane from clathrates stored in the artic and Siberian permafrost on Earth's climate, an EdGCM

simulation was carried out using a linear increase in the concentration of methane in Earth's atmosphere, starting in the year 2040 (Figure 34).

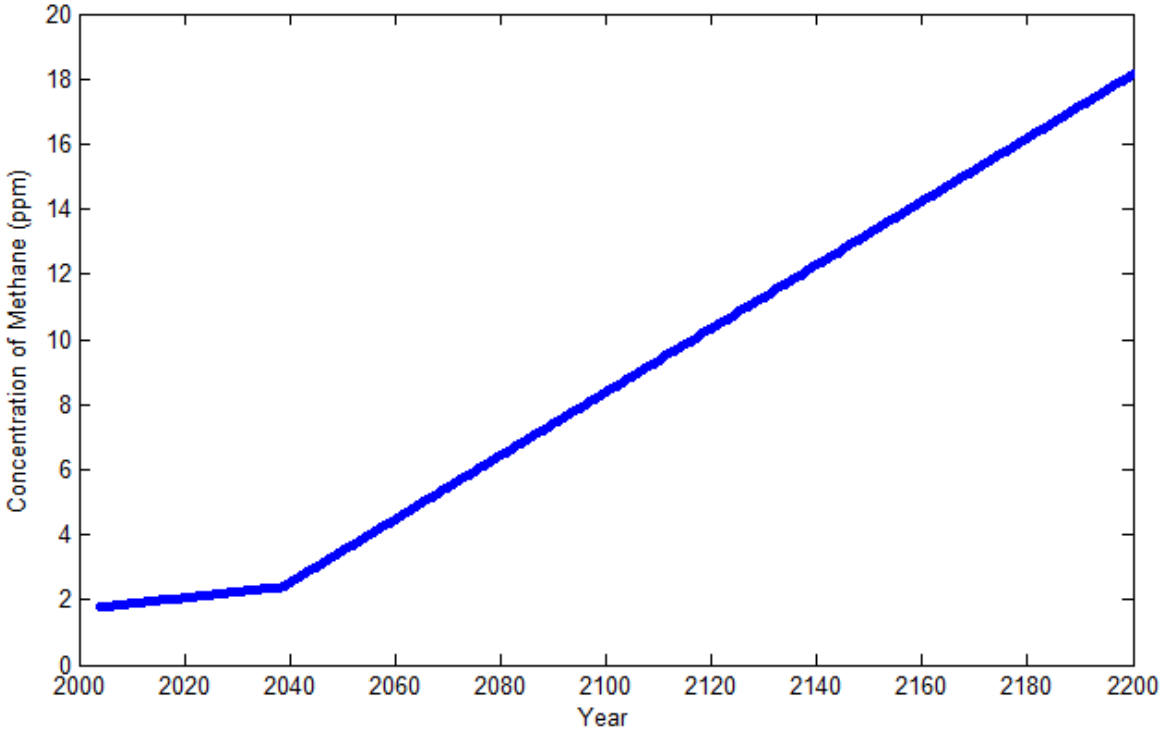


Figure 34. Methane concentration for the clathrate melt case. Initial condition and trending of methane concentration over the simulation period of approximately 200 years.

The initial concentration of methane starts out at 1.774 ppm in the year 2005. From the year 2005 to 2040, there is a linear increase in the concentration of methane of only 0.018 ppm per year. At the start of 2040, there is a continuous release of methane gas from hydrates resulting in a steeper rise in the concentration of the potent greenhouse gas. From 2040 to 2200, there is a change of 0.0976 ppm per year. The concentration of methane reaches approximately 18 ppm at the year 2200. Figure 35 is a Hammer projection map showing the five-year average of the annual surface air temperature as simulated by EdGCM. The top map in Figure 35 shows the surface air temperature at the

start of the simulation, and the second map in Figure 35 shows the surface air temperature after approximately 200

Figure 35. Surface air temperatures for the methane clathrate simulation

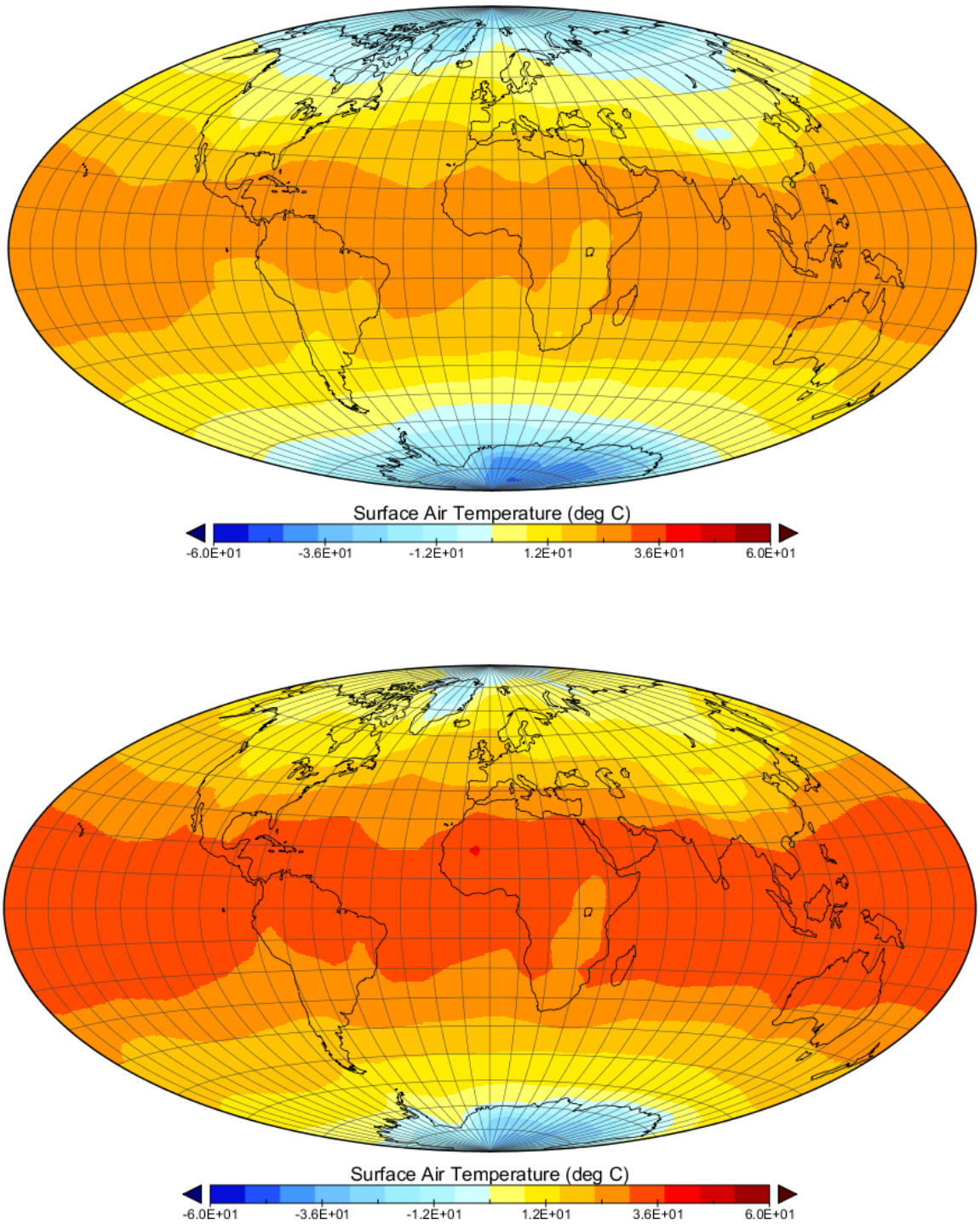

Figure 35 Cont

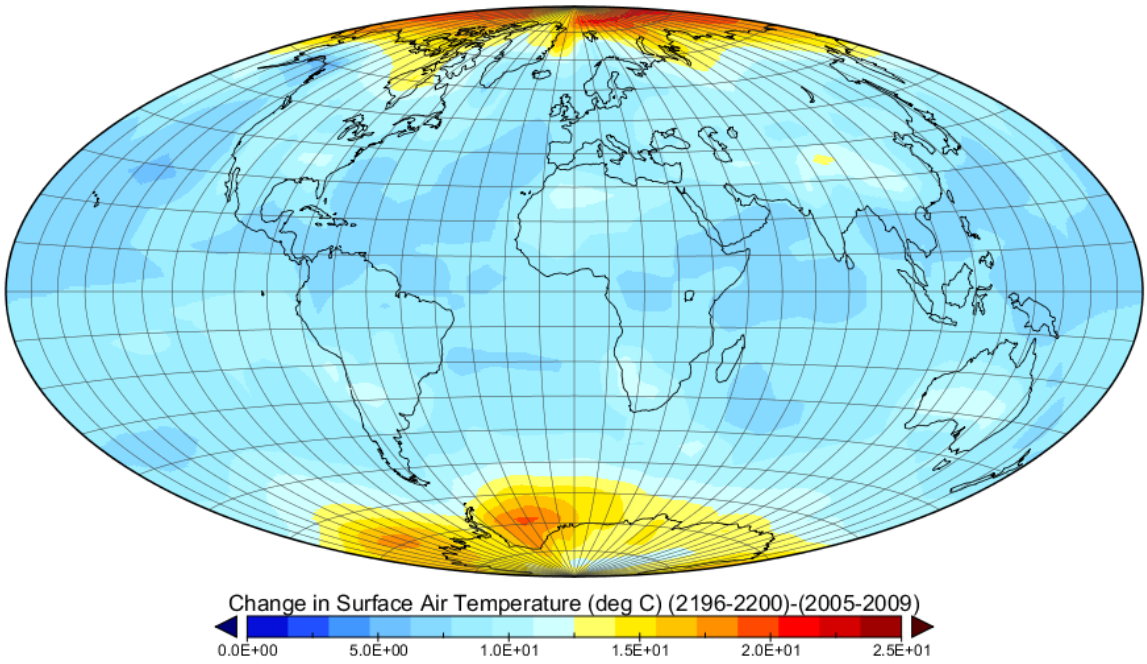


Figure 35. Surface air temperatures for the methane clathrate simulation. (Top): Hammer projection map showing five-year average of the annual surface air temperature from 2005-2009. (Middle): Global distribution of the five-year average of the annual surface air temperature from 2196-2200 (approximately 200 years of simulation time). (Bottom): A difference map showing the change in the surface air temperature between the five-year averages (2196-2200) - (2005-2009). Shades a red show large temperature changes (polar regions) and shades of blue denote smaller differences in the temperature.

years. The is an increase in the temperature of approximately 8℃ over the equator regions and an increase in the surface air temperature of approximately 20-23℃ over parts of the north polar region due to the exponential increase in methane over the 200 year time span. This is better illustrated in the temperature difference map (bottom map on Figure 35) between the five year averages (2196-2200 and 2005-2009) of the annual surface air temperature. As with previous simulations, we see the most significant changes occurring over the polar regions due to radiative forcing resulting from an

exponential increase of methane into the atmosphere – i.e. drastic change in the planet's climate occur over the polar regions first. The temperature increase is illustrated in the zonal average plot of the difference between 2005-2009 and 2196-2200 surface air temperatures (Figure 36.).

The results of the methane clathrate scenario illustrate the important role that future methane emission could have on the global climate. Methane is the most important greenhouse gas apart from carbon dioxide, and it's radiative efficiency is estimated to be approximately $3.7\times10^{-4}$ W/m$^2$/ppb compared to carbon dioxide's radiative efficiency of $1.5\times10^{-5}$ W/m$^2$/ppb. Thus, the radiative efficiency of methane is approximately an order of magnitude greater than carbon dioxide (Ramaswamy et al., 2001). This explains why methane is such a potent greenhouse gas, with a radiative forcing of approximately 0.48 W/m$^2$ (2008) in comparison to preindustrial times (Ramaswamy et al. 2001). It must be pointed out that this simulation represents a worst case scenario, and is subjected to debate as it is not known with high accuracy the amount of methane that could be released due to hydrate instability brought on by global climate warming. The simulation represents a hypothetical experiment to determine one possible outcome as a result of the amplification of the positive feedback mechanism associated with a significant increase in $CH_4$ emission into Earth's atmosphere. It should be noted however, that any release of additional $CH_4$ due to the instability of hydrates within the arctic and Siberian permafrost layers over the next 200 years, would be in addition to current anthropogenic methane gas emissions. This could lead to an even greater enhancement of the resulting positive feedback process (Harvey & Huang, 1995; Prather et al., 2001).

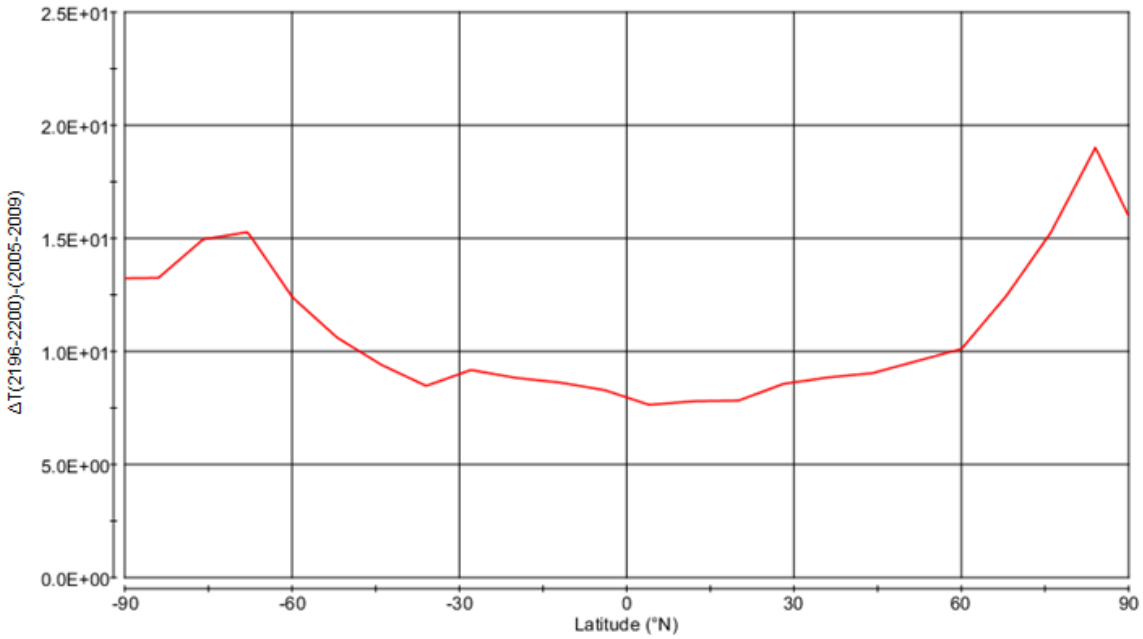


Figure 36. Zonal average difference of air temperatures for methane clathrate case. A zonal average plot showing the difference between the 2196-2200 and 2005-2009 five-year averages of the annual surface air temperature. Note the large temperature changes occurring at the planet's polar regions.

**Simulation of a Long-period Solar Minimum**

The next simulation modeled a hypothetical Maunder minimum or a long period of reduced solar irradiance. The simulation modeled a reduced solar irradiance (1360 $W/m^2$) relative to the normal solar irradiance of 1366 $W/m^2$ at 1 AU just outside of the Earth's atmosphere. The reduced total solar irradiance (TSI) used in the simulation was based on the -5.8 $W/m^2$ value for the TSI over the 70 year period Maunder Minimum (Shapiro et al., 2011). It should be noted that this drop in the TSI is relative to the 2008/2009 solar minimum. The goal of the simulation is to determine the sensitivity of the EdGCM (GISS GCM-II) to a long-term reduction in the solar irradiance of 6 $W/m^2$ over a period of 200 years. It is of interest if the simulation shows results that are identical to those experience during the Maunder Minimum in the late $17^{th}$ century. During the Maunder Minimum of the $17^{th}$ century, regions of the planet experience

significantly lower temperatures relative to the normal temperature, especially in the Northern Hemisphere. The greenhouse emission rate is set to that used for the first simulation carried out in this work. It is of interest to determine whether the radiative forcing due to the present increase in greenhouse gas emissions will dominate the radiative forcing due to a prolonged solar minimum.

The radiative forcing due to a prolonged decrease in the TSI can be estimated from the relation given by Meehl (2003).

$$\Delta F_{TSI} = \frac{0.7 \cdot \Delta TSI}{4} \quad (27)$$

The 1/4 factor in the equation accounts for the spherical geometry, and 0.7 is the albedo parameter (Meehl, 2003). The albedo parameter is determined by the average albedo of the Earth (~30% or ~0.30), and is simply 1.0-A, where A is the average albedo of the Earth. An increase in the radiative forcing due to the change in TSI results in an increase in the planet's energy imbalance. In other words, larger changes in the TSI imply larger effects due to the resulting change in the radiative forcing. As a result of the change in radiative forcing due to the change in the TSI, there is a change in global temperature. The change in temperature is calculated as

$$\Delta T = \lambda \cdot \Delta F_{TSI} \quad (28)$$

where $\lambda$ (℃/[W/m$^2$]) is a parameter describing the sensitivity of climate change due to the radiative forcing. For the decrease in TSI of -6 W/m$^2$ over 200 years in this simulation, the radiative forcing is estimated as

$$\Delta F_{TSI} = \frac{0.7 \cdot \Delta TSI}{4} = \frac{0.7\left(6.0 W / m^2\right)}{4} = -1.05 W / m^2 \quad (29)$$

where 6 W/m$^2$ is the value of the decrease in the TSI due to the prolonged solar minimum. The climate sensitivity parameter, λ, ranges from ~0.54 to 1.2 ℃/(W/m$^2$), as determined for a 2 to 4.5 ℃ increase in temperature as a result of a doubling of $CO_2$ (IPCC 2007). Based on this range estimate for the climate sensitivity parameter, the change in global temperature in response to radiative forcing due to the change in TSI is calculated as

$$\Delta T = \lambda \cdot \Delta F_{TSI} = \left(0.54^{\circ} C / (W / m^2)\right)\left(-1.05 W / m^2\right) = -0.57\ ^{\circ} C$$
$$\Delta T = \lambda \cdot \Delta F_{TSI} = \left(1.2^{\circ} C / (W / m^2)\right)\left(-1.05 W / m^2\right) = -1.26\ ^{\circ} C \quad (30)$$

where 0.54 and 1.2 ℃/(W/m$^2$) are the lower and upper limits of the climate sensitivity parameter.

Results from this simulation indicate a small negative temperature anomaly in the zonal average, ranging from approximately -1.5 ℃ to -0.65 ℃. This compares favorably with the theoretical estimate of the total global temperature change (ranging from -0.57 ℃ to -1.26 ℃), resulting from a prolonged decrease in the total solar irradiance (TSI) over a period of ~200 years. Although this simulation used a minimum period with a much longer duration that the Maunder minimum of ~50 years, other solar type stars could have periods on the order of the one used in this hypothetical case. Furthermore, it is not presently known whether or not the Sun represents a typical solar type star. It is of interest to note, in contrast to the previous EdGCM simulations, the complex pattern seen in the temperature anomaly map (Figure 37). The result of the simulation indicates that there is no distinct contrast in temperature anomaly between the polar regions and the rest of the planet, in contrast to the different greenhouse gas emission scenarios presented earlier in this research. The maximum negative temperature anomaly occurs over a small

region of the arctic (shown as the dark blue shade on the Hammer projected map in Figure 37). The zonal average shows a trend

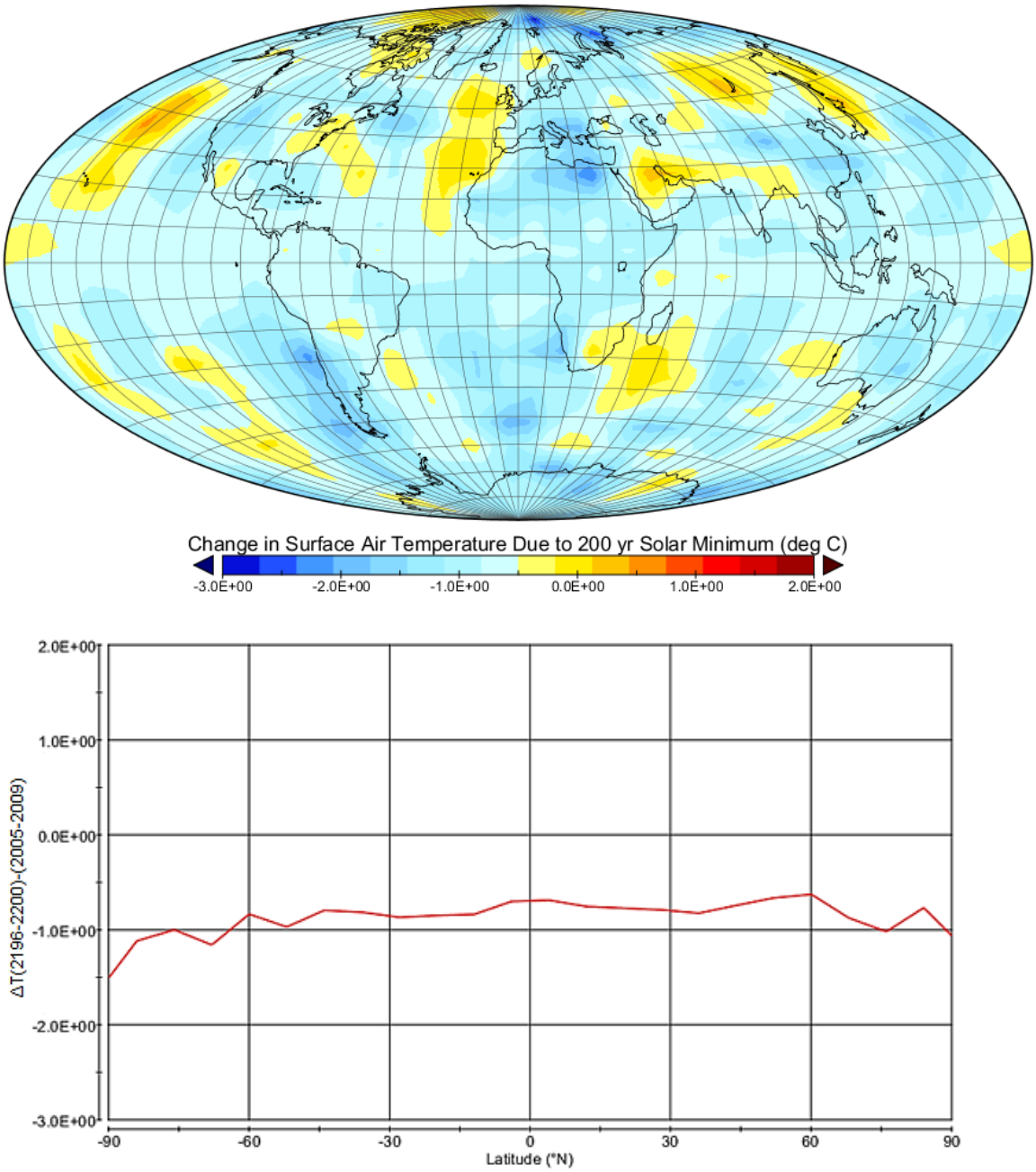


Figure 37. (Top): Difference between the five-year averages (2196-2200) of the annual surface air temperature (in degrees Celsius) for only the greenhouse gas emissions simulations and that including a 200-year decrease in the solar irradiance by 6 W/m$^2$ (a prolonged solar minima). Bottom: The zonal average of the data shown at the top. There is a slight negative temperature anomaly seen in the zonal average plot, ranging from approximately -1.5℃ to -0.65℃.

towards stronger negative temperature anomalies at the polar regions, particularly over the south polar region of Earth. Southern Europe and Northern Africa show negative temperature anomalies ranging from -2.2℃ to -1.2℃. During the last Maunder Minimum in the late 17$^{th}$ century, parts of Europe and North America also experienced colder temperatures.

The difference in net heating of the planet between the case where only the emission of greenhouse gases is assumed and that including the effects due to radiative forcing from a prolonged solar minimum cycle of 200 years is shown in Figure 38. The map displays both negative and positive deficits of net radiation in units of W/m$^2$. Most of the oceanic regions show a negative net heating ranging from -1 to -7 W/m$^2$.

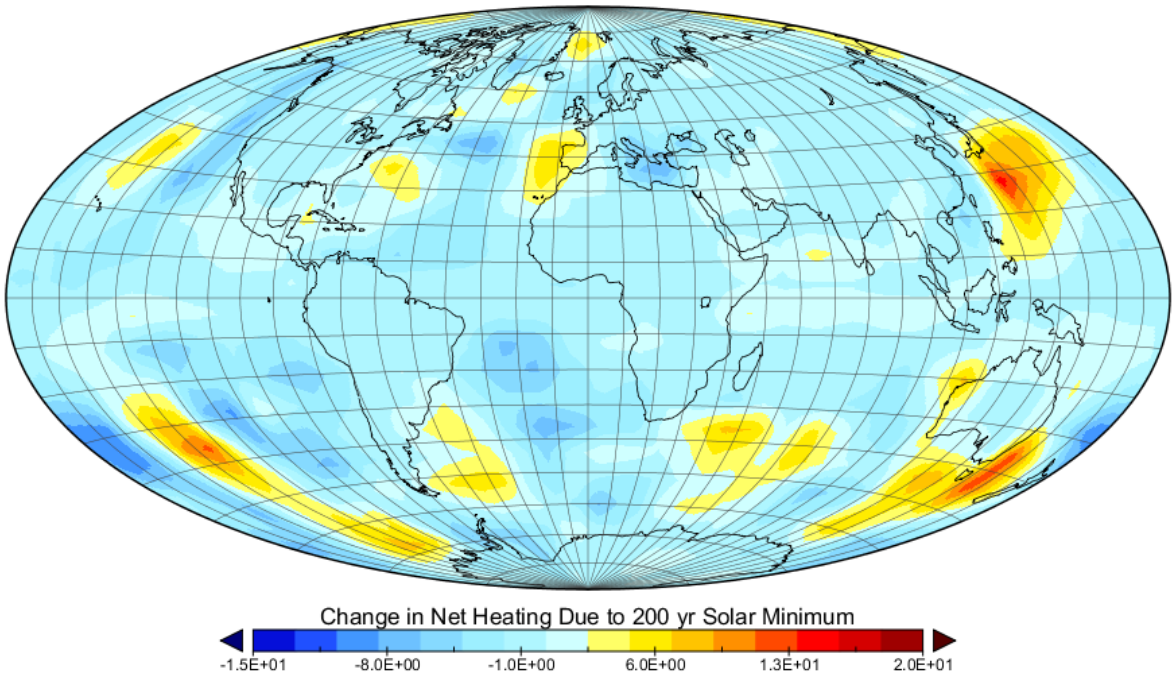


Figure 38. Net heating results for prolonged solar minimum simulation. Net heating (W/m$^2$) experienced by the planet due to a 200-yr prolonged solar minimum of -6 W/m$^2$. A large portion of the planet's oceans experiences net negative heating ranging from -1 to -4 W/m$^2$.

## EdGCM Results for Variations in an Earth-like Planet's Obliquity and Eccentricity

One of the most important factors for determining the climate and habitability of an Earth-like planet is the tilt of the planet's rotation axis from the vertical. This axial tilt, known as the obliquity, governs the amount of stellar radiation each region the planet receives during its orbital cycle around the host star. It is the obliquity of an Earth-like planet that is the primary driver for seasonal changes during its orbit around the parent star, especially for planets with very low orbital eccentricity. Earth-like planets with high eccentricities (those planets with eccentricities greater than about 0.1) have seasons (for non-zero obliquities) governed by their obliquities and eccentricities. For Earth's orbital eccentricity of 0.0167, the primary driver of the seasons is the obliquity of the planet. For an Earth-like planet with zero obliquity (no axial tilt), there would be negligible seasonal activity from year to year, since there would be no net difference in the amount of stellar radiation received anywhere on the planet during the planet's orbital cycle. As the obliquity of an Earth-like planet increases the intensity of seasonal changes becomes greater. In other words, the individual seasons in each hemisphere of the planet would be greatly exaggerated. The summers would be more intense for high obliquities (>45 degrees) since the hemisphere experiencing the summer would be pointed more towards the star. Hence, that hemisphere would receive more direct stellar radiation – i.e. the hemisphere experiencing the summer season on the planet would experience a longer period during which it receives stellar radiation. During the winter season, this hemisphere would experience less time receiving radiation from its parent star, since it

would be oriented away from the stellar radiation. Since there would be a deficit of radiation from the star during the short daytime and long nighttime diurnal cycle, the hemisphere's temperature would decrease. The effects of changing obliquity with time are negligible, since the time span of these climate model simulations is on the order of 200 years.

Earth-like planets with large eccentricities can experience climate changes, in addition to those caused by the planet's obliquity. In contrast obliquity, which produces climatic changes at the planet's polar regions first, eccentricity affects the amount of energy the whole planet receives. The higher the eccentricity, the greater the effect on the planet's climate. If a high-eccentricity planet is at perihelion (the point of closest approach to its parent star) at the same time the planet is experiencing its summer season, than due to the increase in solar irradiance, the summer season will be enhanced. The opposite is true for a high-eccentricity planet experiences its winter season at the same time it is at aphelion, where the entire planet receives less solar insolation.

To explore the effects of both obliquity and eccentricity of an Earth-like planet's climate, EdGCM was used to produce 3-D climate models over short-time periods (less than 30 years). This time limitation was due to instabilities in the climate model code as a result of extreme initial conditions of the axial tilt and eccentricity. Due to the complexity and computer time constraints, the combined effect due to obliquity and eccentricity were not considered in the simulations.

The first simulation uses the same values for the greenhouse gas emissions that were utilized in the first simulation of this work, but with the planet's axial tile (obliquity) set to zero degrees. The results of the EdGCM simulations show that the net

radiation and net heating do not show significant variation during the course of the five orbital cycles (four seasons per orbit cycle). This is expected since a an Earth-like planet with an axial tilt of zero will receive equal amounts of stellar radiation during an orbital cycle (Figure 39).

During all four seasons, the Earth-like planet receives more radiation from the star over its equatorial regions, as is expected for a planet with zero obliquity (Figure 40). The slight variations in the net radiation and heating over the four seasons is due to the eccentricity of the planet's orbit.

The five-year average of the seasonal surface air temperature (2026-2030) shows very little change in the polar regions of the planet (Figure 40), with no significant changes observed over the rest of the planet during the five orbital cycles of the planet. The equatorial regions of the planet show the highest surface air temperatures. The results of this simulation confirm the expected outcome that there are minimal seasonal variations in climate for an Earth-like planet with zero axial tilt (obliquity). Any minor variations from season to season is most likely due to the eccentricity of the planet's orbit, where the planet receivers more or less radiation from the host star (in this case the Sun), depending whether it is at perihelion or aphelion, respectively.

Figure 39. Net radiation (at top of atmosphere) maps for obliquity of zero degrees

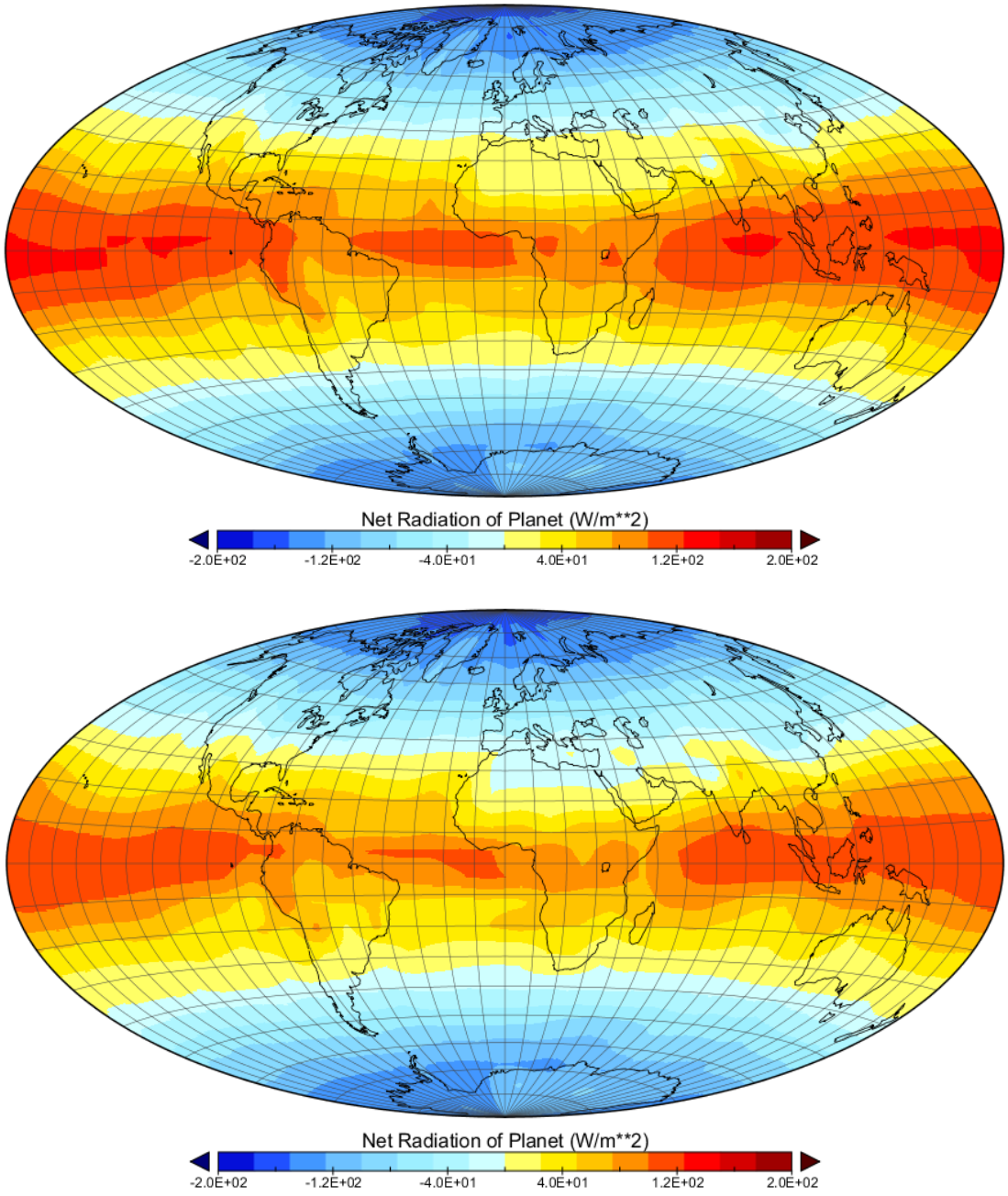

Figure 39 Cont

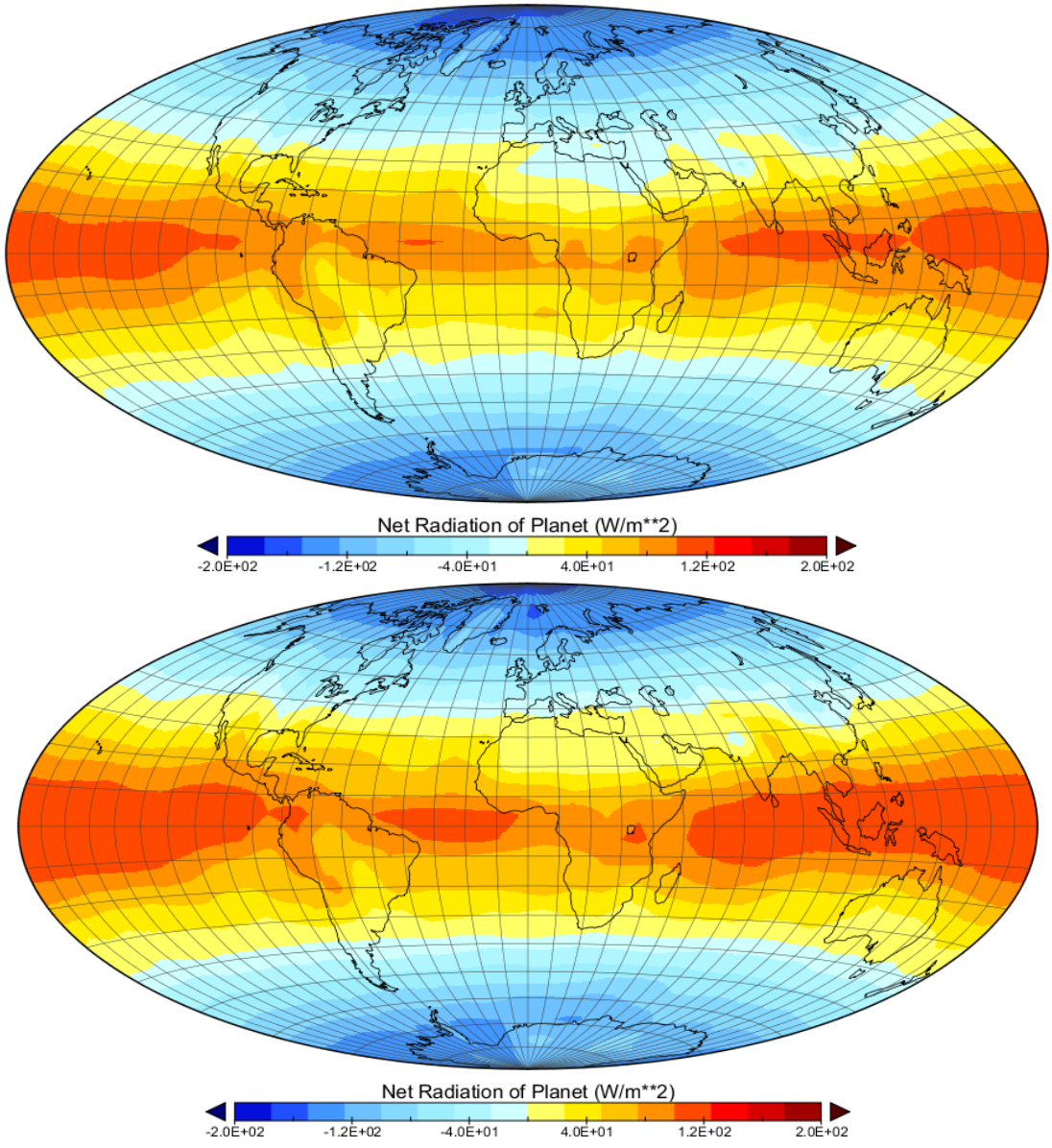


Figure 39. Net radiation (at top of atmosphere) maps for obliquity of zero degrees. The net radiation and heating the Earth-like planet experiences for an obliquity of zero degrees. In both cases, shades of red indicate positive net heating and radiation and shades of blue indicate negative net heating and radiation. The hammer projected maps are based on five-year averages (2194-2197) of the annual net heating and radiation of the planet. Averaging over several years reduces noise in the data. Each season is shown, with Winter at the top, followed by Spring, followed by Summer, and finally Autumn. The net radiation and net heating do not vary significantly over all four seasons (averaged over five orbital cycles), as is expected for a planet with zero obliquity.

Figure 40. Surface air temperature maps for zero obliquity case

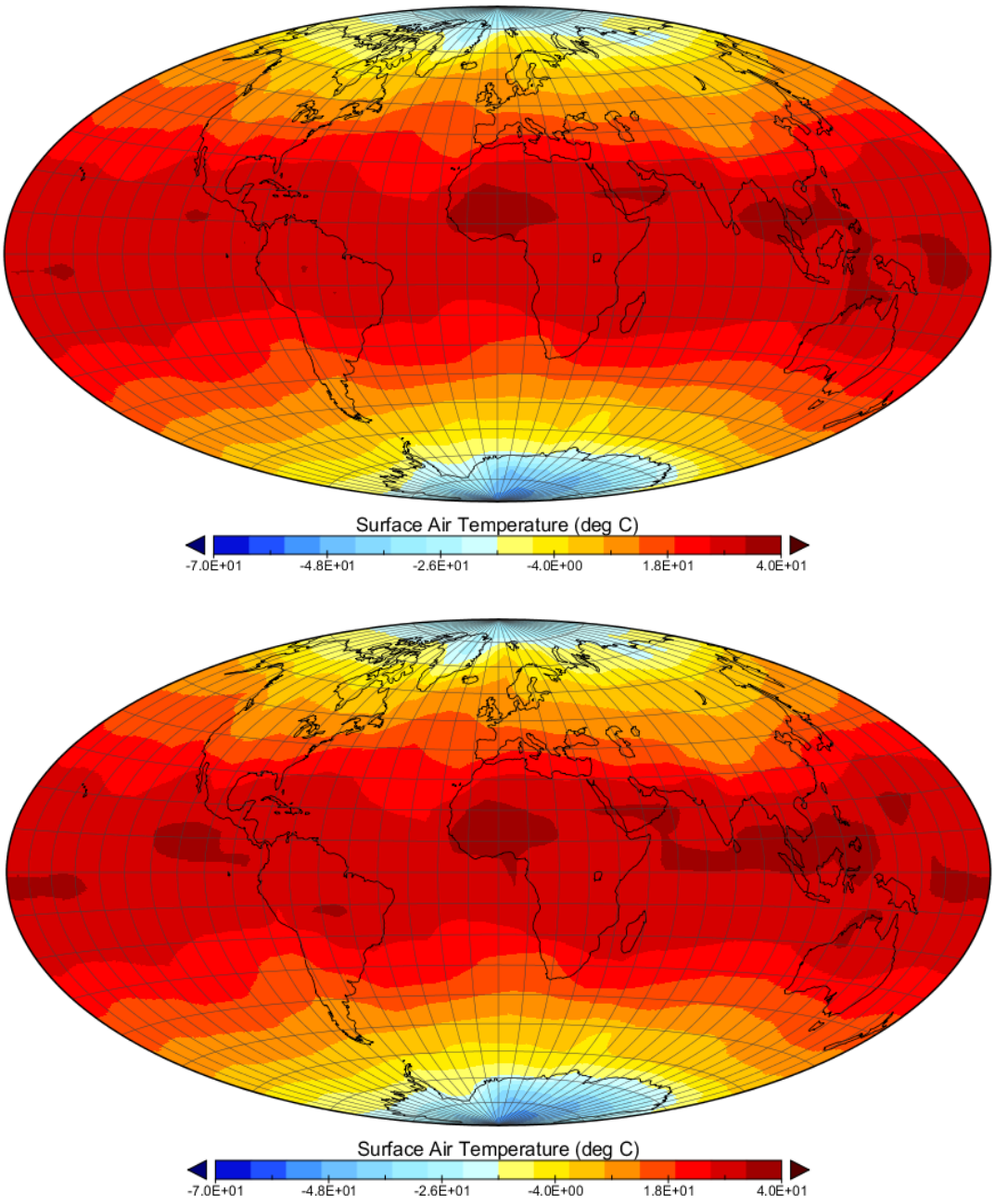

Figure 40 Cont

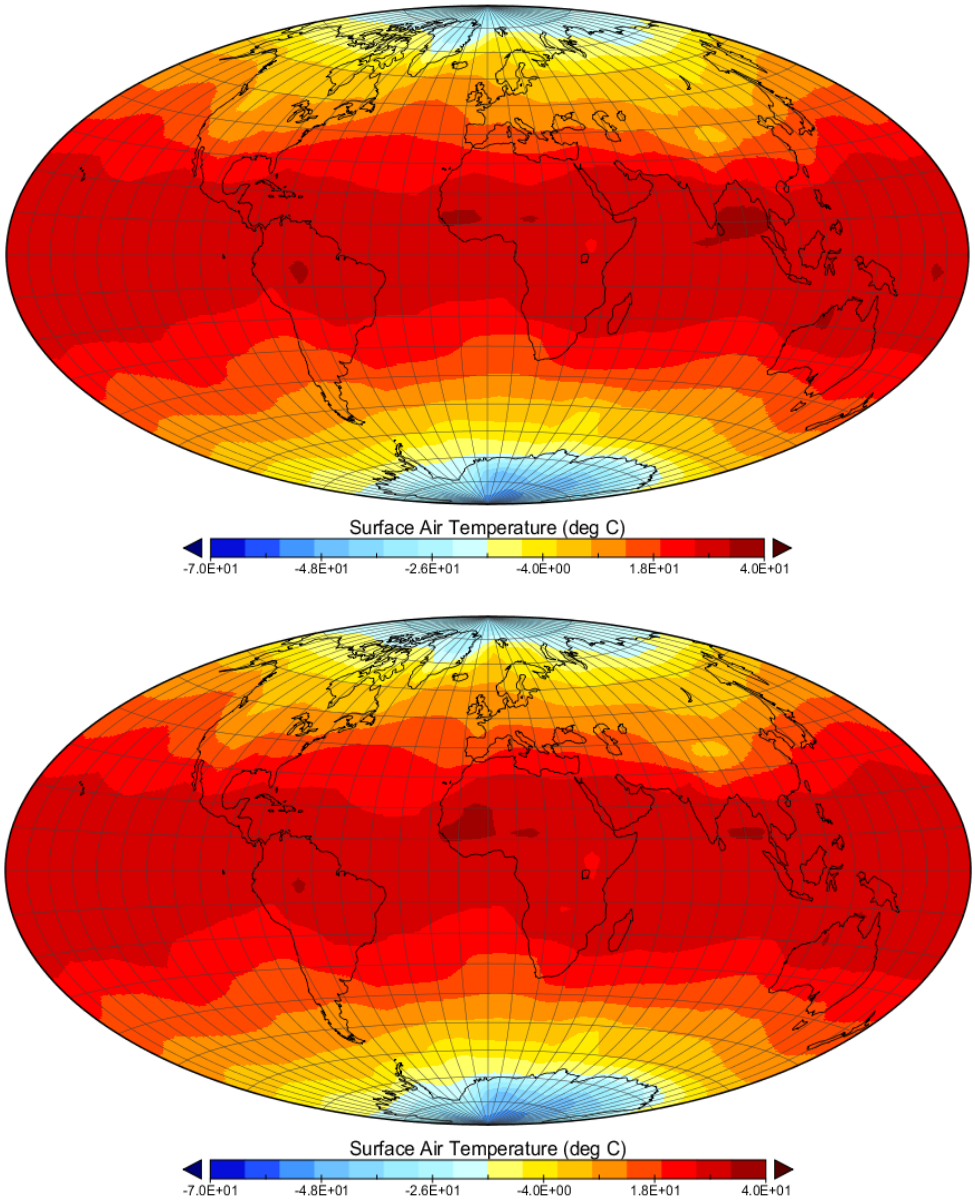


Figure 40. Surface air temperature maps for zero obliquity case. The five-year average (2026-2030) of the "seasonal" surface air temperatures the Earth-like planet experiences for an obliquity of zero degrees. In both cases, shades of red indicate higher temperatures and colder temperatures are represented by shades of blue (polar regions). The is very little variation over the polar regions during the five orbital cycles of the planet, and the hottest regions are observed over the equatorial regions, as is expected for a planet with zero axial tilt. From top to bottom, Winter, Spring, Summer, and Autumn.

The surface albedo of the planet is shown in Figure 41. The polar regions show a very high albedo of approximately 70-80%, with very low albedos over the continents and ocean. The high albedos of the polar regions are the result of very little sunlight reaching those areas on the planet. There is substantial ice and snow at these regions, which has high albedos. Since these polar regions receive very little sunlight due to the planet's zero obliquity, very little ice and snow melting occurs to expose darker terrain. The large area of these regions covered by ice and snow account for their high albedos. There is very little variations in the planet's albedo over the course of five orbital cycles.

Figure 41. Surface albedo maps for zero obliquity case

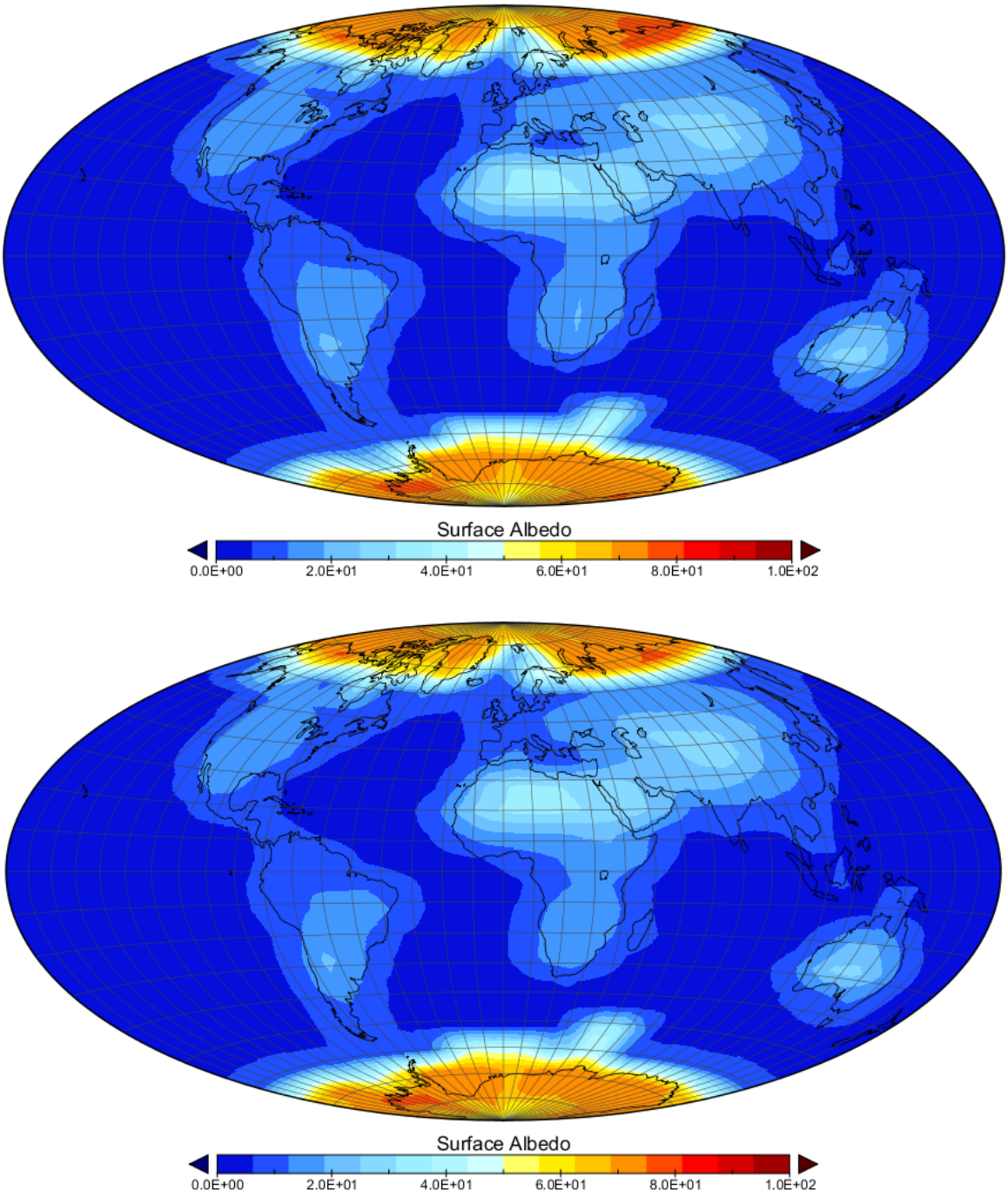

Figure 41 Cont

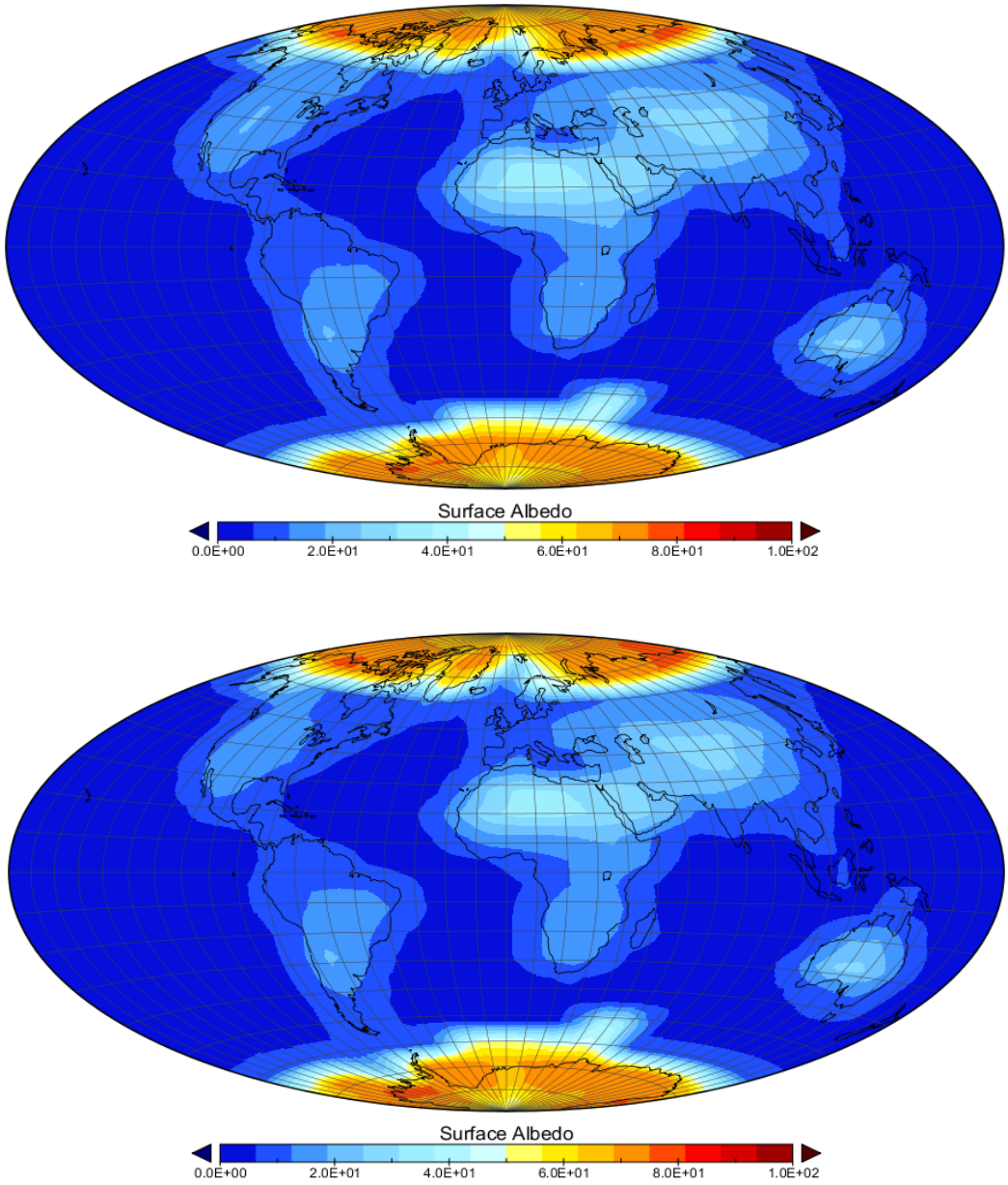


Figure 41. Surface albedo maps for zero obliquity case. The seasonal surface albedo averaged over five years (2194-2197) showing minimal "seasonal" variation, as is expected for a planet with zero obliquity. From top to bottom, Winter, Spring, Summer and Autumn. The "seasons" correspond to the four seasons Earth experiences during its orbit cycle around the Sun. The results show that the planet essentially experiences no climatic variations over the four "seasons" as does the present-day Earth with an obliquity of 23.5 degrees.

The next set of simulations is based on a hypothetical Earth-like planet with a high obliquity of 45 degrees. The expected outcome of the 3-D climate model is an increase in seasonal variation during the course of an orbital cycle. It is suspected that as the obliquity of the planet increase from zero (where there are permanent polar ice caps observed in the simulated data) to higher obliquities, the planet will have more favorable climate as the polar ice cap areas are reduced due to increased stellar irradiance during some portion of the planet's orbital cycle.

The EdGCM simulation for the case of an obliquity of 45 degrees is shown in Figure 42. During the Winter season (Figure 42 first map), the planet receives a higher amount of stellar radiation over its Southern hemisphere as its South Pole tilts toward the parent star. The effect of high obliquity is dramatic as seen in the distribution of net heating over latitude. During the Spring season (Figure 42 second map), the net heating at the surface has shifted from the north polar region to mid-to-low latitudes as is expected during the equinox. During the Summer season (Figure 42 third map) we see the opposite (in contrast to Winter) effect occurring. The tilt of the planet's northern hemisphere towards

Figure 42. Net surface heating maps for 45 degree obliquity case

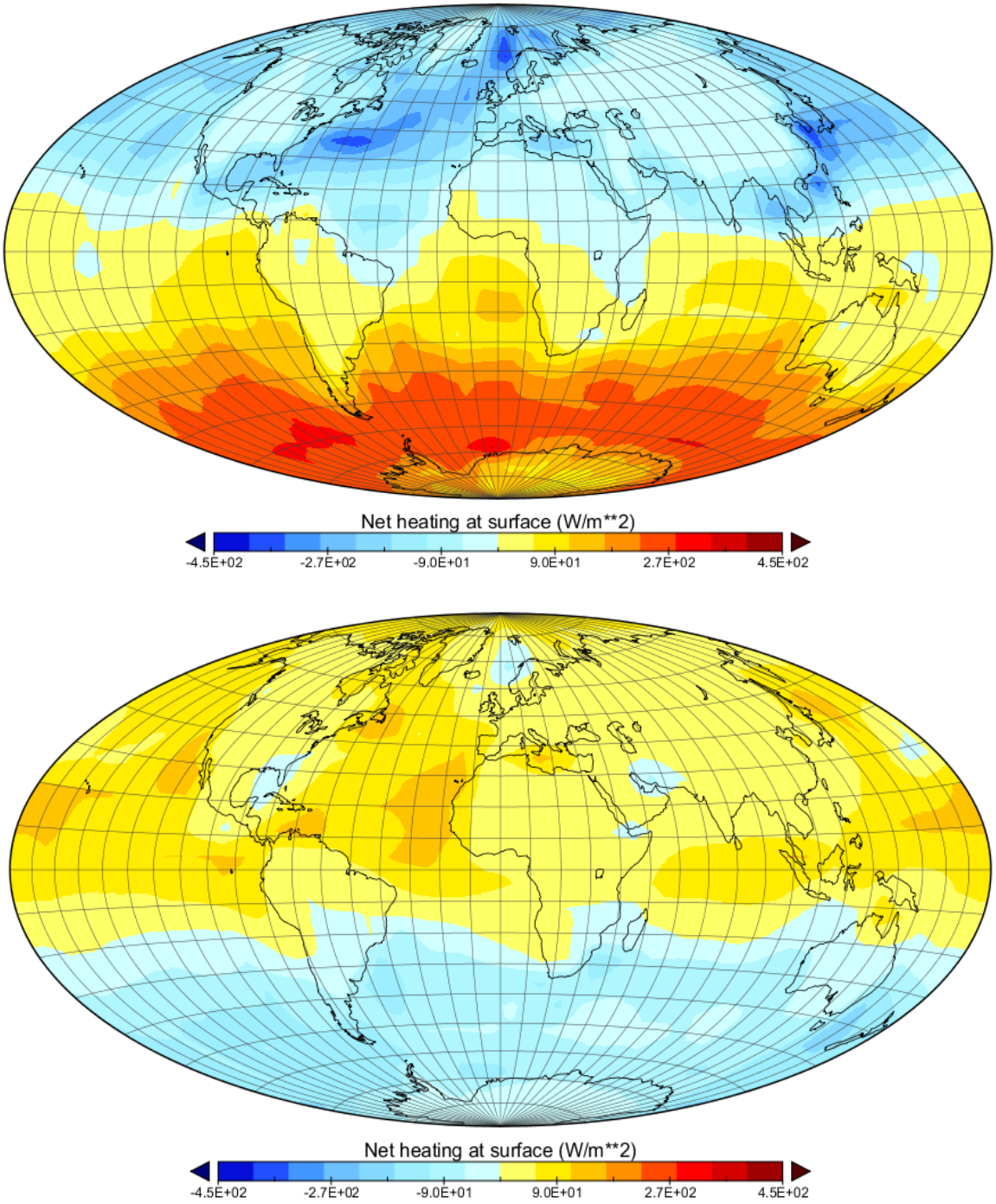

Figure 42 Cont

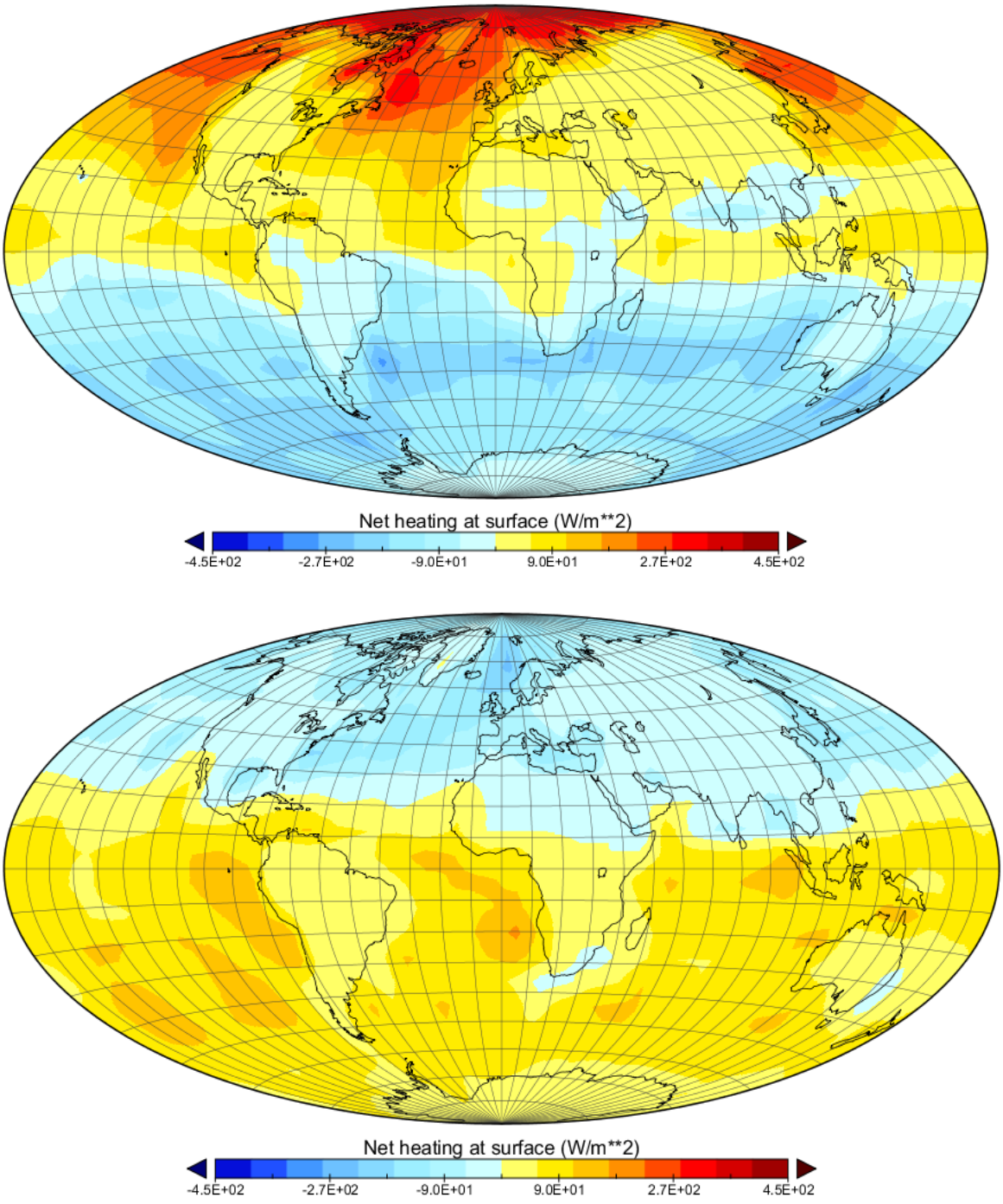


Figure 42. Net surface heating maps for 45 degree obliquity case. Four Hammer projected map showing the four-year (2009-2012) averages of the net surface heating of the planet for an obliquity of 45 degrees during the Winter, Spring, Summer and Fall seasons (Top to Bottom).

the host star is maximum, resulting in most of the planet's north polar region receiving copious amounts of energy. The fall season shows an opposite trend from the spring season in the distribution of net surface heat. There is a shift in net surface heating from mid-to-low northern latitudes to mid-to-low southern latitudes, as a result of the tilt of the planet's axis.

It is seen that EdGCM produces results consistent with what would be expected for an Earth-like planet with high obliquity. As the obliquity is increase from 0 to 45 degrees, the seasonal climatic effects become more pronounced.

The surface air temperature averaged over four years (2009-2012) for an obliquity of 45 degrees show that most of the United States and most of Asia experience extremely cold winters (shown as shades of blue in Figure 43 on the first map). Temperatures in Asia drop to -30 C (-22 F), and temperatures within the United States average around -10 C (14 F). Similar cold temperatures are seen over Greenland. The cold climates experienced in the northerly latitudes over the continents result from the tilt of the northern hemisphere away from the parent star. This results correlates well with the deficit in the net surface heating (Figure 42, first map) experienced during the Winter season. During the Summer season in the Northern hemisphere, a large portion of Asia experiences extremely hot temperatures, approaching 57 C (135 F). The high temperatures experienced in Asia border on the limit of human tolerance. Very high temperatures are also experienced in the eastern half of the United States, with high temperatures reaching upwards of 40 C (104 F). During the northern Summer, most of the southern hemisphere experiences a mild climate. The period during the equinoxes experiences less severe climate shifts, as the star's energy is more evenly distributed.

Figure 43. Surface air temperature maps for 45 degree obliquity case

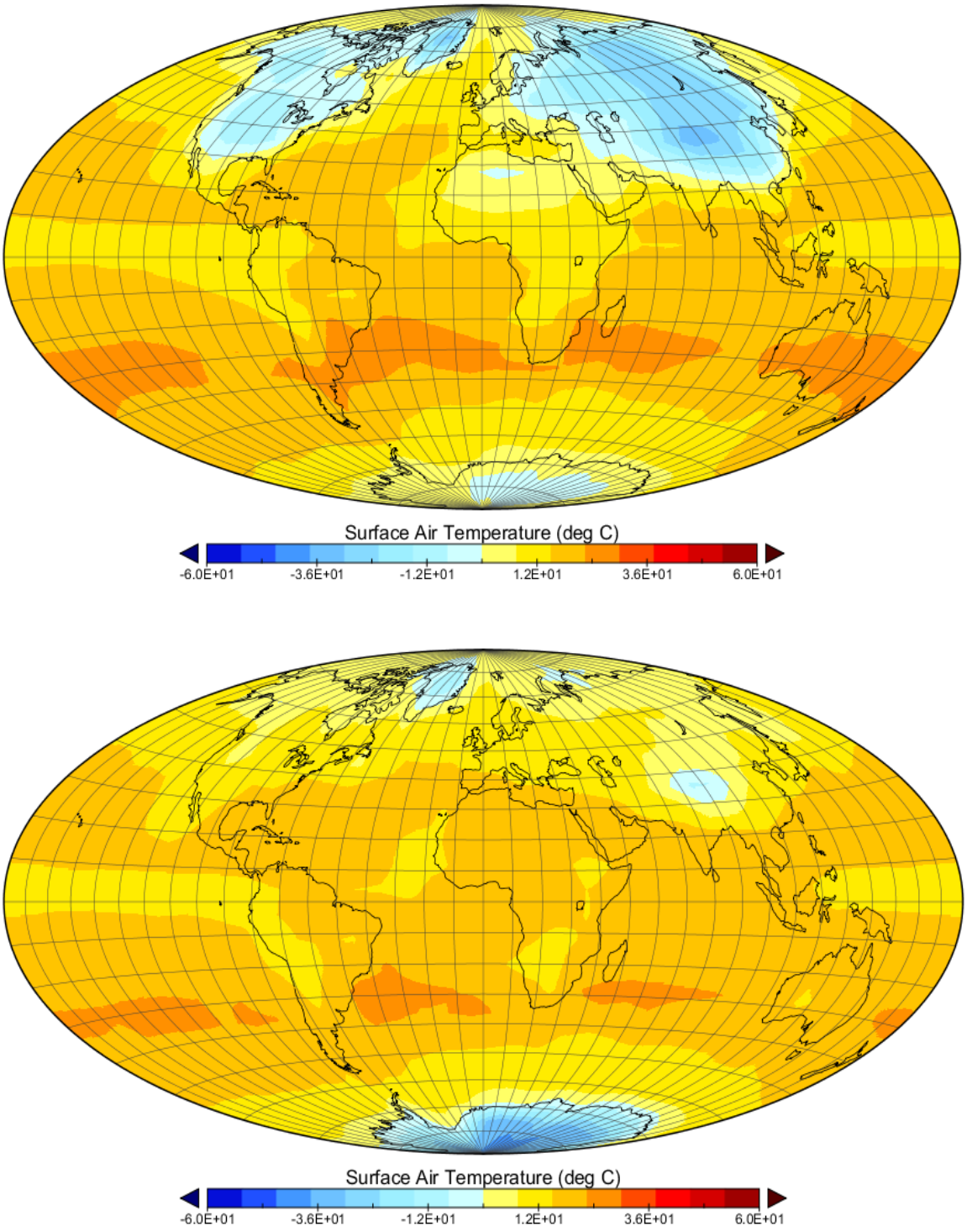

Figure 43 Cont

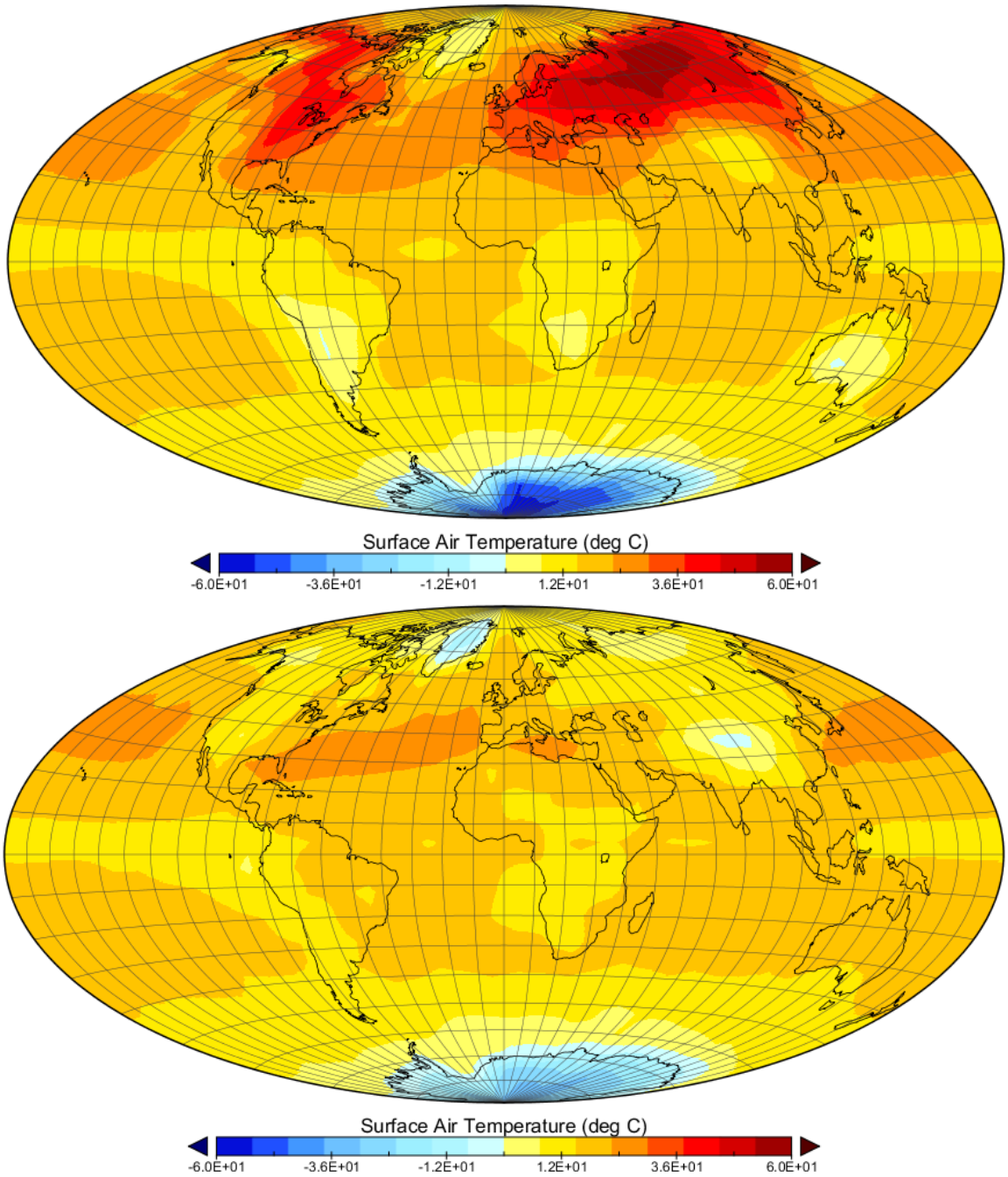


Figure 43. Surface air temperature maps for 45 degree obliquity case. Four-year (2009-2012) average of the surface air temperature over each of the four seasons for a planet with an obliquity of 45 degrees. From top to bottom, Winter, Spring, Summer, and Fall.

The warmest temperatures over the equatorial and mid-latitudes regions of the planet occur during the two equinox periods. This is expected as the equatorial regions of the planet receive more stellar radiation then the two polar regions of the planet during these periods.

As the obliquity of the planet is increase to even higher values (65 degrees), the climate extremes become more pronounced, especially over portions of China, where the temperature drops to ~ -40 C (-40 F) over central China during the Winter season (Figure 44, first map). Most of the United States also experiences a cold climate, similar to the results for the planet with an obliquity of 45 degrees. As is expected during the Winter season in the Northern hemisphere, most of the radiation from the star is directed at the Southern hemisphere. An opposite extreme is seen during the Summer season in the Northern hemisphere, where most of the star's energy is directed at the Northern hemisphere. It is interesting to note that in the summer season, there are extreme temperatures (50-80 °C) over most of the northern hemisphere land masses, in contrast to the summer season in the southern hemisphere, where the temperatures are more moderate. This is the result of the difference in thermal inertia between the large oceanic regions in the southern hemisphere and the land masses, which dominate the northern hemisphere. As with the case for an obliquity of 45 degrees, the most mild climate occurs during the two equinox seasons, where the equatorial region and mid-latitude regions receive most of the energy from the star.

During the Winter season in the Northern hemisphere, the snow coverage increases (Figure 45, top map), and during the Summer season in the North hemisphere,

there is a shift in the snow coverage percentage to the Southern hemisphere (Figure 45, bottom map).

Figure 44. Surface air temperature maps for obliquity of 65 degrees

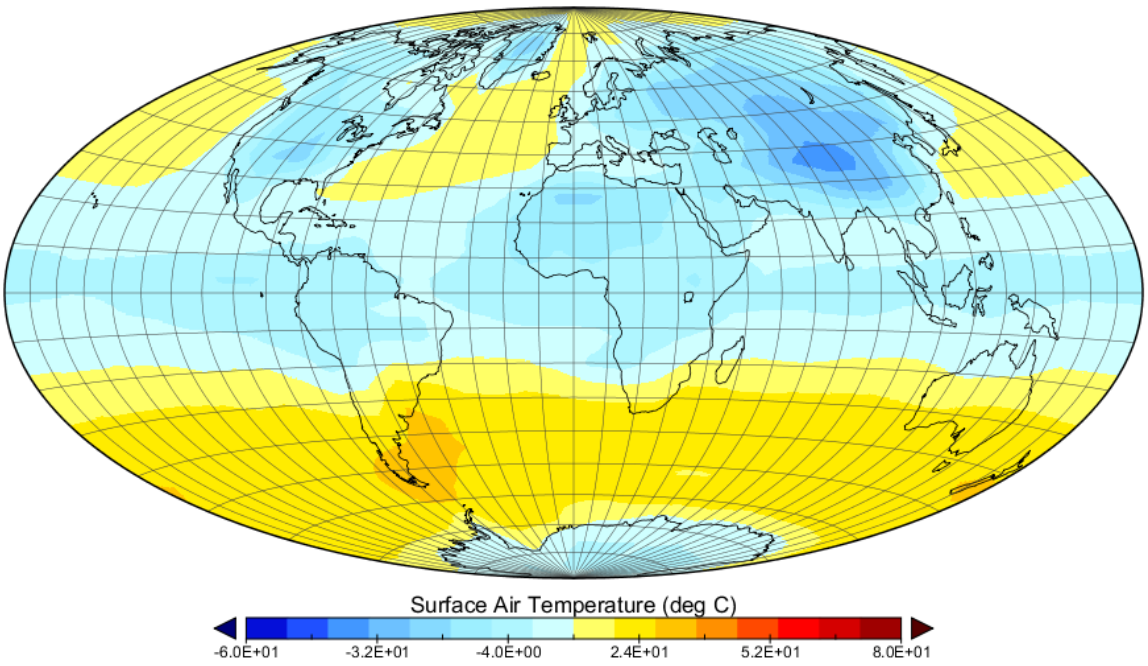


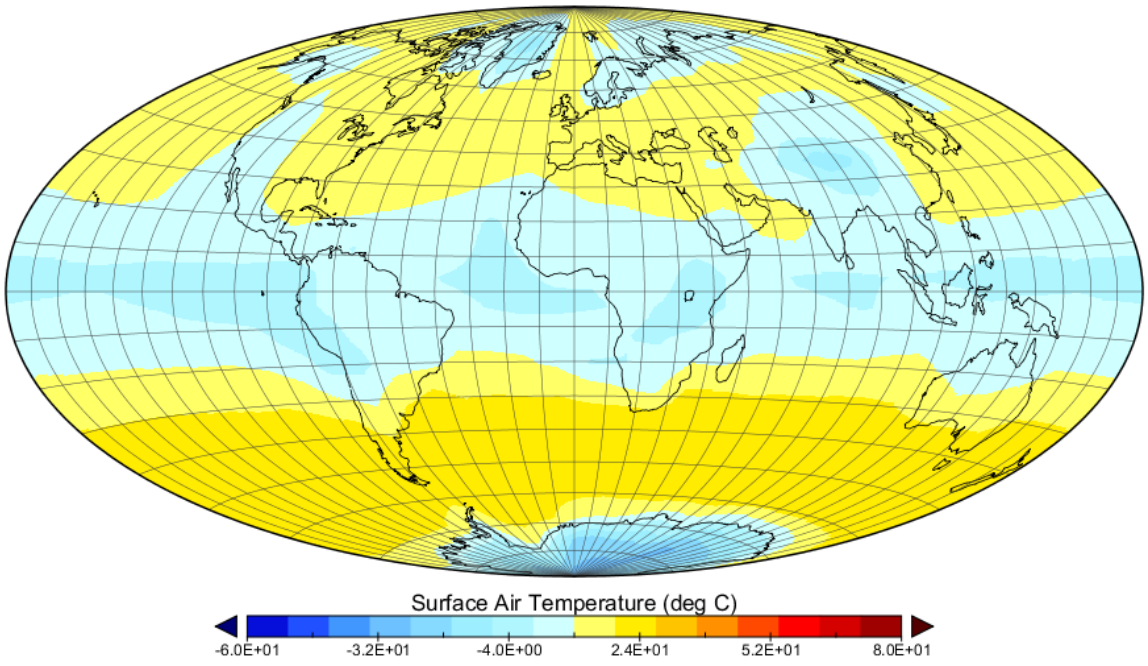

Figure 44 Cont

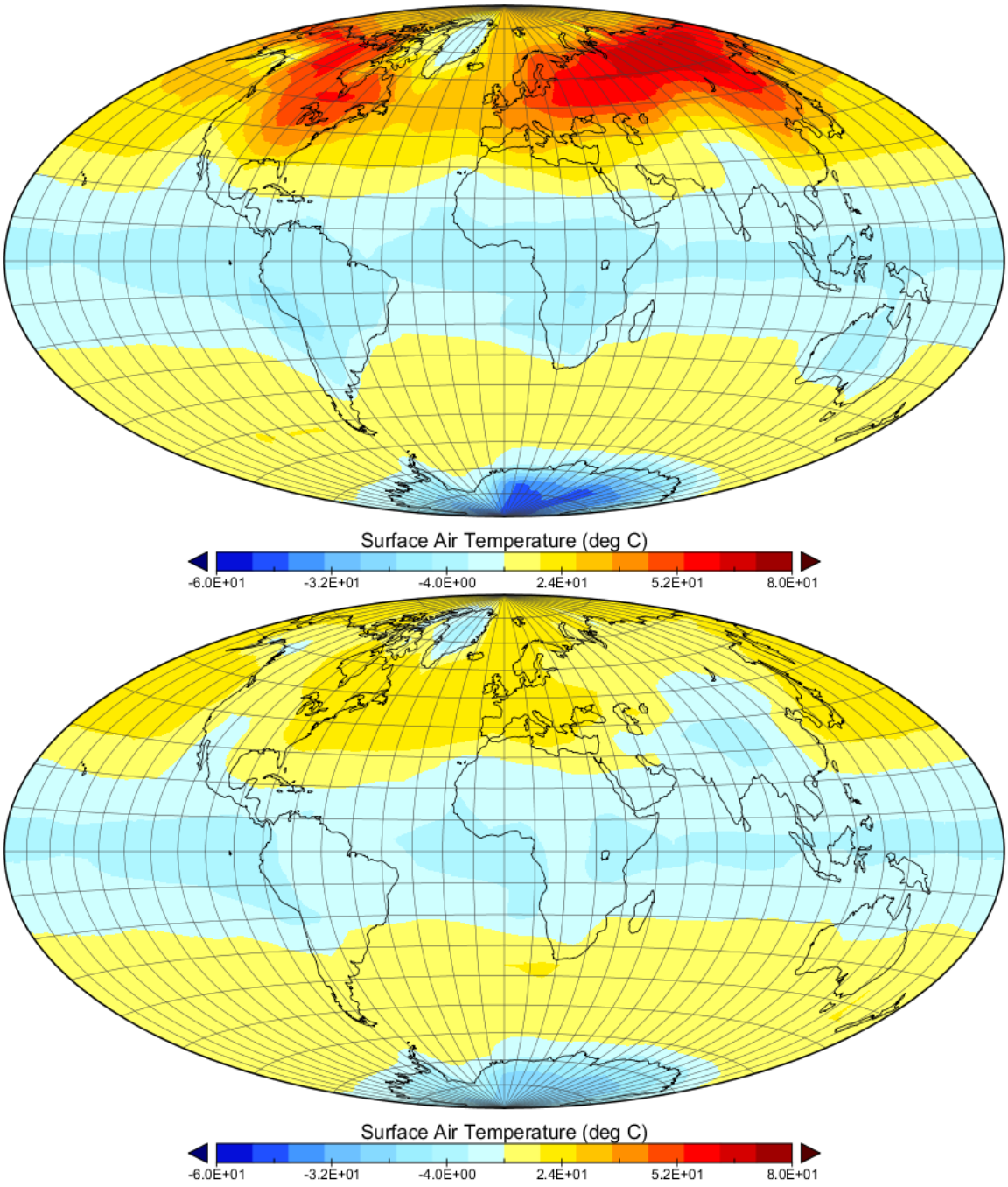


Figure 44. Surface air temperature maps for obliquity of 65 degrees. Four-year averages (2009-2012) of seasonal surface air temperatures for a planet with an obliquity of 65 degrees. From top to bottom, the four Hammer projection maps are for Winter, Spring, Summer, and Fall.

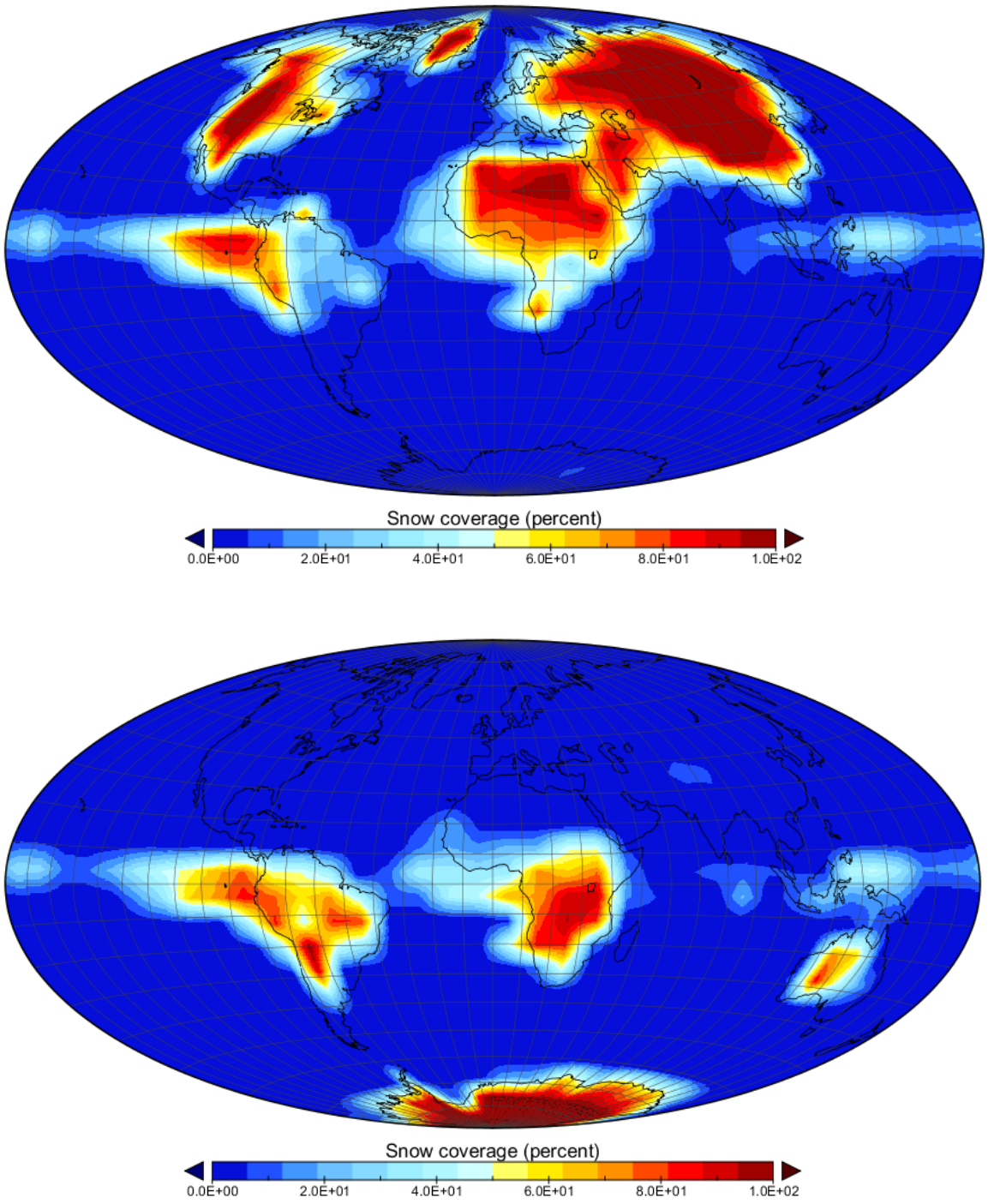


Figure 45. Snow coverage maps for 65 degree obliquity case. Four-year average snow cover maps for Winter season (top map) and Summer season (bottom map). High snow coverage percentages are represented by shades of red.

This is the result of the response of the planet to the changing amount of stellar radiation from the North hemisphere to the south hemisphere. As is expected, the higher the planet's axial tilt (obliquity), the more pronounced the climate extremes. Minimal snow cover occurs during the two equinox seasons, when the climate is more mild. It is seen from these results that the effect of obliquity is to redistribute the amount of stellar insolation from one hemisphere to the other, depending on the time during the planet's orbital cycle. A high obliquity results in an increase in the amount of stellar insolation during the Summer season over the high-latitude regions, at the expense of a deficit of solar insolation over the low-latitude regions. The effect on climate due to the solar insolation is symmetric, depending on the time of year during the orbit cycle.

The amount of snow coverage affects the temperature of the planet's surface, and helps regulate the exchange of heat energy between the planet's surface and atmosphere. The effect from significant snow coverage in Asia (including central China) (Figure 45, first map) is seen on the surface temperature map (Figure 44, first map). There is a direct correlation between the extremely low temperature observed over central China and the heavy snow cover of this location. This illustrates an example of how snow cover can affect climate patterns on local and regional scales.

The last simulation illustrating the effects due to the planet's axial tilt (obliquity) on climate is for the extreme case of 90 degrees obliquity. For zero degrees obliquity, we concluded that there were no (or extremely small) seasonal variations during the planet's orbital cycle. We have already seen that high obliquity (>45) can lead to regional severe climate changes over parts of the United States and Asia. For an obliquity of 90 degrees, one pole will be directed at the host star, followed by the other pole six months later.

When the obliquity reaches high values (>50 degrees), it is possible for the planet to receive more energy from the host star per unit area at the poles than at the equatorial regions. This can lead to the condition where the planet's polar regions actually become warmer than the equatorial region. This can result in very unusual patterns in the meridional temperature gradients that are not anywhere similar to present-day Earth. This presents a challenge to our current understanding of climate models on worlds with extreme obliquities. The simulation presented in this case will provide us with a qualitative understanding of the global climate pattern on the Earth-like planet.

The first two maps show the effect of 90 degrees obliquity on the planet's net heating. During the time when the planet's north pole is oriented towards the star, most of the net heating occurs at high-latitude and the pole (Figure 46, top map). There is a latitudinal gradient in the net heating distribution from strong positive values at the north polar region to negative values in the southern hemisphere of the planet. The reverse trend is observed six months later when the planet's opposite polar region is directed at the host star (Figure 46, bottom map). It is interesting to note that there is an asymmetry observed in the total net heating between the two pole facing events. During the time when the north pole is facing the host star, very high latitude and polar regions receive a net heating ranging from 380 to 900 $W/m^2$. Six months later, when the south pole faces the star, the high southern latitudes and polar region receive a net heating ranging from 300 to 500 $W/m^2$. The asymmetry in net radiation could be due to the effects of thermal inertia from different terrain types between the north and south polar regions. Also, there is less sea ice/snow in the north polar region resulting in lower albedos and greater absorption of stellar energy.

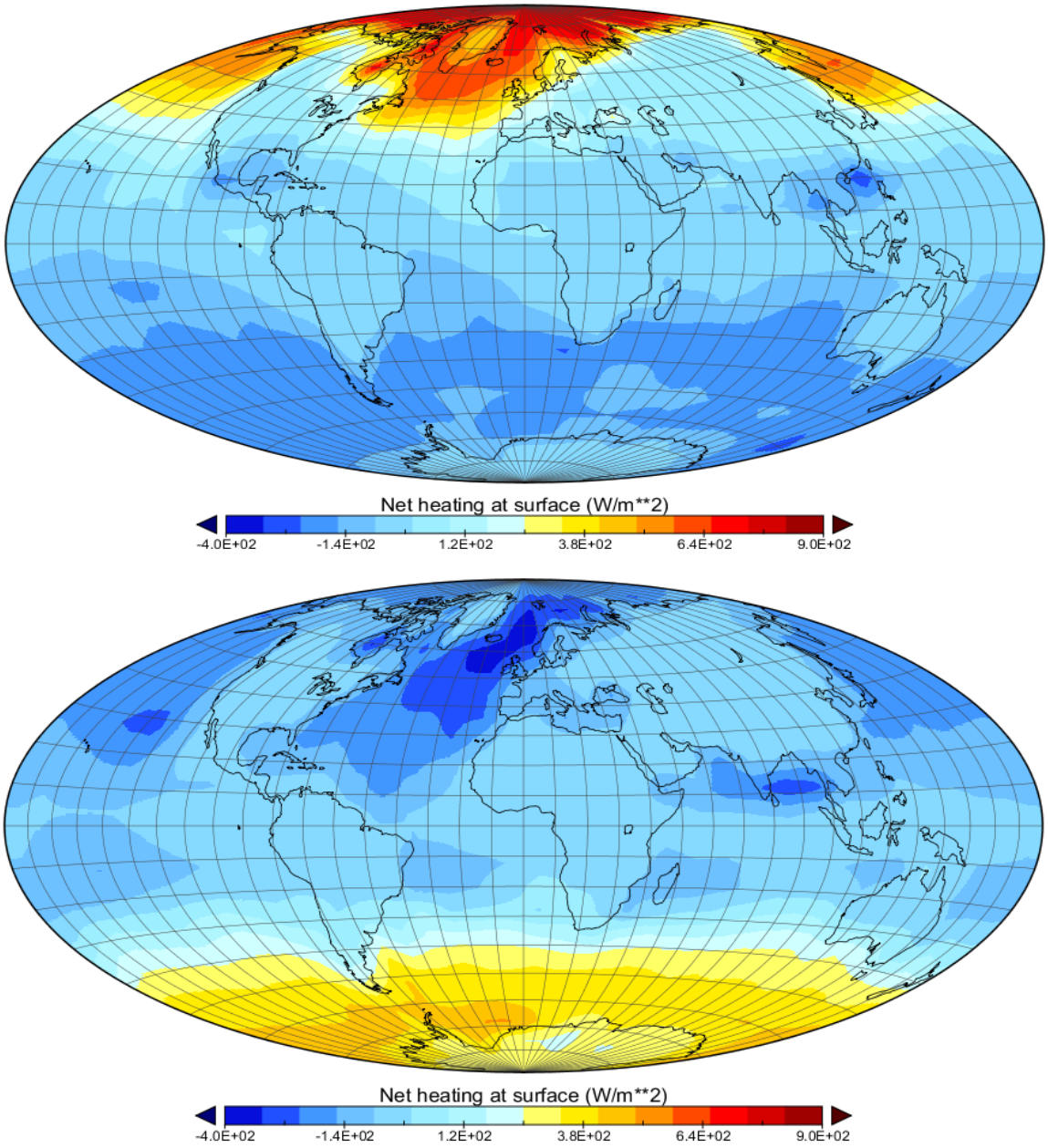


Figure 46. Net heating maps for 90 degree obliquity. Four-year seasonal averages showing the net radiation the planet receives during the time when the north pole faces the star (top map) and when the south pole faces the star (bottom map). Red areas represent strong net heating, and shades of blue represent negative net heating. The asymmetry displayed between the north and south pole facing events is due to opposite polar regions facing the host star every half cycle of the planet's orbit. The increase in neat heating seen at the arctic will lead to increased melting of the ice pack, and a decrease in the albedo over this region of the planet. This leads to an enhancement of the positive feedback effect and warming temperatures due to increase solar absorption.

For the two equinoxes, the net heating is significantly lower than at the polar regions, since the equatorial regions of the planet receive very little energy from the host star during an orbit cycle. The average surface air temperature (Figure 47) shows a similar pattern to the net heating. When the planet's north polar region faces the host star, the temperatures become extreme, and six months later, when the opposite polar region is directed at the star, the temperature increases at that pole. However, the increase in temperature at the south polar region and high latitudes is not as extreme as in the northern hemisphere. This is due to differences between the thermal inertia of the southern oceanic regions and the land-dominated northern hemisphere. It should be noted that an obliquity of 90 degrees will change locations of sea/ice glaciers that are not accounted for in the EdGCM simulation. EdGCM assumes Earth-like oceans, but the distribution of sea ice is likely to change.

Figure 47. Average surface air temperature and snow coverage maps for 90 degree obliquity case

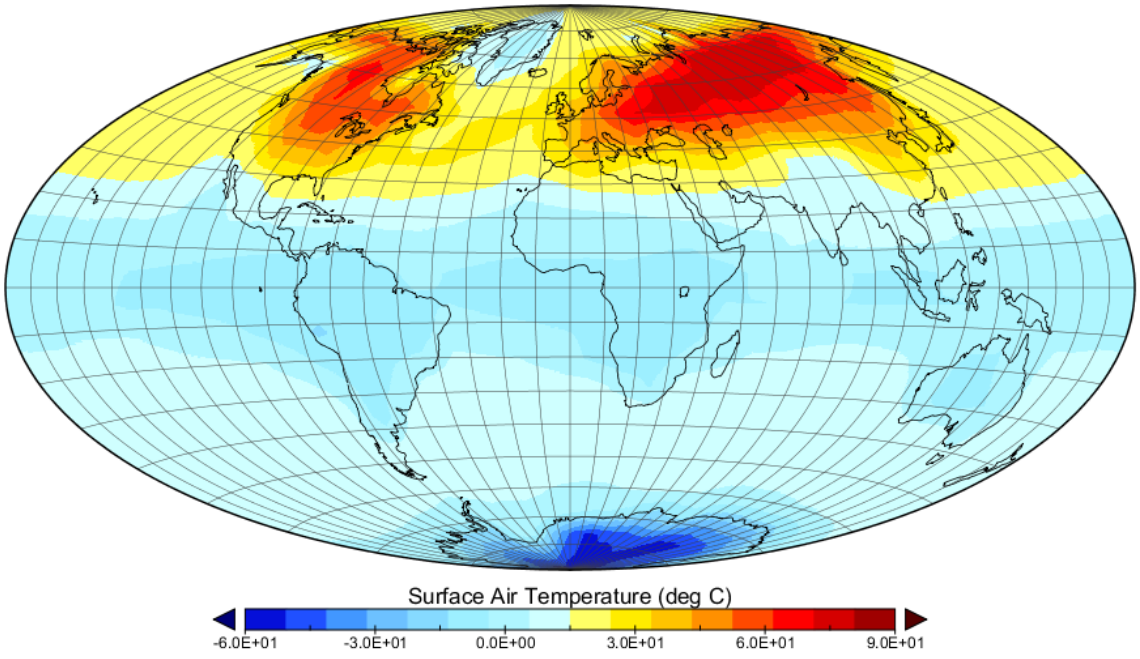

Figure 47 Cont

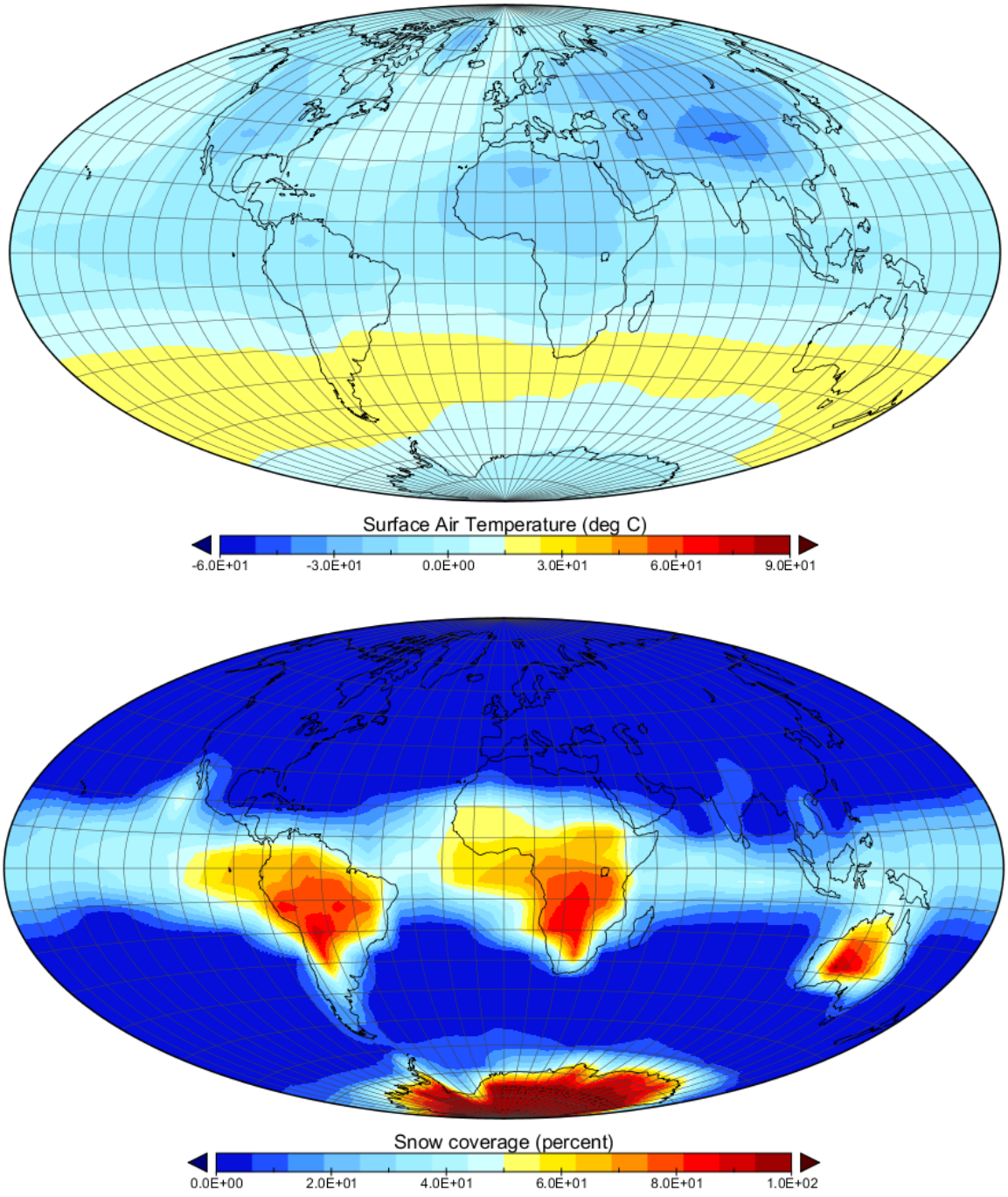

Figure 47 Cont

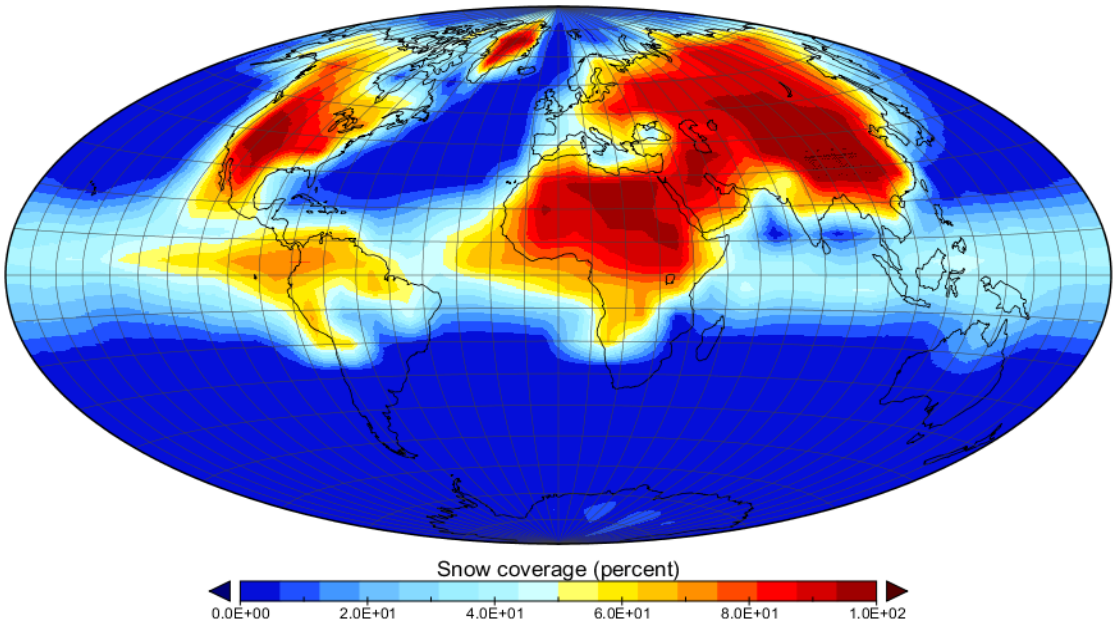


Figure 47. Average surface air temperature and snow coverage maps for 90 degree obliquity case. The distribution of seasonal surface air temperatures averaged over four years for the time when the planet's north polar region faces the star (top map) and six months later when the opposite polar region faces the star (second map). The snow coverage maps are shown for the period during which the planet's north polar region faces the star (third map) and six months later when the opposite polar region faces the star (fourth map). Note the correlation between the amount of total snow coverage and temperature.

The next simulations illustrate the effect of different orbital eccentricities on the global climate of an Earth-like planet, assuming the same land mass configuration as Earth (the assumed default for all simulations in this work). The two eccentricities used in the simulations are 0.2 and 0.3. Higher eccentricities resulted in numerical instability in the EdGCM (GISS GCM-II) computer code, and could not be modeled. Using the expressions for the perihelion and aphelion distances,

$$r_a = a(1+e)$$
$$r_p = a(1-e) \quad (31)$$

the aphelion distance for an eccentricity of 0.2 is 1.2 AU and the perihelion distance is 0.8 AU. For the case of an eccentricity equal to 0.3, the aphelion distance is 1.3 AU and the perihelion distance is 0.7 AU (taking the planet just within the orbit of present-day Venus during the perihelion event). The large variation in heliocentric distance between the perihelion and aphelion for these two cases should result in significant differences in the solar insolation received by the planet. This should lead to an observable change in the global climate throughout the orbit cycle.

Figure 48 shows the symmetry observed in the net heating between the northern hemisphere winter season (top map) and northern hemisphere summer season (bottom map) for an orbital eccentricity of 0.20. The effect of high orbital eccentricity produces a significant difference between the amount of solar insolation received during the northern hemisphere winter (Figure 48: top map) and summer (Figure 48: bottom map) seasons. During the northern winter season, the planet is closer by a factor of 1.5 than in the northern hemisphere summer season when the planet is near its furthest point from the host star. This explains the 170 W/m$^2$ difference in the net heating between the perihelion and aphelion events of the planet's orbit cycle. The obliquity of the planet (23.5 degrees) also contributes to this difference in net heating, since during the northern hemisphere winter the southern hemisphere is directed towards the star, and vice versa. During the time the planet is near perihelion, it receives ~2134 W/m$^2$ (at the top of the atmosphere), and ~949 W/m$^2$ (at the top of the atmosphere) during aphelion. Thus, at perihelion the planet receives ~2.5 times more solar insolation than it does at aphelion. This explains the

extreme difference in the net heating between the northern winter and summer seasons. This is in contrast to present-day Earth, where the small difference in net heating between the summer and winter seasons is primarily due to the planet's axial tilt (obliquity) and not its very low eccentricity. It is interesting to note that the extreme temperature differences in the northern hemisphere caused by the difference between the thermal inertia of mostly the continent dominated northern hemisphere and the ocean dominated southern hemisphere (Figure 49), is not seen in the simulation results. The reverse situation is actually seen in the simulation results (Figure 49). It is the extreme eccentricity (and hence minimum and maximum distances) that dominates the continent-ocean thermal inertia effect (the southern hemisphere oceans take much longer to heat up and cool off than the northern hemisphere continents) observed for very low-eccentricity orbits (e.g. present-day Earth).

Figure 48. Net heating maps for eccentricity of 0.20

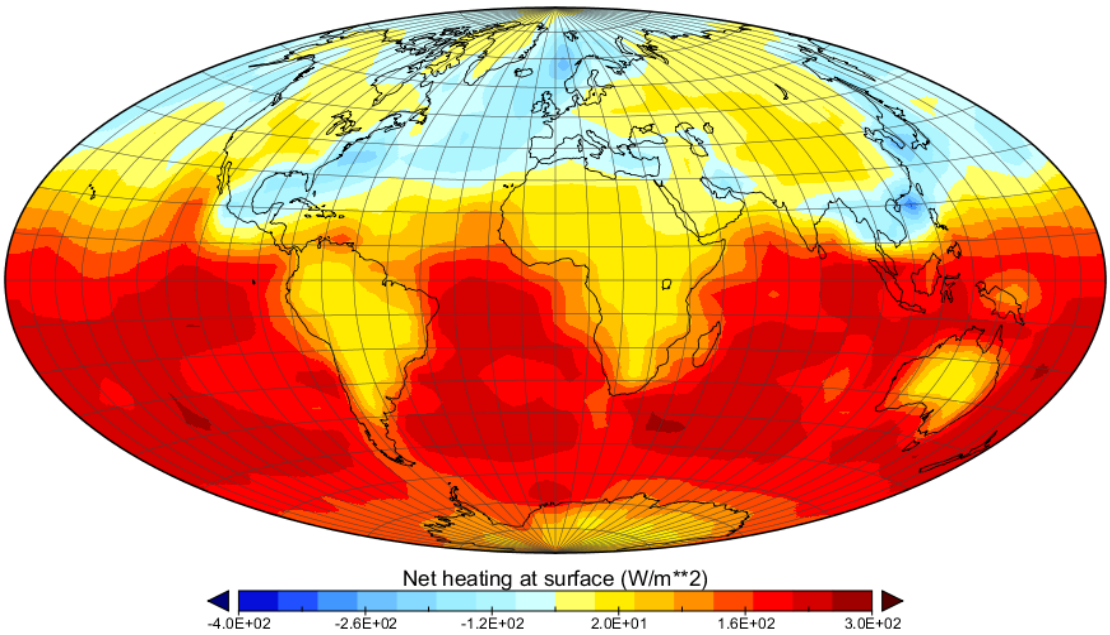

Figure 48 Cont

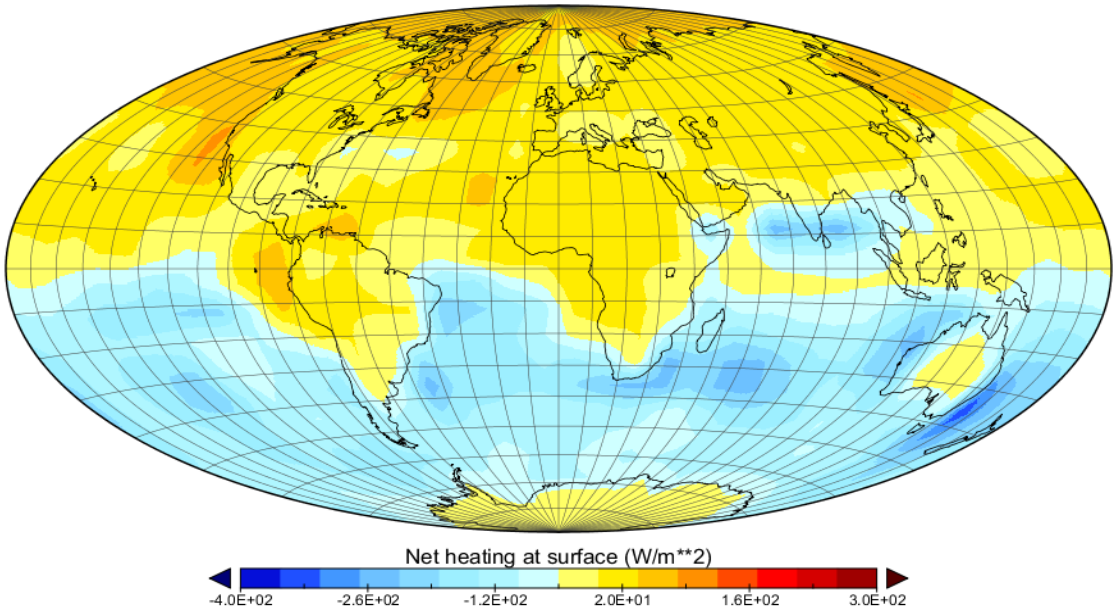


Figure 48. Net heating maps for eccentricity of 0.20. The net heating for winter (top) and summer (bottom) average over four years. During the northern hemisphere winter, the planet is closest to the star and the southern hemisphere receives more of the star's energy due to the planet's obliquity. The reverse is true during the northern hemisphere summer seasonal. Red shades represent positive net heating and blue shades represent negative net heating.

Figure 49. Surface air temperature for an eccentricity of 0.20

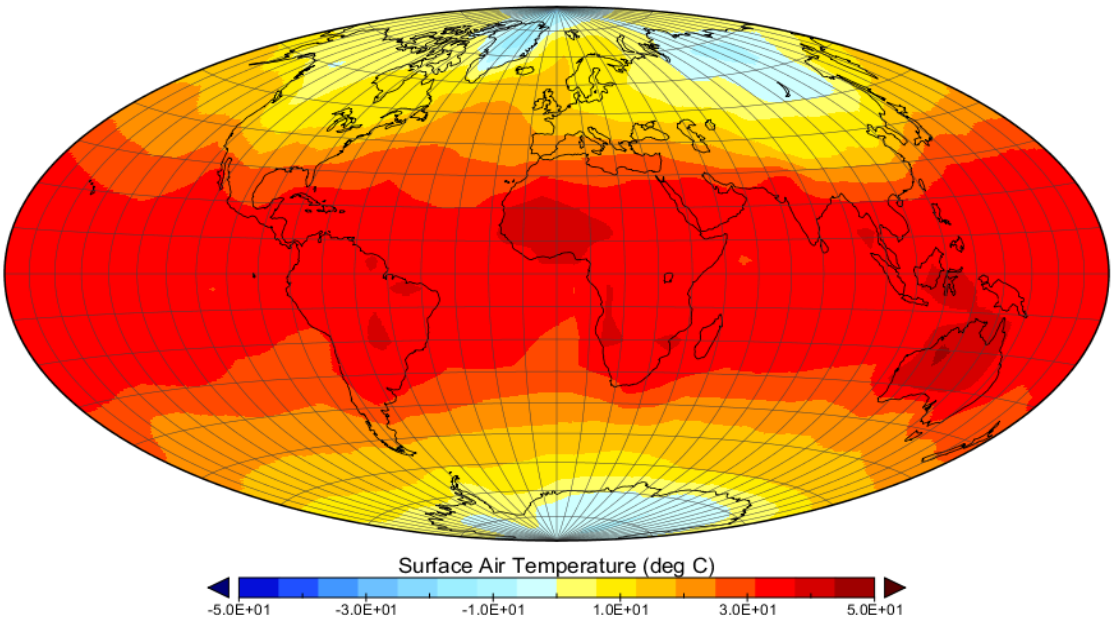

Figure 49 Cont

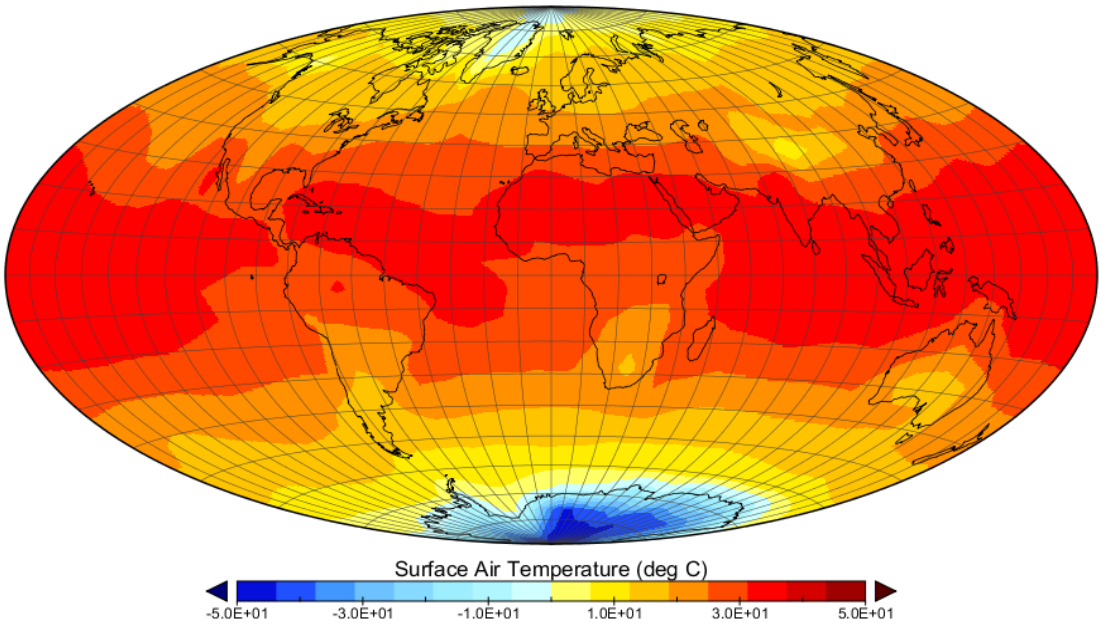


Figure 49. Surface air temperature for an eccentricity of 0.20. Four-year average of the surface air temperature for times when the planet is at perihelion (top map) (northern hemisphere winter) and aphelion (bottom map) (northern hemisphere summer). A qualitative examination of the two maps shows a temperature difference of approximately 9 C between the two extreme heliocentric distances. The orbital eccentricity is 0.2

It is also interesting to note the contrast between the continents and oceans in the southern hemisphere (figure 48). The oceans act as a strong heat sink, storing and conducting the received solar insolation with high efficiency.

The effect of the two extreme distances at perihelion and aphelion can be seen in Figure 49, showing the seasonal ground air temperature, averaged over four years. The eccentricity of 0.2 brings the planet within 0.8 AU, where it receives approximately 2.25 times as much insolation from the star as it does when it is at apogee (1.2 AU). This difference is seen in the large change in the average ground air temperature between the northern hemisphere winter (Figure 49, top map) and summer seasons (Figure 49, bottom map). Most of the heating is seen spread over the equatorial regions to lower latitudes.

The oceans are acting as large heat sinks, absorbing most of the incoming energy from the star. Due to water's high thermal capacity, the oceans tend to act as a heat sink during the summer season and release heat during the winter season.

The is a symmetric change in air temperature over the two polar regions. In the northern hemisphere winter, when the planet's polar region and high latitude regions are directed away from the star, the temperature decreases, and vice versa for the northern hemisphere summer, when the south polar region is directed away from the star. There is also an observed asymmetry in the average surface air temperature between the arctic and Antarctic regions, with the south pole having much lower temperatures. This asymmetry reflects the fact that the Antarctic ice sheet is much thick than the Arctic's ice sheet, and that the ice sheet at the artic floats on top of the ocean. The underlying ocean water under the thin artic ice sheet is above the freezing point of water. This allows some transfer of heat energy through the thin ice sheet to the air above it. In contrast to the very thick Antarctic ice sheet covering land, the Arctic Ocean is in constant motion, resulting in cracks and openings ("leads") that allow heat to escape into the atmosphere. The Antarctic region is colder because the land under the thick ice sheet cools off quicker, in contrast to the ocean under the thin arctic ice sheet which takes longer to cool off. This is seen during the northern hemisphere summer season (Figure 49, top map), where the arctic region's temperature approaches 0℃. This is due to the lack of snow that results during the summer season in the northern hemisphere. This results in warming along with an increase in plant growth that results in lower albedos. Lower albedo allow more solar insolation to be absorbed, thereby raising the temperature. During the winter season, the snow and ice cover increase over the Arctic region. This increases the albedo resulting in

less absorption of energy from the star. Both an increase in albedo and cooling from the increase in snow and ice, result in lower temperatures (Figure 49, bottom map).

For the case where the planet's eccentricity is 0.3, the difference in solar insolation between the perihelion and aphelion events is even more extreme than the case for an eccentricity of 0.2. When the planet approaches perihelion (minimum distance from the star), the received solar irradiance is approximately 2788 W/m$^2$ (for a perihelion distance of 0.7 AU, just within the orbit of Venus for only a short period of time during the orbit cycle). At aphelion, the solar irradiance (at the top of the planet's atmosphere) drops to 808 W/m$^2$. The resulting ground air temperature, average over four years is shown in Figure 50.

Figure 50. Surface air temperature maps for eccentricity of 0.30

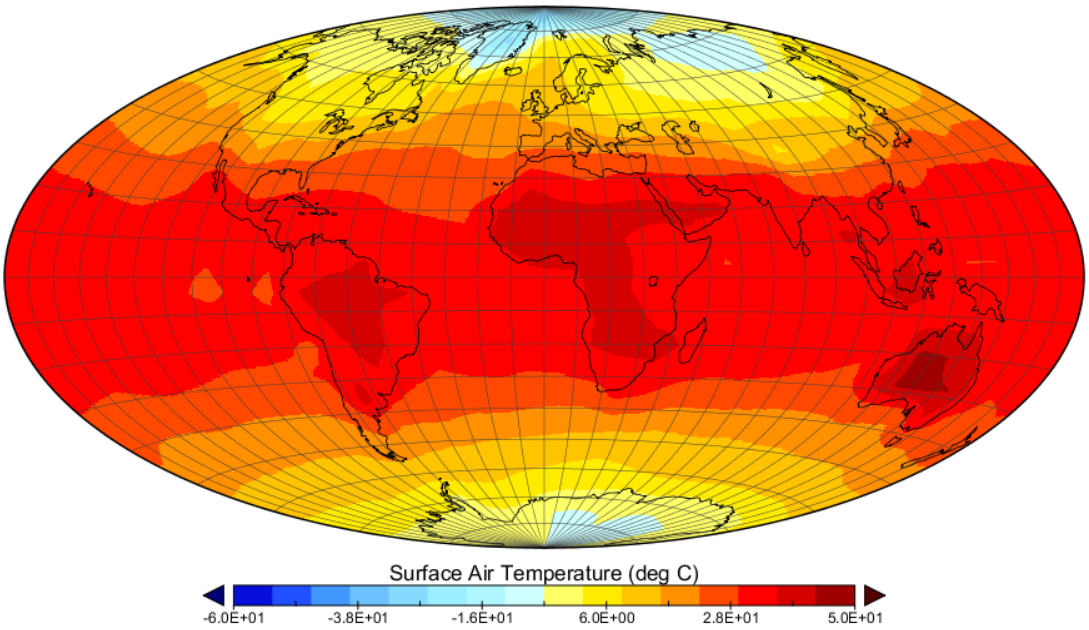

Figure 50 Cont

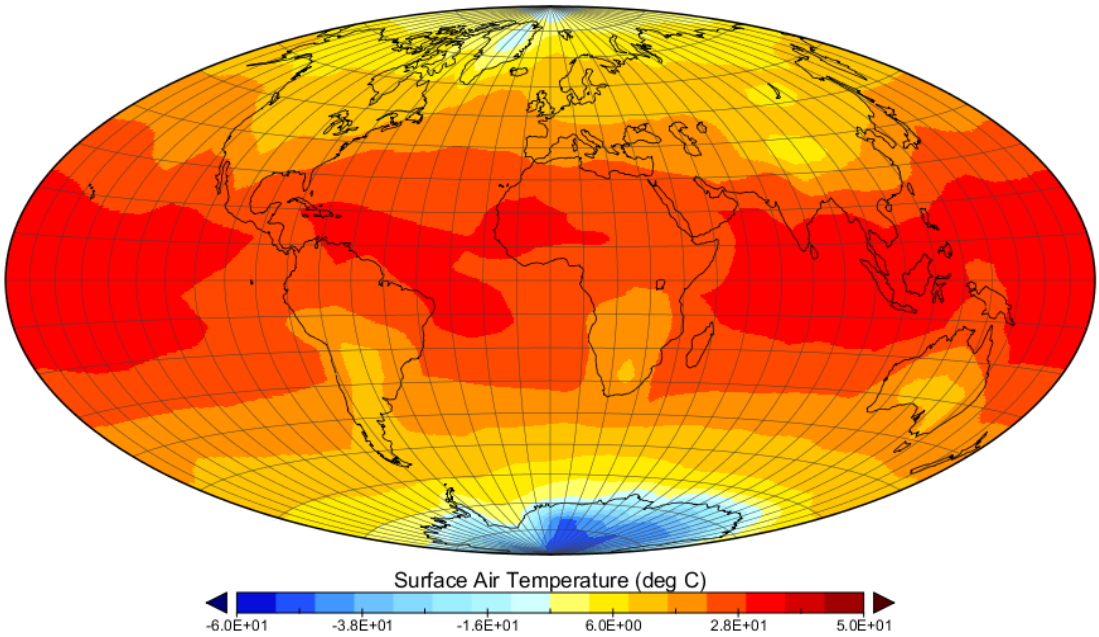


Figure 50. Surface air temperature maps for eccentricity of 0.30. Four year average of the seasonal ground air temperature for the winter season in the northern hemisphere (top map), and the summer season in the northern hemisphere (bottom map). The orbital eccentricity is 0.30.

The net heating at the planet's surface is shown in Figure 51 for the northern hemisphere Winter season (top map) and the northern hemisphere Summer season (bottom map). There is a clear contrast between the net heating on the continents and the oceans in the southern hemisphere. During the northern hemisphere summer the oceans in the southern hemisphere act as a large heat reservoir. The southern hemisphere is dominated by oceans, in contrast to the northern hemisphere, where the effect is not as pronounced. The marked contrast between the oceans and the continents in the southern hemisphere is the result of the different heat capacities between the ocean water and land. The oceans take longer to heat up since their specific heat is larger – i.e. it requires more heat energy to raise the temperature a given number of degrees. In contrast, the continents have a much smaller specific heat, so it takes less time for the land masses to warm up

and cool off. The effects of high orbital eccentricity are also seen between the northern hemisphere summer, when the planet is actually near aphelion and northern hemisphere winter, when the planet is near perihelion. A qualitative assessment of the two maps shown in Figure 51 indicates that during the perihelion, the planet received approximately six times more neat heating at its surface than at aphelion. During the northern hemisphere summer when the southern mid- to high-latitudes are oriented away from the parent star, and the planet is near its aphelion, the continents heat up more rapidly due to their low thermal inertia. The large ocean area in the southern hemisphere has not yet absorbed a significant amount a net heat. In fact, there is a net loss of surface heating occurring. Both the obliquity of the planet and the extreme variation in heliocentric distance due to the high eccentricity of the planet's orbit contribute to the overall global climate pattern observed in the EdGCM simulations.

Figure 51. Neat surface heat maps for eccentricity of 0.30

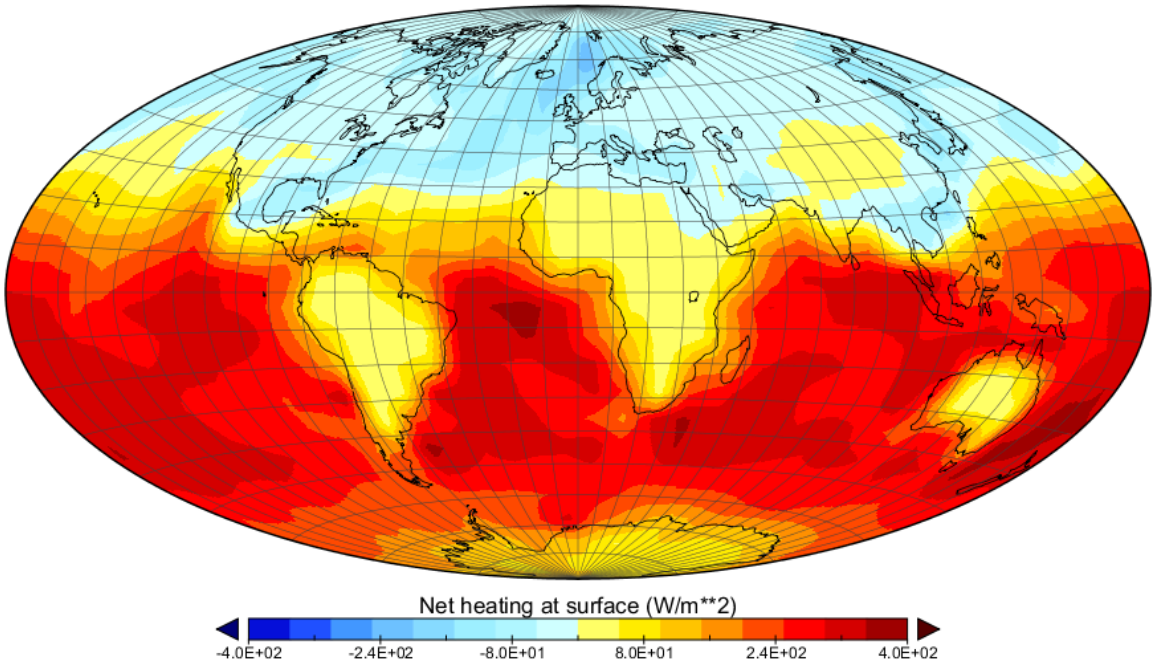

Figure 51 Cont

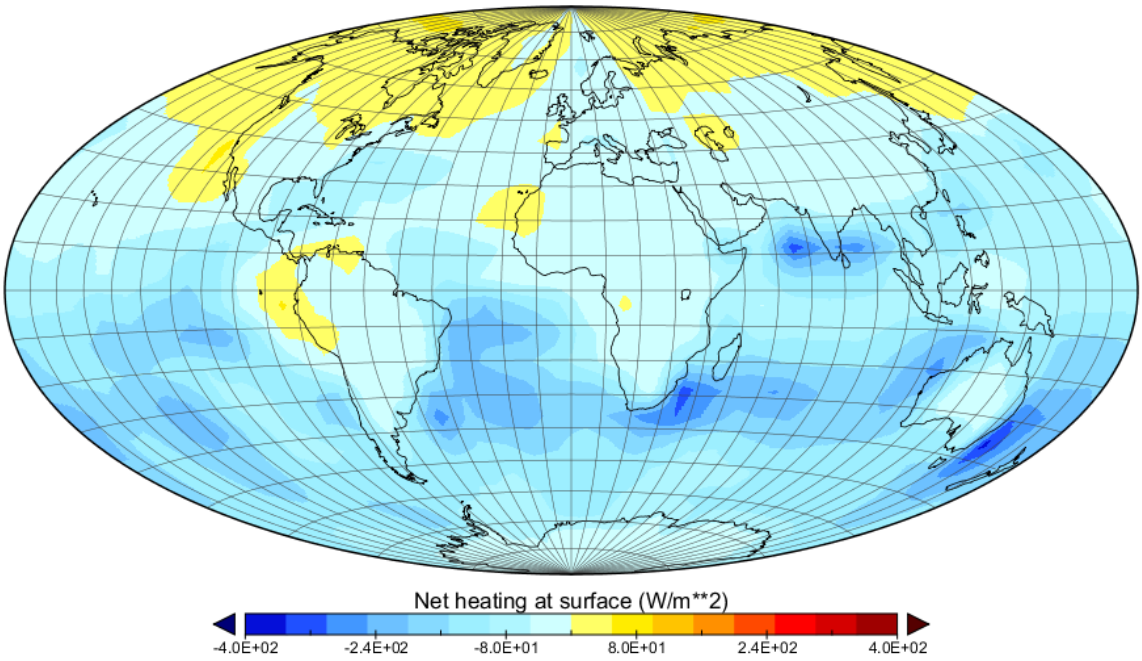


Figure 31. Neat surface heat maps for eccentricity of 0.30. Four-year average of the seasonal neat heating at the planet's surface as simulated by EdGCM. Shades of red represent net positive values of the net heating, and shades of blue represent negative net heating. Northern winter (top map) and Northern summer (bottom map).

The top map in Figure 51 shows the effect of the large oceanic area covering most of the southern hemisphere. During the northern hemisphere winter season when the planet is closer to its parent star, the oceans act to absorb a significant amount of solar radiation. In other words, we see the effect of the oceans acting as a large heat sink (red shaded areas seen in the bottom map of Figure 51). This "heat sink" effect is not seen in the northern hemisphere during the summer season because the total area of oceans is much smaller than that in the southern hemisphere, and also because the planet is located at its furthest distance from its host star, thus it receives a smaller amount of solar insolation.

## EdGCM Results for an Earth-like Planet Located at the Inner and Outer HZ Regions

The next two simulations were carried out using the EdGCM (GISS GCM-II) code to study the effects on an Earth-like planet's global climate pattern as a result of locating the planet at the inner boundary of the Habitable Zone (0.90 AU), and in the outer regions of the Habitable Zone (1.2 AU). Attempts to place the planet at the orbit of Mars (~1.5 AU) produced an instability in the code, which prevented the simulation based on estimates of the very outer edge of the HZ at 1.5 AU. Therefore, the inner and outer boundaries of 0.9 AU and 1.2 AU were used for these simulations. At the inner edge of the HZ, at 0.9 AU, the amount of solar irradiance received at the top of the planet's atmosphere is approximately 1686 $W/m^2$. At the outer region, the planet receives approximately 949 $W/m^2$. The values for the solar irradiance received for these to extreme cases differs significantly from the nominal value of 1366 $W/m^2$ received at Earth's current location within the HZ. It should also be noted that the locations of the inner and outer boundaries of the solar system's habitable zone differ, depending on which model is being used to calculate the effects of the planet's atmosphere on the location of the boundaries. The inner and outer boundaries of the HZ around any star are not simply determined from the range of distance at which water can remain in a stable liquid phase, but must also take into account the effects of the physical properties of the planet, such as atmosphere, geology, obliquity, and tidal locking (for Earth-like planets orbiting M-dwarf stars). The results of these two simulations will allow a qualitative assessment of the global climate patterns that result for an Earth-like planet located at the inner and outer regions of the HZ for a G2V spectral class star like the Sun. The term

"Earth-like" used in this work means that the same configuration of land masses the present-day Earth is used in the models. An improvement to the EdGCM interface to the GISS GCM-II code to allow arbitrary land-mass configurations would be advantageous to studying planets that have similar characteristics to present-day Earth, but with radically different land mass configurations. This would introduce a new variable in the climate modeling results, since the amount and shape of continents can influence global climate patterns, as was the case for the time on Earth where there was one supercontinent.

The results of the EdGCM simulation for Earth placed at the inner region of the Habitable Zone (0.90 AU) is shown in Figures 52 and 53.

During all four seasons, we see that the oceans act as a large heat reservoir (Figures 52 and 53). The large contrast in surface air temperatures between the oceans and land masses is most likely the result of the large heat capacity of water in the oceans. It takes the oceans a long time to heat up as a result of the thermal inertia. The amount of heat energy the oceans gain is directly proportional to the specific heat, $C_p$ of the ocean water, the change in temperature within the oceans, $\Delta$T, and the total mass of the ocean water, $M$.

$$E = MC_p\Delta T \quad (32)$$

Specific heat can be defined as the input of heat energy needed to increase the temperature of a substance or material by one degree Celsius. Mathematically, specific heat can be derived by solving the equation given above for $C_p$,

$$C_p = \frac{E}{M\Delta T} \quad (33)$$

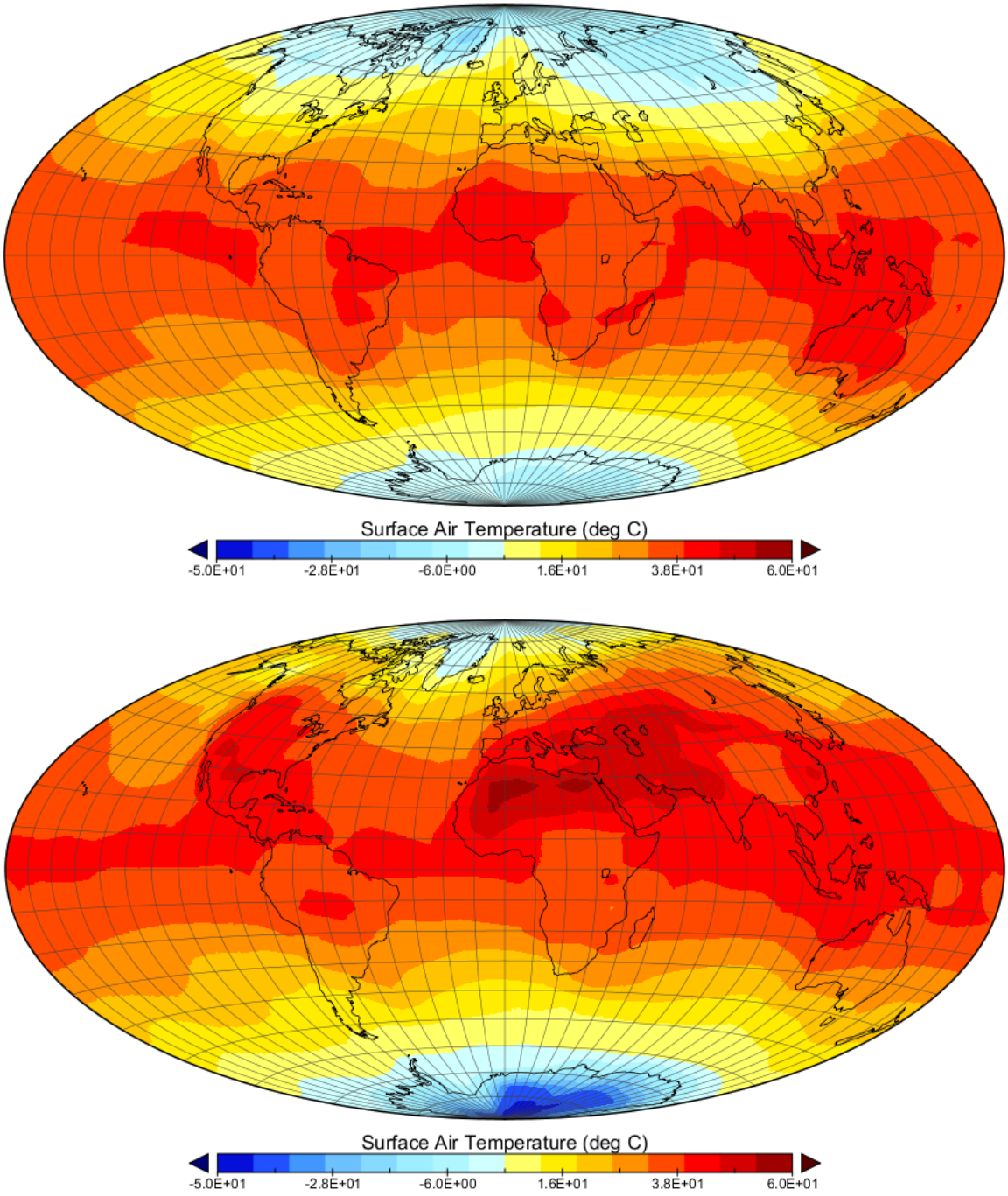


Figure 52. Winter and Summer surface air temperature maps for inner HZ region case. Four-year average of the seasonal surface air temperature for the northern hemisphere Winter season (top map) and Summer season (bottom map). Shades of red denote warmer temperatures and blue shades denote areas with colder temperatures. The seasonal temperatures were averaged over several years in order to reduce inherent noise in the data.

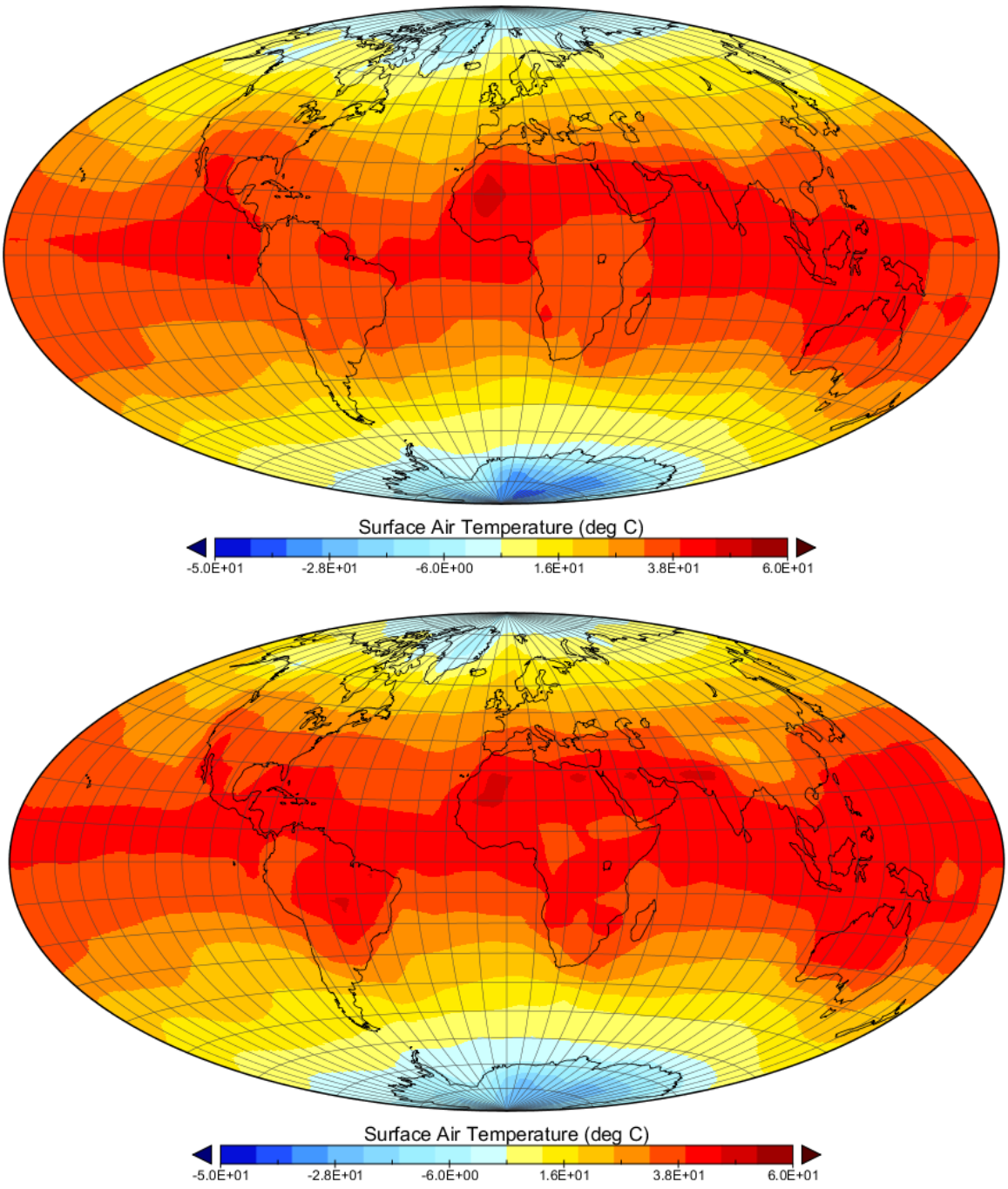


Figure 53. Equinox season air temperature maps for inner HZ region case. Four-year average of the seasonal surface air temperature for the northern hemisphere equinox seasons, Spring (top map) and Fall (bottom map). Shades of red denote warmer temperatures and blue shades denote areas with colder temperatures. The seasonal temperatures were averaged over several years in order to reduce inherent noise in the data.

where $M$ is the mass of ocean water and ΔT the change in temperature. Thus, if the amount of heat energy the oceans have gained, and the total mass of the ocean with a given volume are known, the change in temperature can be estimated within that volume. The above equation can also be rearranged to give the change in temperature.

$$\Delta T = \frac{E}{MC_p} \quad (34)$$

The change in oceanic temperature is therefore inversely proportional to the specific heat of ocean water and the total mass within a given volume of ocean.

Water (including ocean water) is unusual in that it has a relatively high specific heat, approximately 3993 J/kg/K at standard pressure and temperature assuming a salinity of 35 g/kg. It is the high specific heat of ocean water that allows the Earth's oceans to play a key role in regulating the planet's temperature. There is an imbalance in the net heating between the planet's equatorial regions and the polar regions as a result. It is this imbalance that is responsible for oceanic and atmospheric current – i.e. the planet's "heat engine". The description of the role the oceans play in the planet's climate presented above is simplified as there are several other processes that redistribute heat energy throughout the oceans, including convection and conduction characteristics of ocean water, and diffusion properties of the atmospheric layers just above the ocean water.

The orbital period of the planet located at 0.90 AU is shorter than it would be for present-day Earth. The increased amount of solar insolation, which does not vary significantly as a result of the near-circular orbit of the planet, together with the large heat capacity of the oceans results in continuously warm temperatures over the oceans. The oceans do not have time to cool off significantly during the course of an orbit cycle – i.e.

there is a significant inertial lag involved. As a result of the increase solar insolation during the year, there are parts of North Africa, Australia, and Middle East with average surface temperatures approaching 50℃ (122℉).

The case for placing the Earth at the outer region of the Habitable Zone (1.2 AU) is shown in Figures 54 and 55. The original initial condition involved placing the Earth-like planet at 1.5 AU (approximately the orbit of Mars), but numerical instability in the climate model code prevented this case from running. The first global climate pattern seen on the maps in Figures 54 and 55 is the effect of the Arctic region receiving less heat energy during the northern winter season, where four-year average temperatures over portions of the north polar region approach -75℃ (-103℉). During the winter season in the northern hemisphere, the higher latitude regions are directed away from the host star. The effect of the obliquity, in addition to the placement of the planet at 1.2 AU, where the planet receives only approximately 0.59 times the amount of solar insolation received when the planet is at perihelion, leads to the extremely cold temperatures at the polar regions. During the summer season in the northern hemisphere, when the high latitude regions in the southern hemisphere are directed away from the host star, portions of the Antarctic regions have four-year average temperatures reaching -95℃ (-139℉). Most of the heat energy is being absorbed by the oceans over the equatorial to mid-latitude regions of the planet. Temperatures are quite mild over the equatorial regions, with four-year average seasonal temperatures near 21℃ (~70℉) during the summer and winter seasons in the northern hemisphere. Very cold temperatures extend further down from the polar regions to high-latitude regions as a result of the planets location within the outer regions of the Habitable Zone.

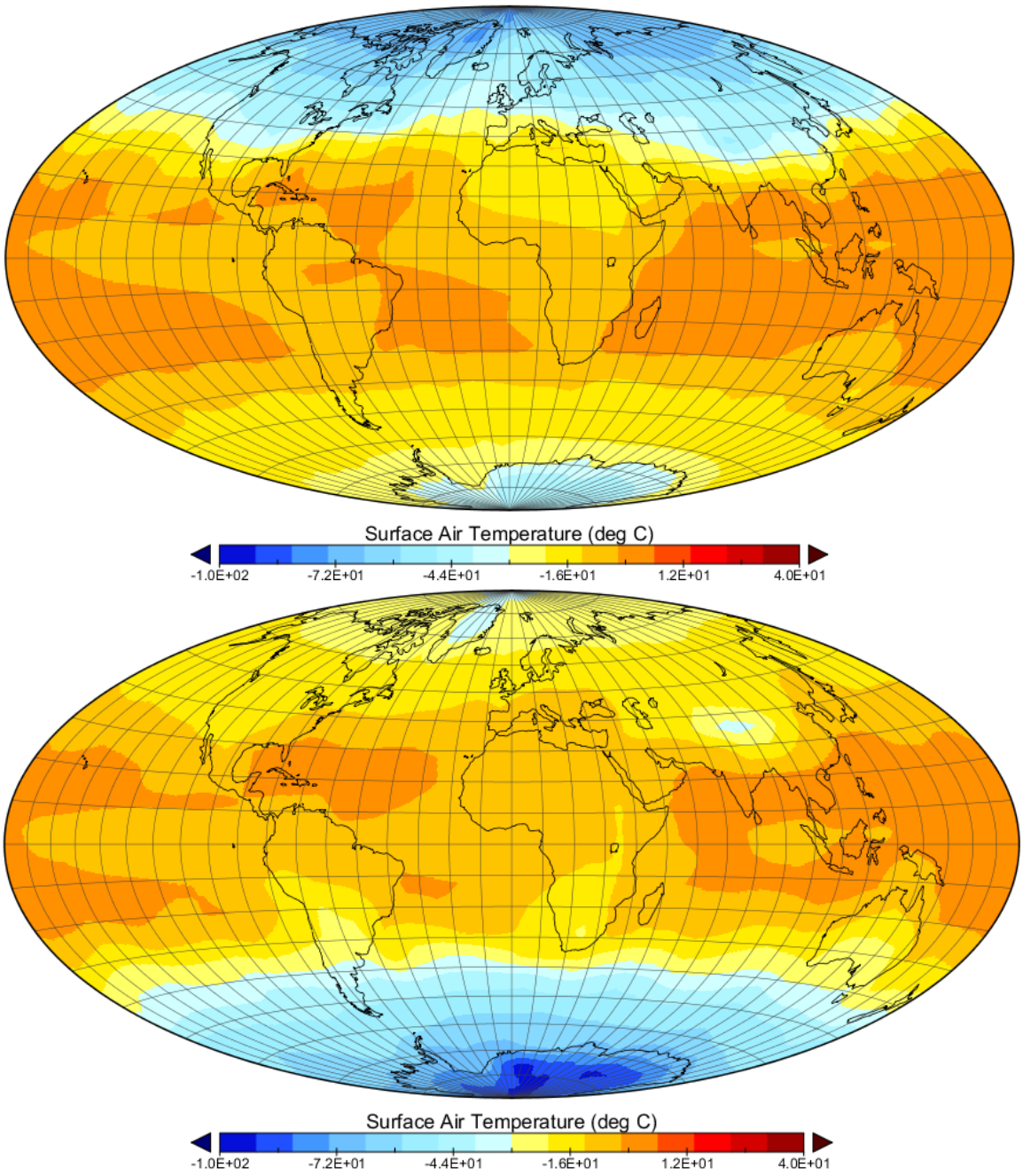


Figure 54. Winter and Summer air temperature maps for outer HZ region case. Four-year average for the seasonal surface air temperatures for the case of the planet located in the outer region of the Habitable Zone (at 1.2 AU). Shades of red denote higher temperatures, and blue shades denote colder temperatures. The oceans absorb most of the heat energy from the star, with extremely cold temperatures near the polar regions, extending down to high-latitude regions during winter (top map) and summer (bottom map) seasons in the northern hemisphere. The temperature for the northern hemisphere winter is shown in the top map, and the northern hemisphere summer in the bottom map.

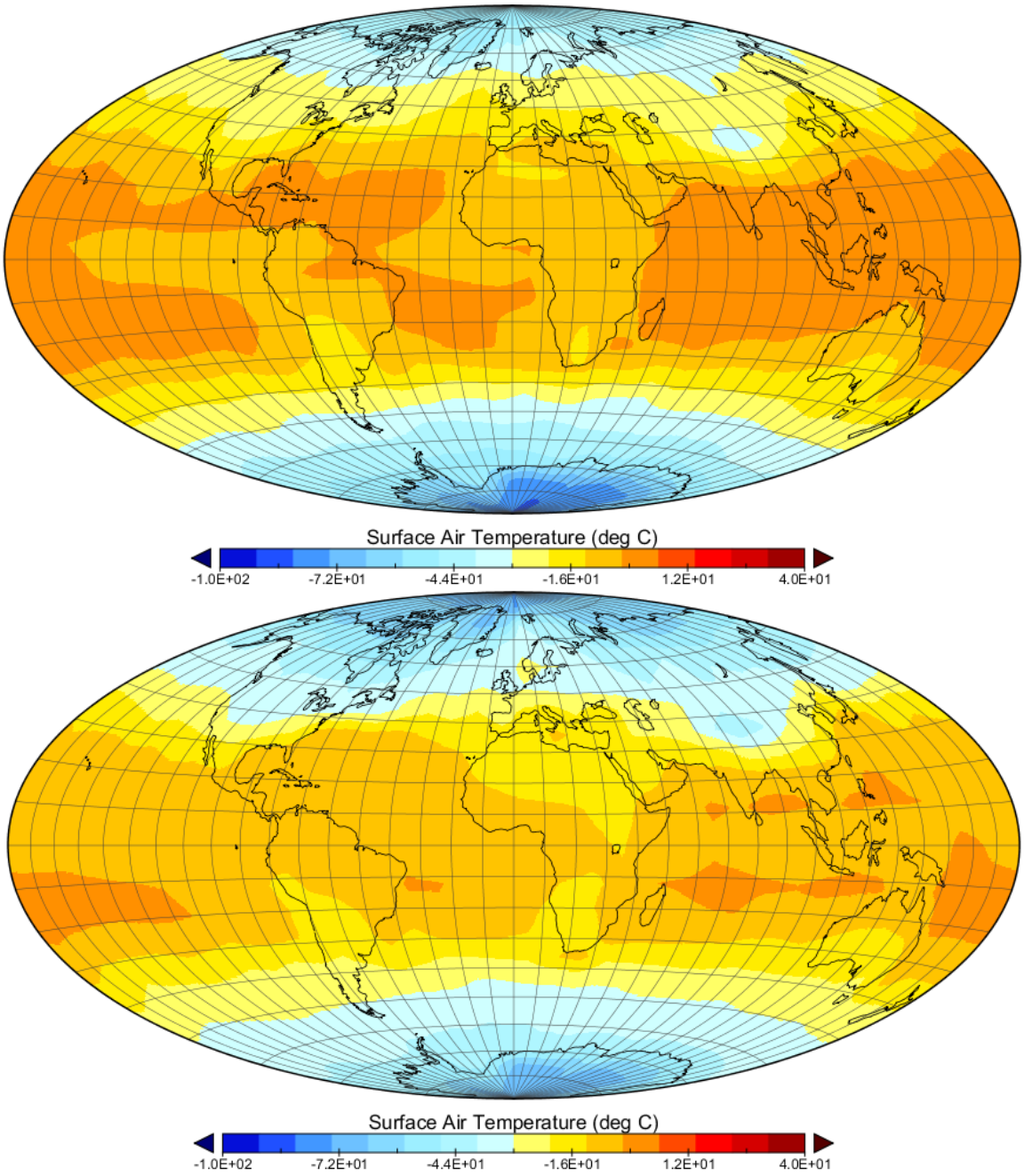


Figure 55. Surface air temperature maps near equinox seasons for the outer HZ region case. Four-year average for the seasonal surface air temperatures for the case of the planet located in the outer region of the Habitable Zone (at 1.2 AU). Shades of red denote higher temperatures, and blue shades denote colder temperatures. The top map shows the surface temperature during the spring season in the northern hemisphere, and the bottom map shows the temperature during the fall season in the northern hemisphere.

The fall season over most of the United States would experience very cold temperatures, ranging between -20℃ down to -30℃ (-4℉ to 22℉). Central to southern Asia would also experience similar temperatures, with central china experiencing even lower temperatures (Figure 55: cyan color seen in central China on the bottom map). Most of South America, Africa, and Australia do not experience temperatures below 0℃ (~31℉).

Figure 56 shows the percentage of snow coverage for the northern hemisphere winter (top map) and summer (bottom map) seasons. The snow pack extends to ±40˚ latitude in both hemispheres. The extent of the snow cap appears to correlate well with the temperature extremes experienced north and south of 40 degrees latitude for the northern and southern hemispheres, respectively. The planet's low eccentricity (near-circular) orbit at 1.2 AU from its host star (solar type star) has resulted in a permanent snow pack ranging from the polar regions down to the upper mid-latitude regions. Climatic conditions on this planet would be survivable, but average temperatures would not exceed 40℉.

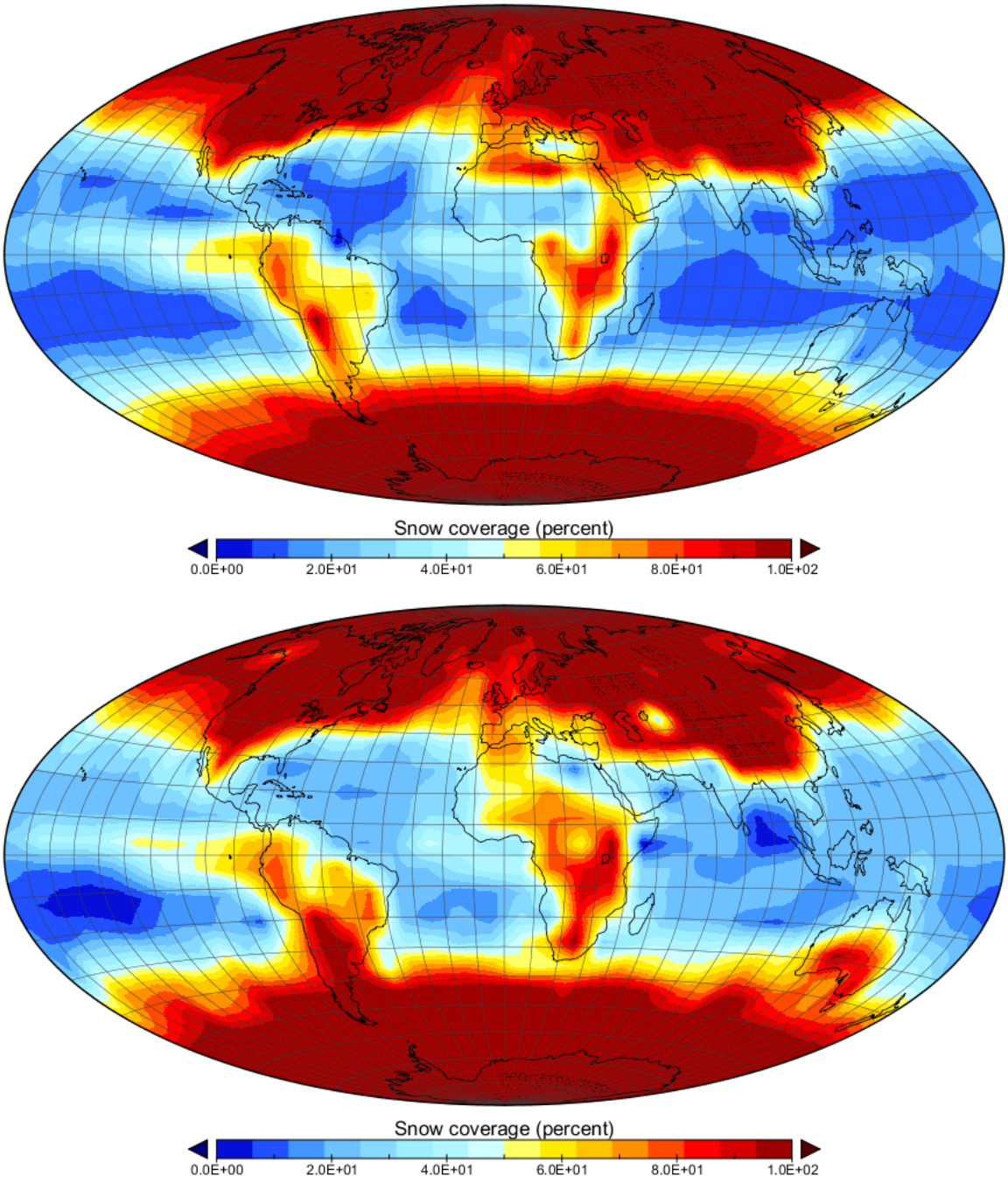


Figure 56. Snow coverage map for outer HZ region case. The amount of snow coverage is shown for the northern hemisphere winter (top map) and summer (bottom map) seasons. The data has been average over four-years to reduce inherent noise in the data. The snow cap extends to approximately 40°N and 40°S latitude during both winter and summer, and reaches near 100%. Light snow is seen to exist over most of the planet's oceans.

**An Advanced Civilization Neglects Their Home World – The Case of an Exponential Increase in Chlorofluorocarbon Emissions**

The last simulation deals with the case of a hypothetical Earth-like world whose advanced civilization never quit using Chlorofluorocarbons (CFCs). The model's initial conditions were set to the 2005 levels of CFC-11 and CFC-12, and a 5 percent per year exponential increase in CFC-11 was used. For CFC-12, a seven percent per year exponential increase in the powerful greenhouse gas was assumed. On Earth, CFCs were banned during the Montreal conference in Canada in 1987 (known as the Montreal Protocol). This action was taken to prevent further damage to the Earth's ozone layers, caused by the chlorine atom from the chlorofluorocarbon molecule. Solar UV-C radiation dissociates the CFC molecule, producing an organic radical and chlorine atom. The Ozone ($O_3$) then combines with free chlorine atoms in the atmosphere for form the molecule ClO. The chemical process continues when oxygen atoms combines with ClO, producing another chlorine atom (Cl) plus molecular oxygen ($O_2$). The whole chemical reactions can be symbolized as (for CFC-11)

$$CCl_3F + UV - C \rightarrow CCl_2F + Cl$$
$$Cl + O_3 \rightarrow ClO + O_2$$
$$ClO + O \rightarrow Cl + O_2$$

where a similar process can occur for the CFC-12 molecule.

In the simulation, the initial values of the chlorofluorocarbons were 0.000250 ppb for CFC-11 and 0.000530 ppb for CFC-12. The two greenhouse gases were allowed to increase exponentially by 5 percent per year out to the year 2200 (approximately 200 year time span). The results of the surface air temperature averaged over five years from 2188 to 2192 are shown in Figure 57. In Figure 57, parts of Northern Africa, Saudi Arabia, and

Northwestern India  reach five-year average temperatures upwards of 50 °C (122 °F), and a large portion of the United States has average surface air temperatures ranging from 36 to 45 °C (97-113 °F). Extreme temperatures (~113 °F) occur over most of Australia, Mexico, Northern South America, and Central Africa. The equatorial ocean region shows temperatures over 100 °F, and the north and south polar regions have temperatures approaching 12 °C and -10 °C, respectively. Over a 200 year time span, the effects due to an exponential increase in CFC emissions are profound, resulting in average maximum surface air temperatures that would be uncomfortable for human habitation.

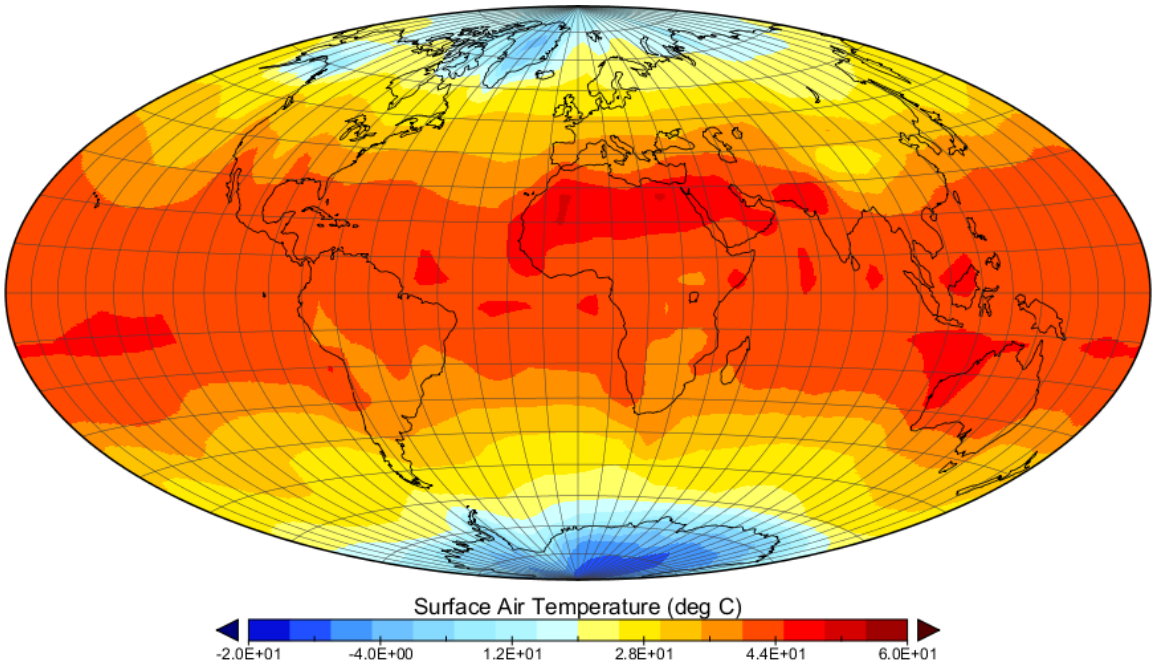


Figure 57. Five-year average surface air temperature averaged over five years (2188-2192) for the CFC scenario. Red shades indicate warmer temperatures and shades of blue represent colder temperatures.

The profound effect of the continued CFC emissions for this hypothetical scenario can be seen in Figure 58. The two hammer projection maps show the total global snow coverage (in percent) averaged over two different five-year periods. Note the dramatic decrease in total snow coverage near the end of the 200 year simulation period. Very little

snow coverage exists at the north polar region of the planet, with the exception of Greenland. The snow pack at Antarctica has decreased significantly at the end of the 200 year time span.

Global warming due to the five percent per year exponential increase in CFC-11 and seven percent exponential increase in CFC-12 could also lead to the melting of methane clathrate in the permafrost layer near the north polar regions, leading to further amplification of the positive feedback mechanism. It is fortunate that these two potent greenhouse gases were eliminated during the Montreal Protocol, else the consequences for Earth could have been profound.

Figure 58. The drastic effects of decreasing total snow coverage due to CFC emissions are seen in these two global maps.

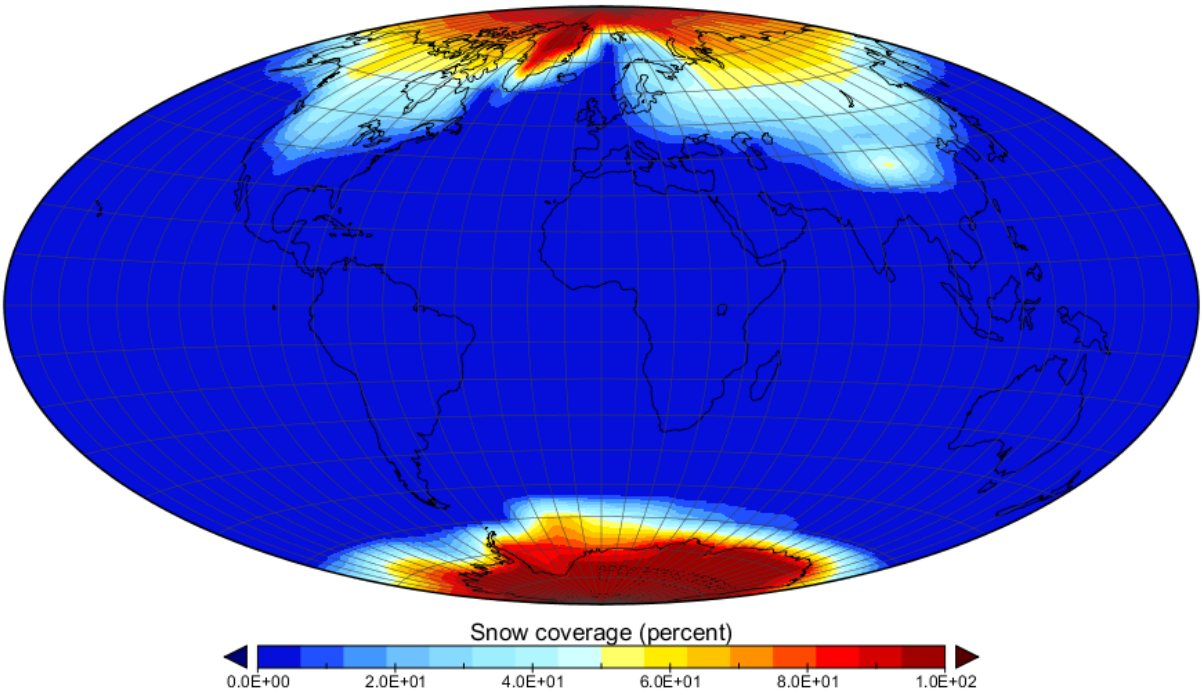

Figure 58 Cont

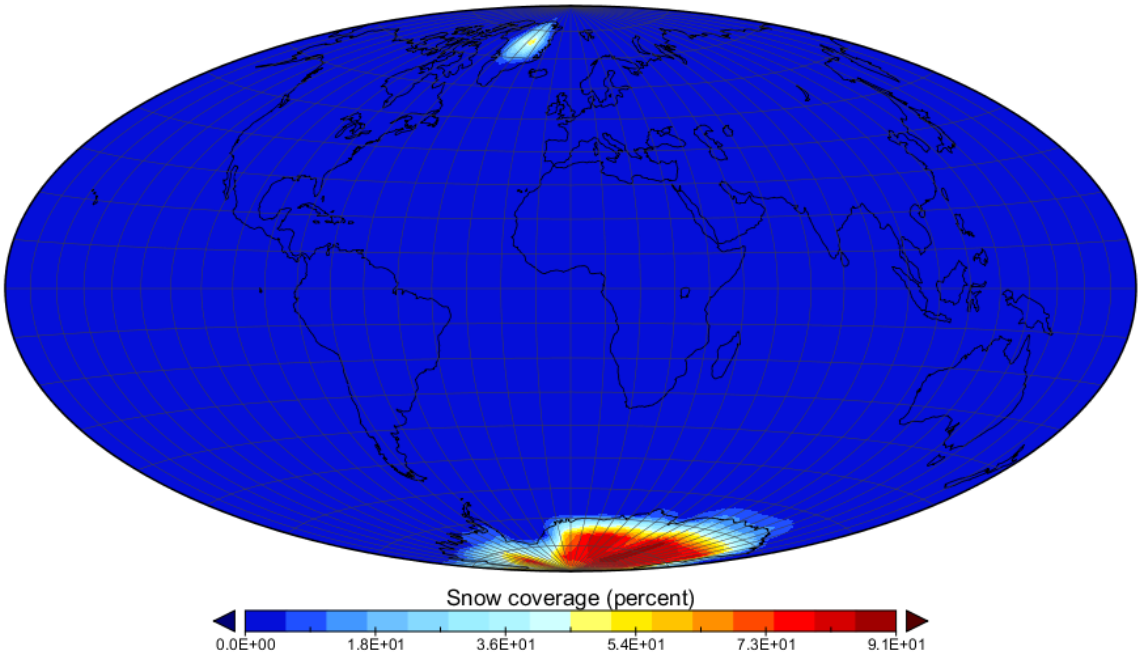


Figure 58. The drastic effects of decreasing total snow coverage due to CFC emissions are seen in these two global maps. The top map shows the total snow coverage averaged over five years from 2005-2009, and the bottom map shows the same total snow coverage distribution averaged over five years from 2188-2192.

Figure 59 shows the difference between the average surface air temperature for the years 2005-2009 and 2188-2192. The greatest temperature changes occur near the polar regions of the planet. This is expected as dramatic shifts in global climate occur at the polar regions first. Significant changes in the average surface air temperature also occur of most of North America and Asia. The continents in the Northern Hemisphere show greater changes in the average surface air temperature, most likely the result of their lower thermal inertia. In other words the land regions tend to heat up and cool off quicker than the oceans. It is interesting that the thermal inertia effect does not seem to occur over portions of South America and Africa.

It would be of interest to modify EdGCM to include the ability to calculate destruction of ozone ($O_3$) as a result of the UV dissociation of chlorofluorocarbons in the planet's stratosphere. In its current form, EdGCM only calculates the dynamical effects of climate evolution and does not take into account atmospheric chemistry.

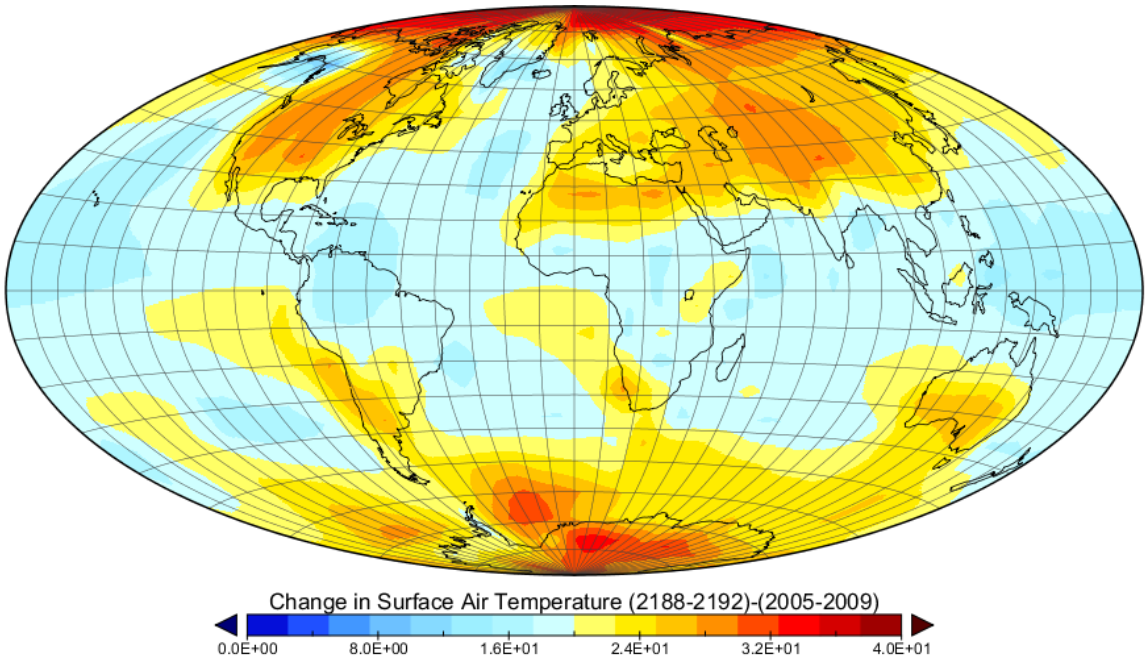


Figure 59. A hammer projected map showing the change in average surface air temperature between two different five-year averages (2188-2192 and 2005-2009) for the CFC scenario. The greatest changes occur at the planet's polar regions, as is expected. Minimal change in the average temperature occurs over the equatorial regions.

As with all the previous cases of 3-D climate model simulations carried out in this research, we see that dramatic effects due to both natural and anthropogenic increases in greenhouse gases, natural variations in solar irradiance, a change in orbital parameters of the planet, and location within the host star's habitable zone, result in climate change that occurs at the planet's polar regions first.

# CHAPTER IV

## COMPARISON WITH OBSERVATIONAL DATA

To verify the validity of the NASA GISS GCM-II, several simulated climate models are compared with observational data obtained by the Clouds and the Earth's Radiant Energy System (CERES). The CERES science instrument is used to measure the amount of solar radiation that is reflected at the top of Earth's atmosphere down to the surface of the planet. The instrument also measures the amount of emitted radiation at longer wavelengths (from 8 to 12 microns) as a function of depth in the Earth's atmosphere.

Figure 60 shows a comparison between the net radiation as measured by the CERES instrument, and the net radiation simulated using the NASA GISS GCM-II. The observational data was obtained during the month of July for the year 2007. The net radiation is essentially the net radiation that is available to influence the Earth's climate, and is a result of energy balance (between incoming and outgoing radiation at the top of the planet's atmosphere). Energy is input to the climate system when solar radiation that is transparent to the atmosphere reaches the surface of the planet. Energy can be output by several process; reflection from cloud layers, aerosols and other particulates (e.g. volcanic eruptions), and by thermal emission from the Earth's surface and atmosphere. If the energy balance is out of equilibrium (i.e. energy balance not equal to zero), the global mean temperature will either rise or fall over the course of the planet's orbital cycle. As

seen in the global maps, there is a surplus of energy over the equatorial regions, and a deficit over the polar regions of the planet. The imbalance between equatorial and polar net energy is a fundamental driver for oceanic and atmospheric circulation, which governs the overall climate pattern on Earth-like planets.

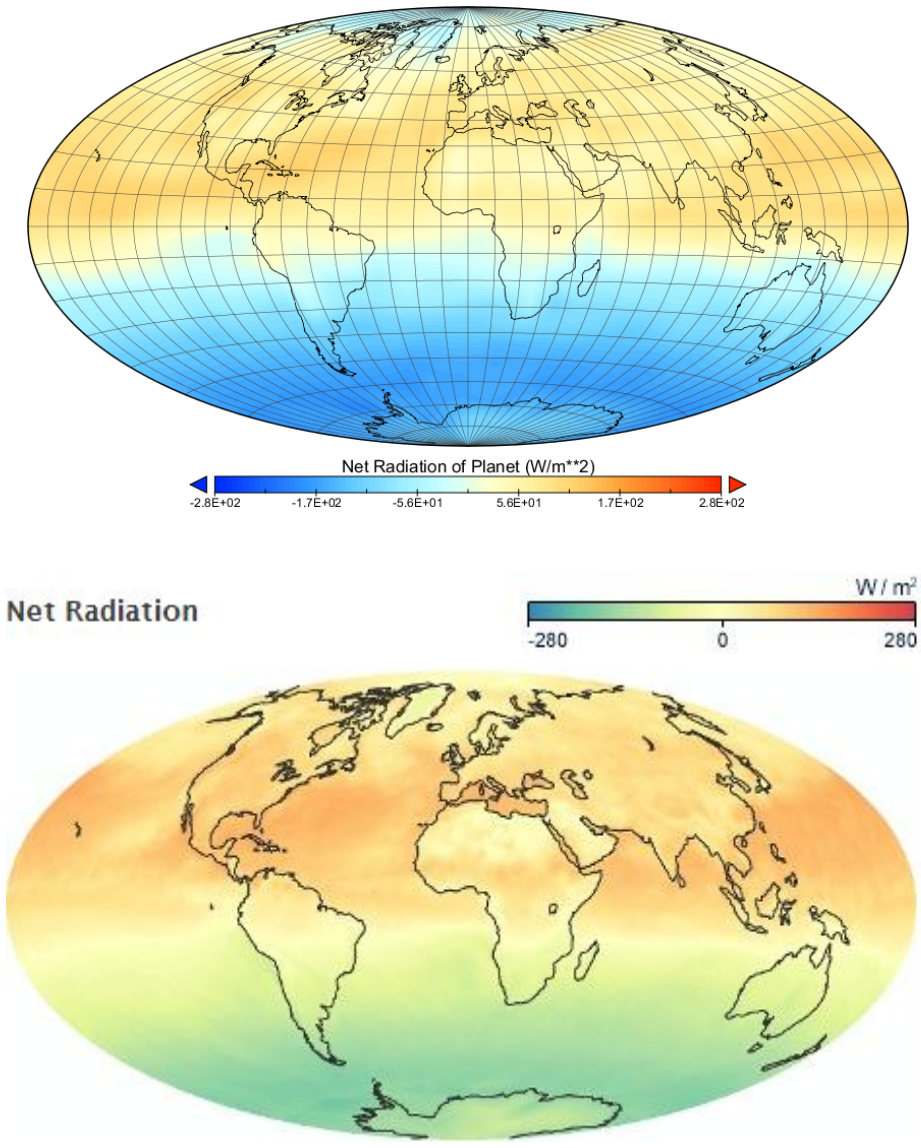


Figure 60. A comparison between CERES (bottom map) observations and climate model simulation (top map) for the net radiation averaged over the month of July for the year 2007. Both observational and simulated data agree qualitatively. There is a deficit of net radiation over the south polar region due to the obliquity of the planet, resulting in the southern hemisphere being directed away from the Sun. The equatorial region receives a surplus of net radiation.

Figure 61 shows a comparison between CERES observations and simulated climate model data using the NASA GISS GCM-II computer code. The data was obtained over the month of December for the year 2006.

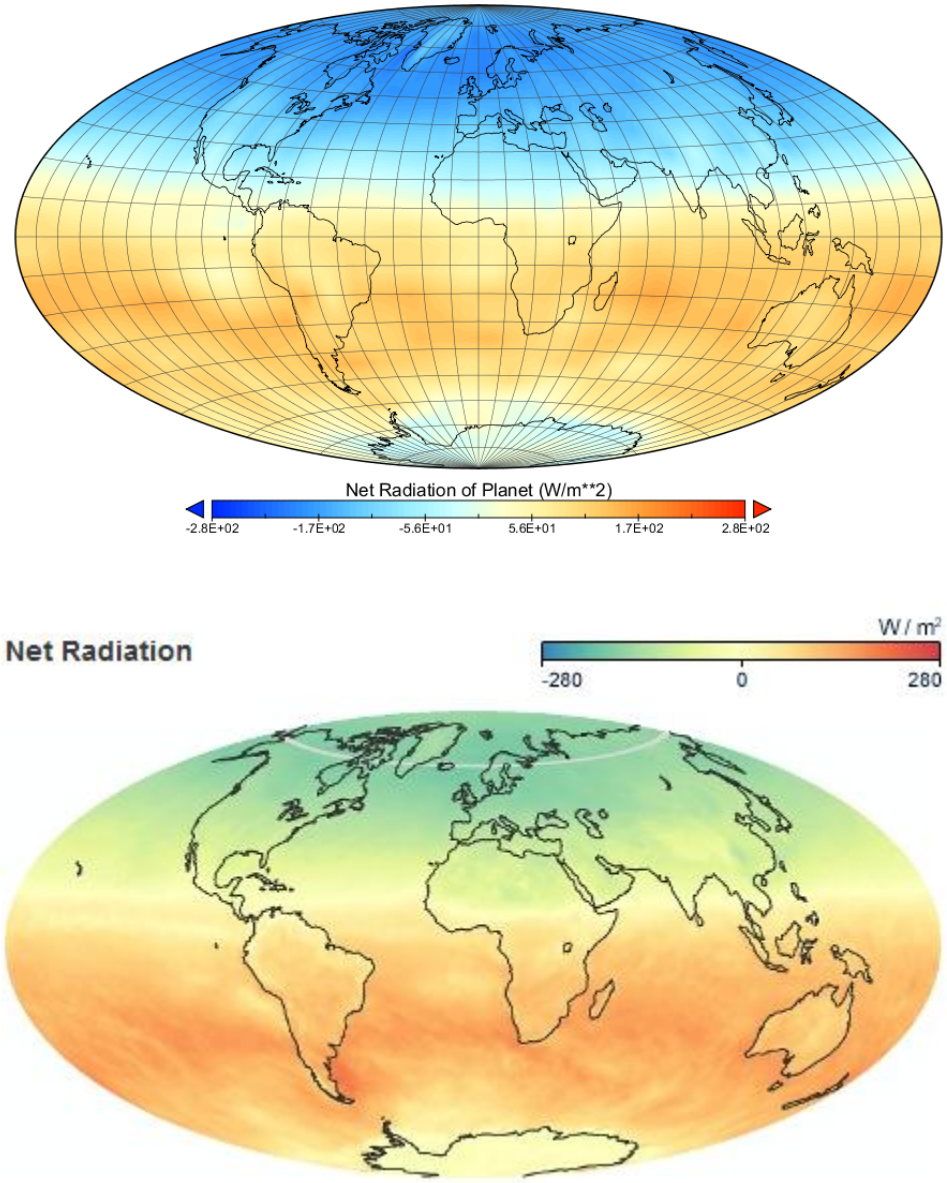


Figure 61. CERES (bottom map) versus GCM-II (top map) comparison of net radiation for December 2006. There is good qualitative agreement between the simulated and observed data. A net deficit of net radiation is seen in the northern hemisphere due to the tilt of the northern hemisphere away from the Sun.

During the equinox seasons, the planet's equator receives a majority of the solar insolation. This can be seen in a comparison of CERES observations of the net radiation with the net radiation as simulated using the GISS GCM-II (Figure 62).

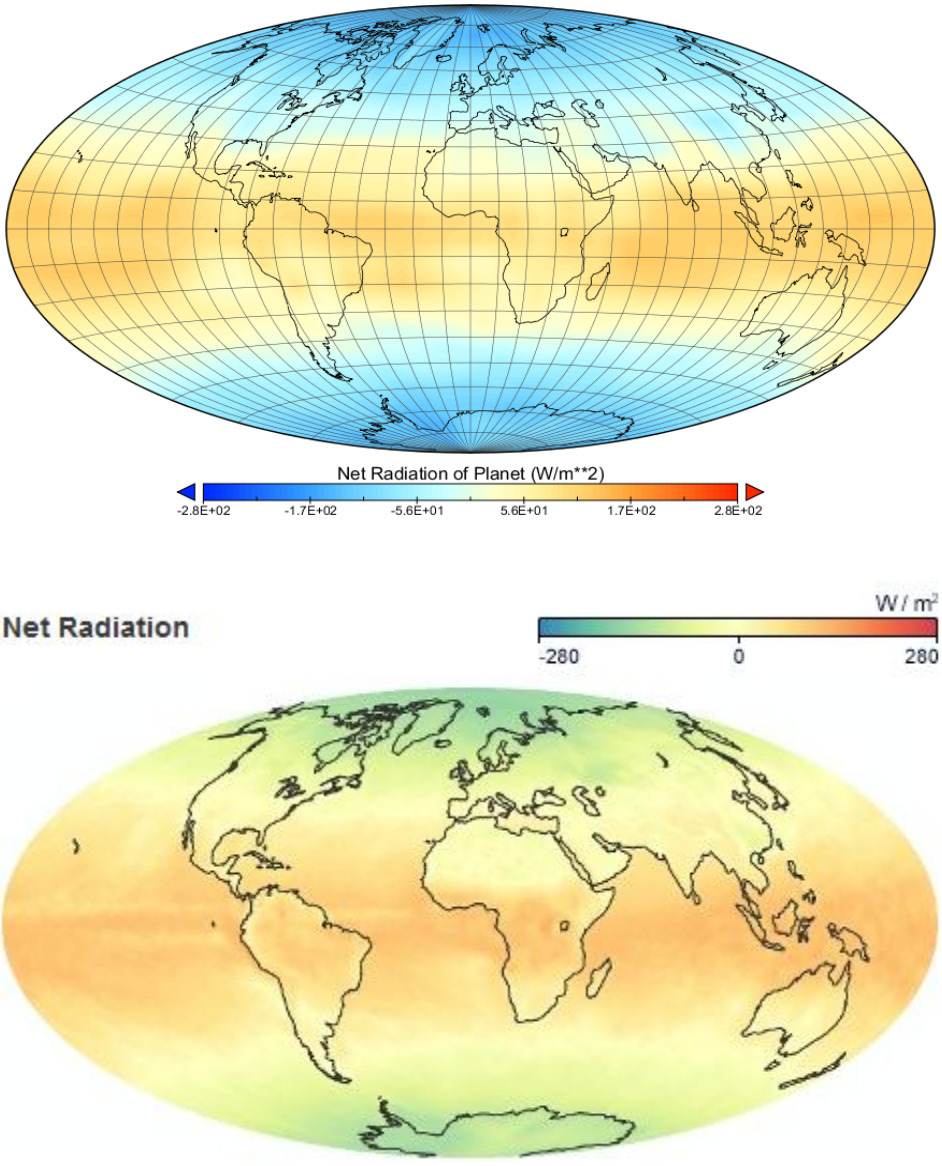


Figure 62. CERES (bottom map) versus GCM-II (top map) comparison of net radiation for March 2007. There is good qualitative agreement between the simulated and observed data. A net surplus of net radiation is seen over the equatorial region, with a net deficit observed over the planet's polar regions.

The total cloud fraction for the planet as measured by the CERES instrument shows good qualitative agreement with simulated data from the GCM-II (Figure 63). It is interesting to note that there can be large differences between simulated and observed cloud fraction, as clouds represent one the major sources of uncertainties in 3-D climate models. This is not the case for the January 2005 comparison.

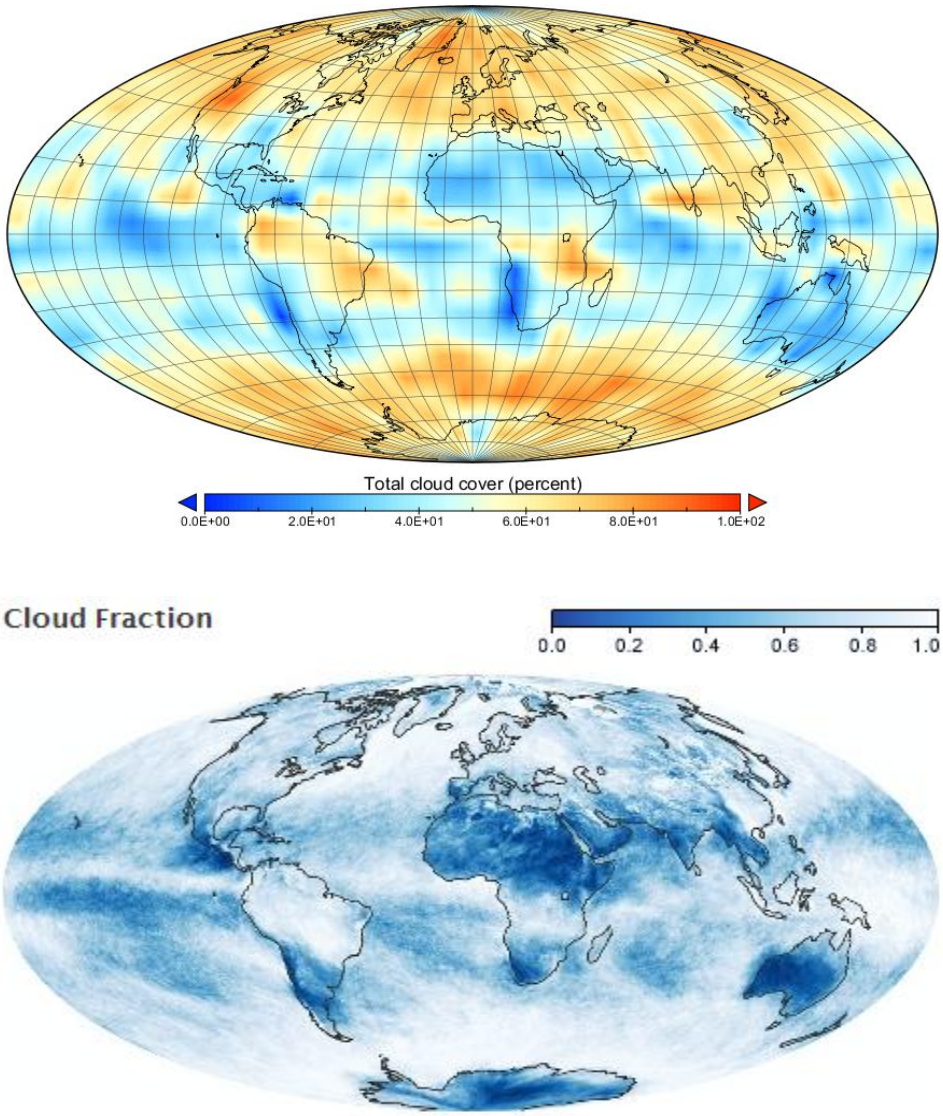


Figure 63. CERES (bottom) versus GCM-II (top) total cloud fraction for January 2005.

# CHAPTER V

# LESSONS LEARNED AND SUMMARY OF RESULTS

## Conclusion

The simulations presented in this thesis provided an evaluation of the EdGCM interface to the GCM-II. The interface allows one to have access to most of the initial conditions and different radiative forcing within the GCM-II. The first series of simulations involved extreme cases of global warming as a result of greenhouse gas emissions. Three major greenhouse gases were modeled in GCM-II, including carbon dioxide, nitrous oxide, and methane. The effect of chlorofluorocarbons on greenhouse warming was also examined on a hypothetical Earth-like planet whose civilization (if such civilizations exist) failed to stop the use of CFCs. The benefit of studying the effect of CFCs on global warming is also of interest to Astrobiologists interested in planetary terraforming. The use of chlorofluorocarbons have been suggested as one possible solution to raising the temperature of Mars as an initial stage in terraforming the planet.

The GCM simulations presented in this thesis have illustrated the basic effects from radiative forcing from four greenhouse gases. We see that the radiative forcing acts as a perturbation to the climate system. In other words, a change in the total mass of a particular greenhouse gas in the planet's atmosphere results in a radiative forcing. The planet's global radiative budget is perturbed by this radiative forcing, thereby affecting

the global climate pattern on the planet. The radiative forcing leads to an increase in global temperature given by (Jacob 1999)

$$\Delta T_0 = \lambda \Delta F \qquad (34)$$

where $\Delta F$ is the radiative forcing, defined as (Jacob 1999)

$$\Delta F = \frac{\Delta f}{2} \sigma T_0^2 \quad (35)$$

where $\sigma$ is the Stefan-Boltzmann constant, $\Delta f$ is the change in the absorption efficiency of the atmosphere, and $T_0$ is the surface temperature of the planet. Global climate model simulations predict a range of 0.3-1.4 K/m$^2$/W (model dependent) (IPCC) for the sensitivity parameter, denoted by $\lambda$ in equation 34. The IPCC gives a total radiative forcing of ~2.33 W/m$^2$ for the combined effect of $CO_2$, $CH_4$, $N_2O$, CFC-11, and CFC-12 greenhouse gas emissions since preindustrial time. This yields a change in the global temperature since preindustrial time of ~0.7 K to 3.3 K for the range in the climate sensitivity parameter predicted by global climate model simulations. The amount of global warming observed is estimated to be ~0.6 K. Thus, we see that global climate models tend to over-predict the change in temperature due to greenhouse gas emissions. This over prediction could be due to an inaccurate treatment of atmospheric aerosols, hazes, and clouds in the 3-D climate model. The total cloud cover represents a major source of uncertainty in the response of the climate model to radiative forcing. However, climate model simulations carried out using the GISS GCM-II (and other GCMs) show that a linear relationship exists between the change in temperature and the initial radiative forcing. The slope of the linear relationship determines the degree of difference of results generated by the various global climate models.

The effect of change in surface and planetary albedo (surface plus clouds, etc.) can effect the degree of radiative forcing, as seen in some of the 3-D climate model simulations presented in this research. For example, if Earth's total albedo were to increase just 0.005 (1.67%) since preindustrial times, the radiative forcing would amount to (Jacob 1999)

$$\Delta F = \frac{F_{\odot}\Delta A}{4} = \frac{1366 W/m^2 \times -0.005}{4} = -1.70 W/m^2 \quad (36)$$

where $\Delta A$ is the change in planetary albedo (- sign for an increase in albedo since it provides a negative feedback). The radiative forcing due to an increase in albedo (e.g. due to an increase in average cloud cover) leads to a negative feedback effect ($\Delta T_0$ ~ -0.5 °K for a sensitivity parameter of 0.3), which could help cancel some or all of the positive feedback effects due to increasing greenhouse emissions. However, it is not certain whether clouds lead to a negative or positive feedback effect, since increasing water vapor content in the planet's atmosphere could lead to an increase in precipitation (condensation). The increase in precipitation would result in a decrease in the total cloud cover. The complex interaction among radiative forcing due to greenhouse gas emissions and change in planetary albedo represent provides a good example of the difficulties encountered in 3-D climate modeling of Earth-like planets.

Three simulation scenarios were explored. The first involved a linear increase of the three greenhouse gases according to recent estimates by the Intergovernmental Panel on Climate Change (IPCC). The second simulation was a scenario based on an exponential increase in carbon dioxide over 200 years (to the year 2100), and the third simulation was based on a worst case scenario involving the hypothetical melting of

clathrates within the arctic and Siberian permafrost layers. All of the scenarios demonstrated the positive feedback mechanism associated with the buildup of greenhouse gases within Earth's atmosphere over a 200 year simulation time period. An interesting result in all of the greenhouse gas emission scenarios is an increase in temperature over Northwest Africa over the next 200 years. This is particularly important for climatic effects within the United States since the Atlantic hurricane season depends on warm air rising over Central and Northwest Africa. More severe hurricanes over the Atlantic Ocean could have severe repercussions on the economy of the United States, as billions of dollars in damage can result from hurricanes that impact the eastern coastline.

Another main result from the greenhouse gas simulations is that the total cloud cover of the planet plays a major role in determining the radiation budget of the lower atmosphere (troposphere). The cloud cover regulates the total radiation budget by reflecting, scattering, absorbing incoming solar radiation. This effects the amount of solar radiation reaching the planet's surface. The clouds also play a role in regulating the overall albedo of the planet. Increasing the albedo results in higher reflectivity and less absorption of solar insolation. Less cloud cover results in lower albedos that allow more absorption of solar energy. Together with radiative forcing due to both natural and anthropogenic greenhouse emissions, the overall albedo plays a key role in regulating the planet's surface air temperature. However, modeling the total cloud cover of the planet is one of the largest sources of error in 3-D climate models. Modern climate models like the GCM-II code can reproduce the latitudinal temperature profile with a high degree of accuracy. However, these models have difficulty reproducing the planet's cloud cover to the same accuracy of the temperature distribution. The low error in simulating the

latitudinal temperature profile is the result of the fact that most 3-D climate models solve the equations of energy flow. The strong correlation between thermal radiation emission and temperature is the result of the Stefan-Boltzman law, which states that the emitted radiation is directly proportional to the fourth power of the temperature. This means there is a correspondent proportionality in the error in the temperature distribution predicted by modern climate models.

The GCM-II 3-D climate model greenhouse scenarios also demonstrated a correlation between the net heating over the equatorial regions and net radiation. The gradient in the net heating as a function of latitude is the result of variations in albedo and the amount of solar insolation as a function of latitude. The results of the greenhouse gas simulations showed that temperature change is related to the albedo over a particular region of the planet. For instance, as the temperatures rise over the arctic region of the planet due to 200 years of greenhouse gas emissions, the more land masses are exposed. These darker land masses have lower albedos, which result in an increase in absorption of solar energy. This, in turn, causes a further rise in temperature which leads to more ice melt. This ice-albedo positive feedback mechanism was noted in the results of the greenhouse gas simulations. All of the simulations demonstrated that significant climatic changes occur over the polar regions of the planet first.

The next simulation involved setting a prolonged solar minimum for approximately 200 years, longer than the Maunder Minimum that occurred during the late $17^{th}$ century. The solar irradiance over this time span was -6 $W/m^2$ less than the present-day value of ~1366 $W/m^2$. The results of this simulation revealed a small negative temperature anomaly in the zonal average, ranging from -1.5 to -0.65 degrees

Celsius. This compares favorably with the theoretical estimate of the total global temperature change, ranging from -0.57 to -1.26 degrees Celsius, for a prolonged drop in the solar irradiance of -6 $W/m^2$ over a period of 200 years. Stronger negative temperature anomalies were noted over the Arctic region, and the zonal average shows a general trend towards stronger negative anomalies at the polar regions. This demonstrates that climate changes in response to radiative forcing, whether due to greenhouse gas emissions or solar irradiance variations, tend to occur first at the planet's polar regions.

The next series of climate model simulations investigated the effects of different axial tilts (obliquities) on the overall global climate pattern of an Earth-like planet. In the context of the simulations carried out in this work, the term "Earth-like" means that the same land mass configuration was used in all of the simulations. This is due to the inability to easily change the configuration of the present-day land mass of Earth to any arbitrary land mass with the EdGCM program. The main conclusion from the obliquity simulations is the following. The higher the planet's obliquity, the more radical the climatic extremes become. The GCM-II code demonstrated the effect of a zero degree obliquity on global climate. The results showed very little seasonal variations in climate over the course of an orbit cycle. This is the result of an equal distribution of daytime hours at all latitudes. Thus, there is little seasonal variation and the polar regions remain very cold. In reality there will be some annual variations due to the different thermal inertia and heat capacity of terrain types covering the planet's surface.

In contrast to the simulation for an obliquity of zero degrees, the simulation results for a hypothetical Earth-like planet with an extreme obliquity of 90 degrees demonstrated large annual variations in climate. This is the result of significant variations

in the amount of solar radiation absorbed as a function of orbital phase. The angle of solar radiation with respect to the normal incidence also undergoes large annual variations. Therefore, for the case of an obliquity of 90 degrees there are extreme seasons. This is clearly demonstrated in the results from the GCM-II simulations, where the polar regions have extreme temperature increases during the summer season, followed by periods of cold climate conditions during the winter season.

The next series of simulations explored the global climate patterns associated with high-eccentricity orbits of Earth-like planets. Due to numerical instabilities encountered using the GCM-II code, the two cases used were for eccentricities of 0.2 and 0.3. The case for an eccentricity of 0.3 resulted in a perihelion distance of 0.7 AU (just within the orbit of Venus) and an aphelion of 1.3 AU. Results of these simulations showed extreme temperature differences, especially in the northern hemisphere. The results illustrated the contrast between the oceans and continents in the planet's southern hemisphere, with the large area covered by ocean water acting as a strong heat sink. In other words, the oceans store the majority of the received solar insolation, and conduct the insolation with high efficiency. The extreme variation in climate is due to the high eccentricity of the planet's orbit and the obliquity (axial tilt) of the planet's rotation axis. It is suspected that land mass configuration and ocean area coverage will have profound effects on the global climate pattern of these worlds. A rather interesting result from the high-eccentricity simulations is the lack of an extension of a snow cap during the time when the planet spends on long time during its aphelion when it is moving slowest in its orbit around the host star. This may be the result of  a large thermal inertia from the oceans that cover

approximately 70% of the planet's surface. The thermal inertia acts as a buffer against global freezing.

The general conclusion for the scenarios involving planets with high orbital eccentricities is that planets on orbits with higher eccentricities tend to show more latitudinal variation in average surface air temperature and other climatic parameters than those on nearly-circular orbits. Producing a catalog of climate model simulations for a wide range of orbital eccentricities would be of great benefit to the scientific community, since many of the newly discovered exoplanets have non-circular eccentricities. This suggest that Earth-like planets with nearly circular orbits like Earth only sample a very small subset of potentially habitable planets. It is therefore important for future work in this area to expand the climate modeling of Earth-like worlds to those with a wide range of orbital eccentricities.

The final set of simulations involved placing the Earth at the inner region (0.90 AU) and outer region (1.2 AU) of the Sun's habitable zone. The eccentricity was set to Earth's current value, a nearly circular orbit. The original initial condition of the inner HZ boundary (locating the orbit of Earth at the present-day heliocentric distance of Venus at 0.72 AU) resulted in numerical instability in the GCM-II computer code. It is suspected that this was the result of a runaway greenhouse effect that prevented the code from completing the simulation run. However, the two simulation scenarios using 0.9 AU for the inner HZ boundary and 1.2 AU for the outer boundary represent the conservative estimate of the Continuously Habitable Zone (CHZ). The CHZ is defined as that region within the Solar System that allows an Earth-like planet to remain habitable since the heavy bombardment epoch came to an end.

The most interesting results from these two simulations is the permanent snow pack ranging from the polar regions down to the upper mid-latitude regions for the case where the planet is located in the outer region of the Habitable Zone. The temperatures on this Earth-like planet orbiting at 1.2 AU from its parent star would never exceed 40℉. Temperatures across most of the United States would be very harsh, ranging between -4℉ and 22℉. During the winter season at the south pole, four-year average surface air temperatures reach -139℉ over portions of Antarctica. This is in contrast to the average temperature of approximately -80℉ during the winter season.

The extreme surface air temperatures experienced during the simulation period for the case of the inner and outer Habitable Zone regions would have profound effects on any inhabitants living on these planets. The results of the simulations indicate that habitability conditions of Earth-like worlds would depend strongly on the heliocentric distance, since the distance from the host star determines the amount of solar irradiance the planet receives. The amount of solar insolation received by an Earth-like planet play a key role in determining the strength of the planet's greenhouse effect. In turn, it is the amount of greenhouse warming that determines the precise location of the boundaries of the habitable zone for a given planet. A global decrease in food production due to harsh environmental conditions experienced by Earth-like planets orbiting in the inner and outer regions of the Habitable Zone would lead to wide spread starvation of any inhabitants living on these planets. The drastic change in climate patterns would result in further damage to the global environment, with possible mass extinction events.

The results from all of the simulations carried out using the EdGCM interface to the GCM-II code has illustrated the effects of natural and anthropogenic greenhouse gas

emissions on global climate by changing the atmospheric composition of a hypothetical Earth-like planet.

The increased greenhouse gases in the planet's atmosphere results in radiative forcing that changes the planet's surface air temperature. Orbital parameters and solar irradiance also affect the planet's atmospheric composition, which also affects the total radiative forcing and resulting temperature change. Radical changes in planetary climate, particularly the surface air temperature can have profound effects on any society inhabiting the planet. On Earth, impacts on society and the global environment/ecosystem are primary drivers of policy and administrative actions, which, in turn, can lead to further anthropogenic changes in the global climate (Figure 64).

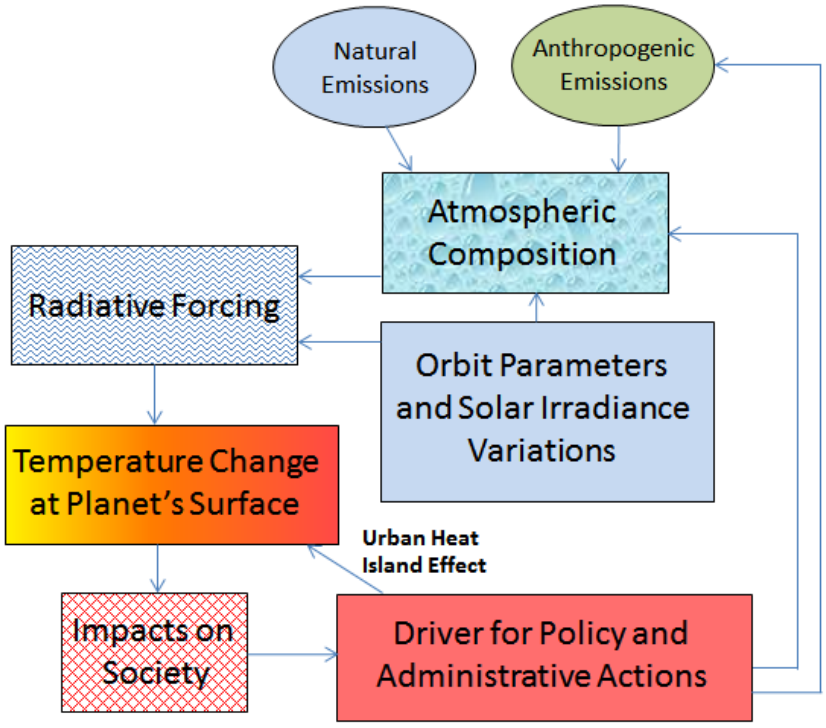


Figure 64. Interrelationship diagram. The interrelationship between greenhouse gas emissions, orbital parameters, planetary surface air temperature, global climate, and administrative policy.

The climate modeling results also lead to suggestions on improving the EdGCM interface to the GCM-II model, including the model itself. The various factors involved in improving any 3-D global climate model code are illustrated in Figure 65. Various satellite and airborne observations can be used to improve atmospheric chemistry and dynamics. These theoretical constructs are used to derive analytic approximations, parameterizations and numerical solutions to create the 3-D global climate model. The climate model requires additional data, including boundary conditions, initial conditions and the various radiative forcings. These can be obtained using the observational data provided by satellite and airborne sensors. The results of global climate model simulations can be used as a validation of the theory behind the GCM. If the results of the climate model simulations differ significantly from measured values of climate parameters, the model must be improved and/or changed until agreement is achieved with observational data to within a certain degree of accuracy.

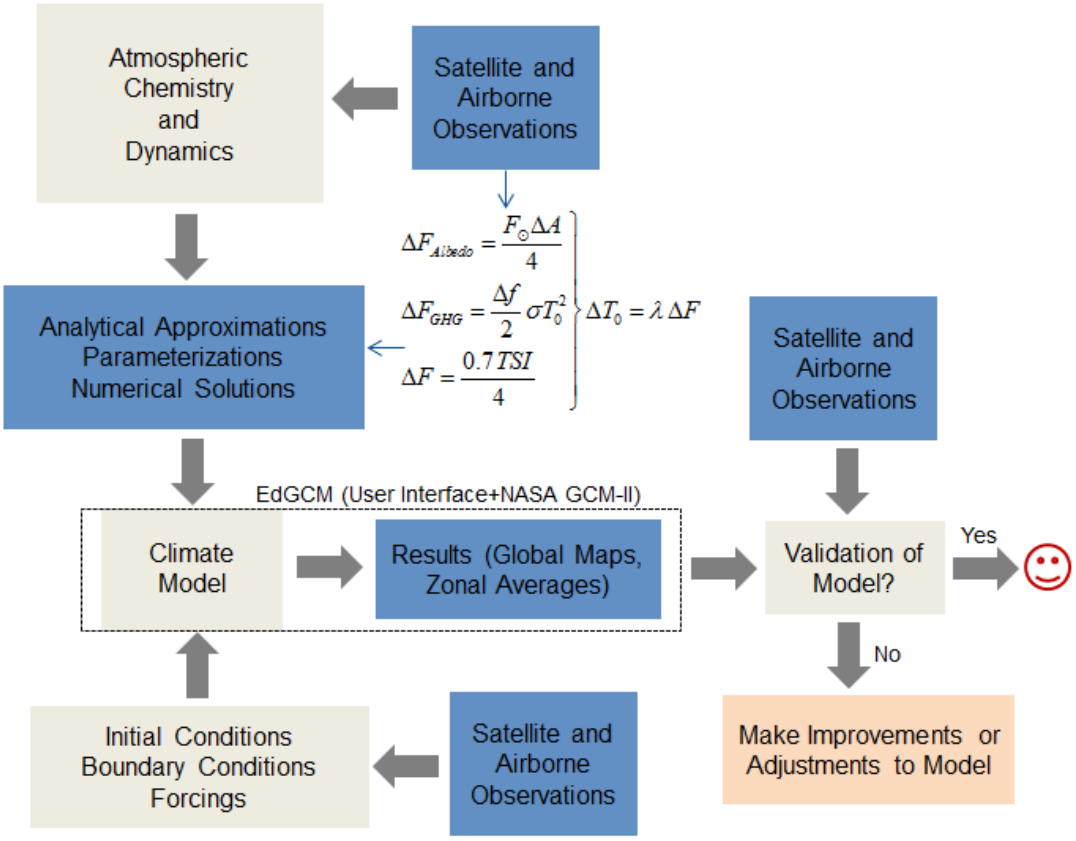


Figure 65. Illustration of the scientific method of global climate model validation.

To sample a wide variety of possible Earth-like planets, the code should be capable of changing the land mass distribution to an arbitrary configuration. Current modeling is limited to using the Earth's land mass distribution, or several fixed paleoclimate land mass configurations. The land mass distribution and ocean coverage play a key role in determining the overall climate patterns on Earth-like planets due to the difference between the thermal inertia and specific heat capacity of surface terrain. The ability to change the planet's mass and rotational period would allow sampling of a large set of possible Earth-like planets, including the ability to model the climate patterns on super-Earth planets (rocky terrestrial planets with masses ranging between 1.5 and 10 Earth masses). An improvement in the numerical stability of the code to allow more

extreme scenarios to be modeled without terminating the simulation. In its current configuration, the EdGCM interface to the GCM-II provides university students the ability to explore the effects of global climate change over course resolution based on three major greenhouse gas emissions (carbon dioxide, nitrous oxide, and methane), plus two chlorofluorocarbon (CFC) species. The student is able to specify trends in the emission rates of these gases over time either through specifying a specific analytical function or using an external trend data file. The ability to add additional greenhouse gases, especially trace gases would allow more detailed analysis of their effects on global warming. The ability to change the planet's orbital parameters (eccentricity and obliquity) allows students to explore the effects of axial tilt on the seasonal variations of global climate. The EdGCM interface and GCM-II do not currently allow the student to specify trends in these two orbital parameters as a function of time. Including this capability in future versions of the computer code could allow simulations to be carried out over extremely long time spans to explore variations in climate patterns with time resulting from oscillations in obliquity and eccentricity. This capability would be very beneficial for exploring the climate on Mars as a result of changing obliquity. This would provide the capability to simulate global climate variations on Earth-like planets that have no large moon capable of stabilizing the planet's obliquity as is the case for Earth.

A final modification to the GCM-II code is to include the effects due to urban heat islands. As metropolitan areas on Earth continue to expand with time, the so-called Urban heat Island Effect is contributing to changes in temperatures, particularly within and near major urban centers. This is especially important, as temperature increases due to the urban heat island effect can be a major driver for policy and administrative actions

needed to plan future mitigation strategies. Many of the 3-D climate model simulations for extreme cases, resulted in global temperature changes (>4 °C) that could lead to a continuous sea level rise over the next two centuries. The sea level rise is caused by the expansion of ocean water as a result of global warming, and the melting of planetary glaciers. An equation for estimating the change in sea level as a function of global temperature change has been derived by Roper (2012). In terms of the change in temperature (measured in degrees Celsius), the equilibrium sea level (measured in meters) can be determined using the following cubic function:

$$d = T\left(0.54T^2 + 0.39T + 7.7\right) \quad (37)$$

where $T$ is the temperature change (relative to 1990), and $d$ the equilibrium sea level. For a global temperature change of at least 4 °C (resulting from several of the climate model simulations presented in this work), the estimated equilibrium sea level would be ~72 meters. This would put a large majority of the coastal urban zones beneath the water, resulting in significant loss of life, and relocation of a substantial fraction of the human populous.

## REFERENCES


Biastock, A. *et al*. 2011. Rising arctic ocean temperatures cause gas hydrate destabilization and ocean acidification. *Geophysical Research Letters*, 38.

Bruhl, C. 1993. The impact of the future scenarios for methane and other chemically active gases on the gwp of methane. *Chemosphere*, *26*, 731-738.

Archer, D., Buffett, B., & Broukin, V. 2009. Ocean methane hydrates as a slow tipping point in the global carbon cycle. *PNAS*, 106.

Chandler, M. A., Richards, S. J., & Shopsin, M. 2005. EdGCM: Enhancing climate science education through climate modeling research projects. In Proceedings of the 85th Annual Meeting of the American Meteorological Society, 14th Symposium on Education, Jan 8-14, 2005, San Diego, CA, pp. P1.5 http://edgcm.columbia.edu.

Evans, W. F. J., & Puckrin, E. 1999. A comparison of gcm models with experimental measurements of surface radiative forcing by greenhouse gases. 10th Symposium on Global Change Studies, American Meteorological Society, 378-381, 10-15 January 1999, Dallas, Texas.

Feulner, G., & Rahmstorf, S., 2010. On the effect of a new grand minimum of solar activity on the future climate on earth. *Geophys Res Lett*, *37*, L05707.

Ghil, M. 1984. Climate sensitivity, energy balance models and oscillatory climate models. *J Geophys Res*, *89*, 1280-1284.

Goode, P. R., et al. 2001. Earthshine observations of Earth's reflectance. *Geophy Res Lett*, 28, 1671-1674.

Halliday, A. N. 2000. Terrestrial accretion rates and the origin of the moon. *Earth and Planetary Science Letters*, 176, 17-30.

Hansen, J., Sato, M., & Ruedy, R. 1997. Radiative forcing and climate response. *J Geophys Res*, *102*, 6831-6864.

Hansen, J., et al. 1988. Global climate changes as forecast by Goddard Institute for Space Studies three-dimensional model. *J Geophys Res*, *93*, 9341-9364.

Hansen, J., Lacis, A., Rind, D., & Russell, G. 1984. Climate sensitivity: Analysis of feedback mechanisms, climate processes and climate sensitivity. *AGU Geophysical Monograph*, 29, Maurice Ewing Vol. 5, 130-163.

Hansen, J. G., et al. 1983. Efficient three-dimensional global climate models for climate studies: Models I and II. *M Wea Rev*, *111*, 609-662.

Harvey, L. D., & Huang, Z. 1995. Evaluation of the potential impact of methane clathrate destabilization on future global warming. *J Geo Phys Res*, *100*, 2905-2926.

Hauglustaine, D. A., Grainer, C., & Brasseur, G. P. 1994. Impact of Increased Methane Emissions on the Atmospheric Composition and Related Radiative Forcing on the Climate System. In: Non $CO_2$ Greenhouse Gases [van Ham, J. et al. (eds.)]. Kluwer Academic Publishers, 253-259.

Held, I. M., & Soden, B. J. 2000. Water vapor feedback and global warming. *Annual Review of Energy and the Environment*, *25*, 441-475.

Henderson-Sellers, A., & McGuffie, K. 1988. A climate modeling primer. New York, John Wiley & Sons, Inc.

Gorodetskaya, I. V., Cane, M. A., Temblay, L. B., & Kaplan, A. 2006. The effects of sea-ice and land-snow concentrations on planetary albedo from the earth radiation budget experiment. *Atmos. Ocean, 44*, 195-205.

Jacob, D. J. 1999. Introduction to Atmospheric Chemistry. Princeton University Press.

Kane, S. R., & Gelino, D. M. 2011. The Habitable Zone Gallery. *PASP* in press (arXiv: 1202.2377).

Kasting, J. F., & Williams, D. M. 1997. Habitable planets with high obliquities. *International Journal of Solar System Studies*, *129*, 254-267.

Kasting, J. F. 1988. Runaway and moist greenhouse atmospheres and the evolution of Earth and Venus. *Icarus, 74*, 472-494.

Koenderink, J. J., & Richards, W. A. 1992. Why is snow so bright? *J. Opt Sci Am A*, 9, pp. 643-648.

Krey, V. *et al*. 2009. Gas hydrates: entrance to a methane age or climate threat? *Environmental Research Letters*, 4, 034007.

Laskar, J., Joutel, F., & Robutel, P. 1993. Stabilization of the Earth's obliquity by the moon. *Nature*, *361*, 615-617.

Lean, J., Beer, J., & Bradley, R. 2012. Reconstruction of solar irradiance since 1610: implications for climate change. *Geophys Res Lett*, 22, 3195-3198.

Levitus, S., Antonov, J. I., Boyer, T. P., Baranova, O. K., Garcia, H. E., Locarnini, R. A., Mishonov, A. V., Reagan, J. R., Seidov, D., Yarosh, E. S., Zweng, M. M. 2012. World ocean heat content and thermosteric sea level change. *Geophys Res Lett, 39*, L10603.

Lissauer, J. J., Barnes, J. W., & Chambers, J. E. 2011. Obliquity variations of a moonless Earth. *Icarus*, *217*, 77-87.

Meehl, G. A., Washington, W. M., Wigley, T. M. L., Arblaster, J. M., & Dai, A. 2003. Solar and greenhouse gas forcing and climate response in the twentieth century. *J Climate*, *16*, 426-444.

O'Halloran, T. L., Law, B. E., Goulden, M. L., Wang, Z., Barr, J. G., Schaaf, C., Brown, M., Fuentes, J. D., Göckede, M., Black, A. and Engel, V. 2012. Radiative forcing of natural forest disturbances. *Global Change Biology*, *18*, 555–565.

Prather, M., et al. 2001. Atmospheric chemistry and greenhouse gases, in *Climate Change 2001: The Scientific Basis. Third Assessment Report of the Intergovernmental Panel on Climate Change*, edited by J. T. Houghton, Y. Ding and D. J. Griggs, pp. 239-287, Cambridge University Press, Cambridge UK.

Ramaswamy, V. et al. 2001. Radiative forcing climate change, in climate change 2001: The Scientific Basis, pp. 349-416, Houghton, J. T. et al. (eds.). Cambridge U. Press, Cambridge, 2001.

Rasoonl, S. I., & de Bergh, C. 1970. The runaway greenhouse effect and the accumulation of $CO_2$ in the atmosphere of Venus. *Nature*, *226*, 1037-1039.

Roper, D. 2012. Sea Level Versus Temperature. Retrieved from http://www.roperld.com/science/sealevelvstemperature.htm.

Schuiling, R. D., &Krijgsman, P. 2006. Enhanced weathering: an effective and cheap tool to sequester $CO_2$. *Climate Change*, 74, 349-354.

Shakhova, N., Semiletov, I., Salyuk, A., & Kosmach, D. 2008. Anomalies of Methane in the Atmosphere Over the East Siberian Shelf: Is There Any Sign of Methane

Leakage From Shallow Shelf Hydrates?. *Geo Res Abs*, *10*, EGU2008-A-01526, 2008. SRef-ID: 1607-7962/gra/EGU2008-A-01526. EGU General Assembly 2008.

Shapiro et al. 2011. A New Approach to the Long-Term Reconstruction of the Solar Irradiance Leads to Large Solar Forcing. *A&A 529*, A67.

Shindell, D. T., Schmidt, G. A., Mann, M. E., Rind, D., & Waple, A. 2001. Solar forcing of regional climate change during the Maunder Minimum. *Science*, *294*, 2149-2152.

Shindell, D. T., 2009: Maunder Minimum. In Encyclopedia of Paleoclimatology and Ancient Environments. V. Gornitz, Ed., Encyclopedia of Earth Sciences Series. Springer, pp. 550-551.

Wielicki, B. et al. 2005. Changes in earth's albedo measured by satellite. *Science*, 308, p. 825.

Williams, D. M., & Pollard, D. Extraordinary climates of earth-like planets: three-dimensional climate simulations at extreme obliquity. *International Journal of Astrobiology*, 2, 1-19.

Williams, D. M., & Pollard, D. Earth-like worlds on eccentric orbits: Excursions beyond the habitable zone. *International Journal of Astrobiology*, *1*, 61-69.